

**A NOVEL TECHNIQUE FOR THE ANALYSIS OF SHEAR WALLS
WITHIN MANUFACTURED HOMES USING THE FINITE
ELEMENT METHOD**

By

SAMEER BAFNA

A thesis submitted in partial fulfillment of the requirements for the degree
of

MASTER OF SCIENCE

WASHINGTON STATE UNIVERSITY
Department of Civil and Environmental Engineering

MAY 2004

To the Faculty of Washington State University:

The members of the Committee appointed to examine the thesis of SAMEER BAFNA find it satisfactory and recommend that it be accepted.

Chair

Acknowledgments

I would like to express my sincere gratitude and appreciation to Dr. William F. Cofer, advisor and chair of my committee, for his support and guidance that he gave me throughout my research. I am fortunate to have him as my advisor and thank him for giving me liberty to work independently and having faith in me.

I am grateful to Dr. James D. Dolan for serving on my committee and for his valuable suggestions and assistance throughout this research. Special thanks to Dr. David Pollock, member of my committee, for his guidance and support.

I would like to thank Idaho National Engineering and Environmental Laboratory (INEEL), especially William D. Richins, Jeffrey M. Lacy, and Thomas K. Larson for providing the much needed full-scale test data for verification purpose. Special thanks to Jeffrey M. Lacy for his help with modeling of manufactured homes. I would also like to thank the National Institute of Standards and Technology (NIST), especially Michael A. Riley, for providing useful test data for validation of the program used to analyze shear walls.

Special thanks to Ravindra Akarapu for his valuable help with C programming. I would also like to thank Ryan Kobbe for the information he provided me on double section manufactured homes. Thanks to Imtiyaz Shaikh and Sachin Saldhana for their help and being very supportive roommates. I want to acknowledge my friends, and fellow graduate students who helped to make graduate school a pleasant and invaluable experience.

I would like to thank my grandmother, brothers and sisters, uncles and aunts, and relatives for their support and prayers. Finally, I would like to dedicate this thesis to my parents, Surekha and Dilip Bafna for their relentless love, endless support, and countless sacrifices. I missed my family a lot, especially my little nieces, Tanvi and Savi, during my stay in Pullman, and nothing was possible without their support.

**A NOVEL TECHNIQUE FOR THE ANALYSIS OF SHEAR WALLS WITHIN
MANUFACTURED HOMES USING THE FINITE ELEMENT METHOD**

Abstract

By Sameer Bafna, M.S.
Washington State University
May 2004

Chair: William F. Cofer

Widespread damage to manufactured homes associated with Hurricane Andrew and other more recent catastrophic events points toward the need for research addressing their structural performance when subjected to high winds. To improve the level of engineering for manufactured housing, the U.S. Department of Housing and Urban Development (HUD) is developing a Desktop Design Tool under the administration of the Idaho National Engineering and Environmental Laboratory (INEEL). The state-of-the-art for lateral load analysis of manufactured homes is not sufficiently accurate to allow current rational design for these complex three-dimensional structural systems. Thus, to predict the behavior of a manufactured home subjected to wind loading, a three-dimensional analysis of the complete structure is required. The purpose for the Desktop Design Tool is to provide a three-dimensional, system-based analysis capability for designers of manufactured homes.

The focus of this research was to develop analysis techniques that can be used to accurately model the behavior of shear walls within manufactured homes. The method presented is an improvement over existing methods because it can be applied without first doing detailed wall testing. Then, a structural analysis module was developed and

verified for use within the Desktop Design Tool to evaluate the performance of manufactured homes when subjected to wind load. The module includes an interface element, which was developed to enable the determination of one of the major results desired from the analysis module, which is the force at connections between walls and diaphragms and across the mating line. The results, in comparison with full-scale tests, are promising in that the model correctly predicts the overall behavior of the structure.

Table of Contents

Acknowledgments	iii
Abstract.....	v
Table of Contents	vii
List of Tables	xi
List of Figures.....	xii
1. INTRODUCTION.....	1
1.1 Background.....	1
1.2 Objectives	4
2. LITERATURE REVIEW.....	6
2.1 Introduction	6
2.2 Testing	7
2.2.1 Manufactured Homes.....	7
2.2.2 Light-Framed Structures	9
2.2.3 Shear Walls	10
2.2.3.1 Sheathing.....	10
2.2.3.2 Effect Of Openings.....	11
2.2.3.3 Aspect Ratio	12
2.2.3.4 Adhesives.....	13
2.2.3.5 Large Sheathing Panels	14
2.2.3.6 Overturning Restraints.....	14
2.2.3.7 Stud Spacing.....	15
2.2.3.8 Panel Width	15

2.3	Modeling.....	15
2.3.1	Entire Structure.....	15
2.3.2	Shear Walls.....	17
2.3.2.1	Analytical Model.....	17
2.3.2.2	Finite Element Modeling.....	19
3.	<i>FEl</i> OVERVIEW.....	21
3.1	Introduction.....	21
3.2	<i>FEl</i> Overview.....	21
3.2.1	Existing Elements.....	22
3.2.2	Modifications in <i>FEl</i>	22
4.	SHELL ELEMENT FORMULATION.....	24
4.1	Introduction.....	24
4.2	Element Formulation.....	24
4.2.1	Formulation of the Plane Stress Portion of the Element.....	25
4.2.2	Formulation of the Plate Portion of the Element.....	29
4.2.2.1	Shear Locking of Plate Element.....	37
4.2.3	Formulation of Shell Element.....	38
4.2.3.1	Transformation from Isoparametric Natural Coordinates (ξ, η) to Cartesian Coordinates (x, y).....	39
4.2.3.2	Orthotropic Material Transformation.....	41
4.2.3.3	Element Transformation from Local Coordinates (x, y) to Global Coordinates (X, Y).....	42
5.	INTERFACE ELEMENT FORMULATION.....	45

5.1	Introduction	45
5.2	Element Geometry	45
5.3	Element Formulation	46
5.3.1	Stiffness Matrix Derivation.....	50
5.3.2	Element Transformation	52
6.	SHEAR WALLS.....	55
6.1	Introduction	55
6.2	Full-Scale Shear Wall Testing (NIST)	55
6.2.1	Introduction.....	55
6.2.2	Test Specimens and Configurations.....	56
6.2.3	Experimental Results	62
6.3	Modeling of Shear Walls Using Orthotropic Shell Element	63
6.3.1	Results.....	65
6.3.2	Drawbacks to the Model with Orthotropic Shells.....	66
6.4	Enhanced Model	67
6.4.1	Results.....	72
7.	DOUBLE-SECTION MANUFACTURED HOME	75
7.1	Introduction	75
7.2	Full-Scale Testing of Double-Section Manufactured Home	75
7.2.1	Introduction.....	75
7.2.2	Double-Section Manufactured Home Description.....	76
7.2.3	Loading	76
7.2.4	Data Acquisition	79

7.3	Modeling of Double-Section Manufactured Homes	79
7.3.1	Introduction.....	79
7.3.2	Model Description	80
7.3.2.1	Foundation System	80
7.3.2.2	Floor System.....	82
7.3.2.3	Wall System.....	84
7.3.2.4	Roof System	85
7.3.2.5	Interfaces	87
7.4	Results	89
7.4.1	Load – Deflection Behavior.....	89
7.4.2	Force Response	92
8.	CONCLUSIONS AND RECOMMENDATIONS	94
8.1	Conclusions	94
8.2	Recommendations	95
	Literature Cited	97
	Appendix A: Equivalent In-Plane Properties for Orthotropic Shell Element	110

List of Tables

Table 6.1: Properties of Orthotropic Shell Element.....	63
Table 6.2: Comparison of Racking Displacement for Unit Load for Orthotropic Shell Model	66
Table 6.3: Properties of Components in the Enhanced Model	71
Table 6.4: Properties of Nails (6d common).....	71
Table 6.5: Comparison of Racking Displacement for Unit Load for Enhanced Model ...	72
Table 7.1: Chassis Properties.....	82
Table 7.2: Floor Properties	84
Table 7.3: Wall Properties	85
Table 7.4: Roof Properties	87
Table 7.5: Interface Properties.....	88
Table 7.6: Global Displacements for Air Bag Test (Uniformly Distributed Load).....	90
Table 7.7: Racking Displacements of the Shear Walls.....	91
Table 7.8: Shear Displacements Along the Mating Line.....	91
Table 7.9: Percentage of Forces in Each Shear Walls	92

List of Figures

Figure 1.1: Components of Manufactured Home	1
Figure 2.1: Lateral Force Resisting System of Light-Framed Building	6
Figure 2.2: Test Setup (Nelson et al., 1985) For Testing Interior Shear Wall Along With Adjacent Structural Elements	8
Figure 4.1: Geometry and Degrees of Freedom for Shell Element	25
Figure 4.2: Degrees of Freedom per Node for the 4-Node Plane Stress Element	26
Figure 4.3: Degrees of Freedom per Node for the 4-Node Plate Element.....	31
Figure 4.4: Stiffness Matrix for Shell Element, $[K]_{\text{SHELL}}$	39
Figure 4.5: Orientation of Orthotropic Material Axes	41
Figure 4.6: Orientation of Local Axes	43
Figure 5.1: Interface Element Geometry	46
Figure 5.2: Degrees of Freedom per Node for an Interface Element.....	47
Figure 5.3: Orientation of the Local Axes	53
Figure 6.1: Framing Dimensions of the Solid Wall Specimen	56
Figure 6.2: Framing Dimensions of the Wall Specimen with a Door Opening.....	57
Figure 6.3: Framing Dimensions of the Wall Specimens with a Window Opening.....	58
Figure 6.4: Edge Dimensions of the Specimen.....	59
Figure 6.5: Wall Test Setup	60
Figure 6.6: Locations of Sensors Connected to the Wall Framing	61
Figure 6.7: Locations of Sensors Connected to the Gypsum Board Cladding	61
Figure 6.8: Locations of Sensors Connected to the OSB Cladding.....	62

Figure 6.9: Load v/s Racking Displacement.....	62
Figure 6.10: Finite Element Model of Wall-1 using Orthotropic Shell Element.....	64
Figure 6.11: Finite Element Model of Wall-2 using Orthotropic Shell Element.....	64
Figure 6.12: Finite Element Model of Wall-3 and Wall-4 using Orthotropic Shell Element	65
Figure 6.13: Enhanced Model of Wall-1 Representing Sheathing (Interior or Exterior) .	68
Figure 6.14: Enhanced Model of Wall-1 Representing Framing Members.....	68
Figure 6.15: Enhanced Model of Wall-2 Representing Sheathing	69
Figure 6.16: Enhanced Model of Wall-2 Representing Framing Members.....	69
Figure 6.17: Enhanced Model of Wall-3and Wall-4 Representing Sheathing	70
Figure 6.18: Enhanced Model of Wall-3and Wall-4 Representing Framing Members....	70
Figure 6.19: Wall Stiffness from the FE Model and Experimental Test for the Solid Wall (Wall-1)	73
Figure 6.20: Wall Stiffness from FE Models and Experimental Test for the Wall w/ Door Opening (Wall-2)	73
Figure 6.21: Wall Stiffness from FE Models and Experimental Test for the Wall w/ Window Opening Sheathed on Both Sides (Wall-3).....	74
Figure 6.22: Wall Stiffness from the FE Model and Experimental Test for the Wall w/ Window Opening Sheathed on Only One Side (Wall-4)	74
Figure 7.1: Typical Layout of Double-Section Manufactured Home.....	77
Figure 7.2: Section View of the Manufactured Home	78
Figure 7.3: Test Home Installation Showing Piers, Tie-down Load Cells, and Reaction Wall with Braces	78

1. INTRODUCTION

1.1 Background

Widespread damage to manufactured homes associated with Hurricane Andrew and other more recent catastrophic events points toward the need for research addressing their structural performance when subjected to high winds. Vulnerability of manufactured homes to severe winds, combined with the uncertainty regarding the magnitude and distribution of the wind pressure on them, highlights the need for research in this field.

Manufactured homes are constructed of various components, such as a chassis, tie-downs, walls, floor, roof, and the mating line, as shown in *Figure 1.1*. The analysis of individual components is not enough to accurately predict the behavior of a manufactured home. Instead, a three-dimensional analysis of the entire system is required.

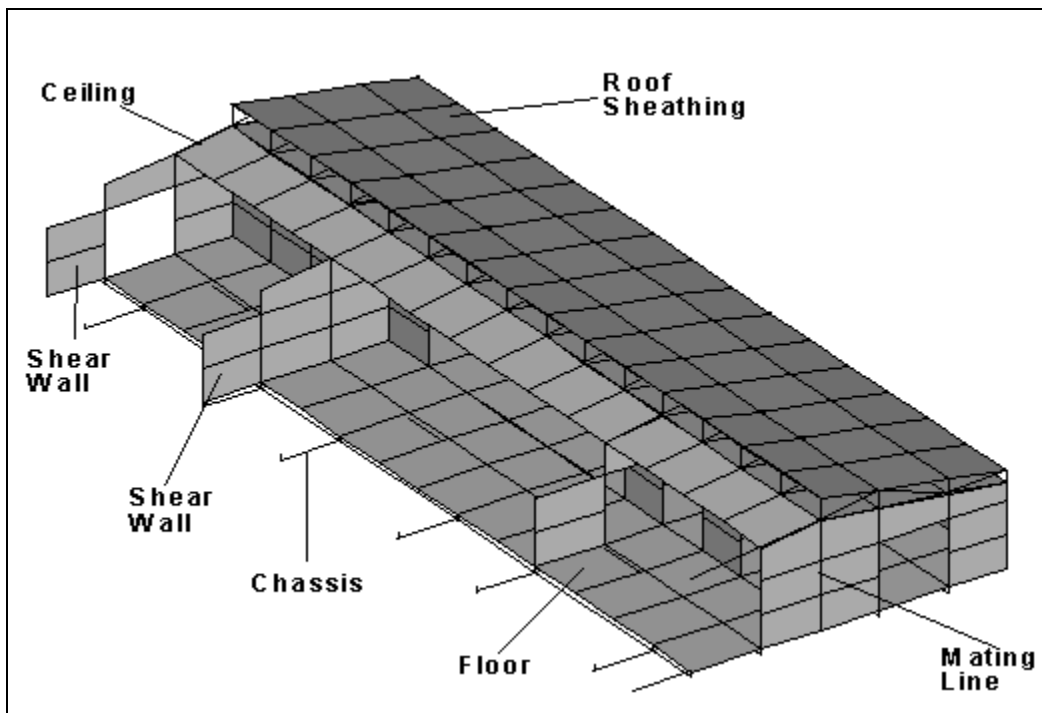


Figure 1.1: Components of Manufactured Home

The Idaho National Engineering and Environmental Laboratory (INEEL) is conducting research to test, analyze, and improve manufactured homes with the goal of making them more durable, wind-storm resistant, and energy efficient. As part of this project to improve the level of engineering for manufactured housing, a Desktop Design Tool is being developed. It is envisioned that the tool should be capable of carrying out performance-based structural design within existing design codes.

The current procedure for the analysis of manufactured homes when subjected to wind relies on the method of tributary areas to assign the lateral loads from the side walls to the shear walls. In manufactured homes/light-frame structures, shear wall systems are often used to efficiently and economically transfer the wind load to the foundation. They not only provide the building with enclosure, but also sufficient strength and stiffness to resist vertical loads, out of plane wind loads, and in-plane lateral forces. Shear walls differ from other, non-structural walls in manufactured homes, referred to as “partition walls”, by the connection of the wall to the roof and the floor system and, in some cases, by the materials used in the construction of the wall. Partition walls may be placed on the floor sheathing between joists, but shear walls are always located over floor joists as their main purpose is to distribute the lateral load to the chassis.

Previous studies have shown that the transfer of load from side walls to the shear walls is more complex than the tributary area method (Jablin and Schmidt, 1996). Load transfer depends on factors such as the stiffness of the roof/ceiling diaphragm, the length and the position of the shear walls, and various other factors. In many cases, the method of tributary areas may be appropriate, but a new rational analysis procedure that is

accurate for any type of design and loading is desired. Moreover, system behavior dominates the structural action of the manufactured homes. To predict the behavior of a manufactured home, a three-dimensional analysis of the complete unit is required. Thus, the state-of-the-art for lateral load analysis of manufactured homes is not sufficiently accurate to allow current rational design for these complex three-dimensional structural systems. The purpose for the Desktop Design Tool is to provide a three-dimensional, system-based analysis capability for designers of manufactured homes.

The state-of-the-art tools for the structural analysis of manufactured homes under lateral loads are, for the most of part, based on methods developed for light-frame (“stick-built”) structures (Goodman et al. 1996). However, the special rigid adhesives used to attach sheathing to the studs significantly alter the behavior of manufactured homes under lateral loading. These adhesives provide a nearly rigid attachment and prevent slip between the sheathing material and framing member and contribute to increased stiffness of the walls. This is the most important difference between manufactured housing construction and other light-frame timber construction and, hence, methods developed for light-frame structures are inappropriate for the analysis of manufactured homes. Also, previous full-scale tests on laterally loaded manufactured homes confirm that conventional analysis methods are not applicable (Stewart et al. 1988).

The behavior of the connections between shear walls and side walls, between shear walls and floor/roof diaphragms, and along the mating line between sections is difficult to model accurately since the load-displacement relationships for them are difficult to develop without using experimental data. The modeling of these types of interfaces has been a focus of research in the past. The difficulty in modeling the

behavior of connections is accurately representing the behavior of a row or multiple rows of individual fasteners, while keeping the number of degrees of freedom at a workable level. The focus of this research is to develop analysis techniques that can be used to accurately model the behavior of shear walls within manufactured homes. The method presented is an improvement over existing methods because it can be applied without first doing detailed wall testing. Then, a structural analysis module is developed that can be used within the Desktop Design Tool to evaluate the performance of manufactured homes when subjected to wind load. It is designed to be simple enough to be part of an automated analysis/design package to be used by semi-professional designers, but accurate enough to evaluate the distribution of forces within the structural system.

1.2 Objectives

The major objectives of this research are:

1. Develop an analysis module for the Desktop Design Tool described earlier.

The analysis module will incorporate an existing finite element program, *FElt* (Gobat and Atkinson, 2000). Several enhancements are required for the existing *FElt* code to be applicable as the analysis module for the Desktop Design Tool for manufactured housing. They are:

- i. The main structural elements for the walls, roof, and floor diaphragm in a structural model of a manufactured home are often modeled with shells. Hence, an orthotropic flat shell element, with combined bending and membrane behavior, must be added to the element library.

- ii. One of the major results desired from the analysis module is the force at connections between shear walls and diaphragms and across the mating line. In order to obtain these forces, an interface/connector element that provides an elastic connection along the edges of adjoining shell elements must be developed and added to the element library.
2. Verify the analysis module by simulating tests of a typical Double-Section Manufactured Home. Forces (such as tie-down strap force, and forces along ridge-line) and displacements (such as global displacements, racking deformations, shear displacement along the ridge-line, and interface slip displacements) obtained from experimental results are compared to results obtained from the finite element analysis.
3. Develop a simplified analysis method that captures the essential stiffness properties of exterior and interior shear walls within manufactured homes without the need to perform detailed full-scale tests.

2. LITERATURE REVIEW

2.1 Introduction

The demands for inexpensive housing have led to an increase in popularity of manufactured homes. Prior to the mid 1970's, research on the structural behavior of manufactured homes was limited, the majority of which was performed on the behavior of light-framed structures subjected to lateral loading.

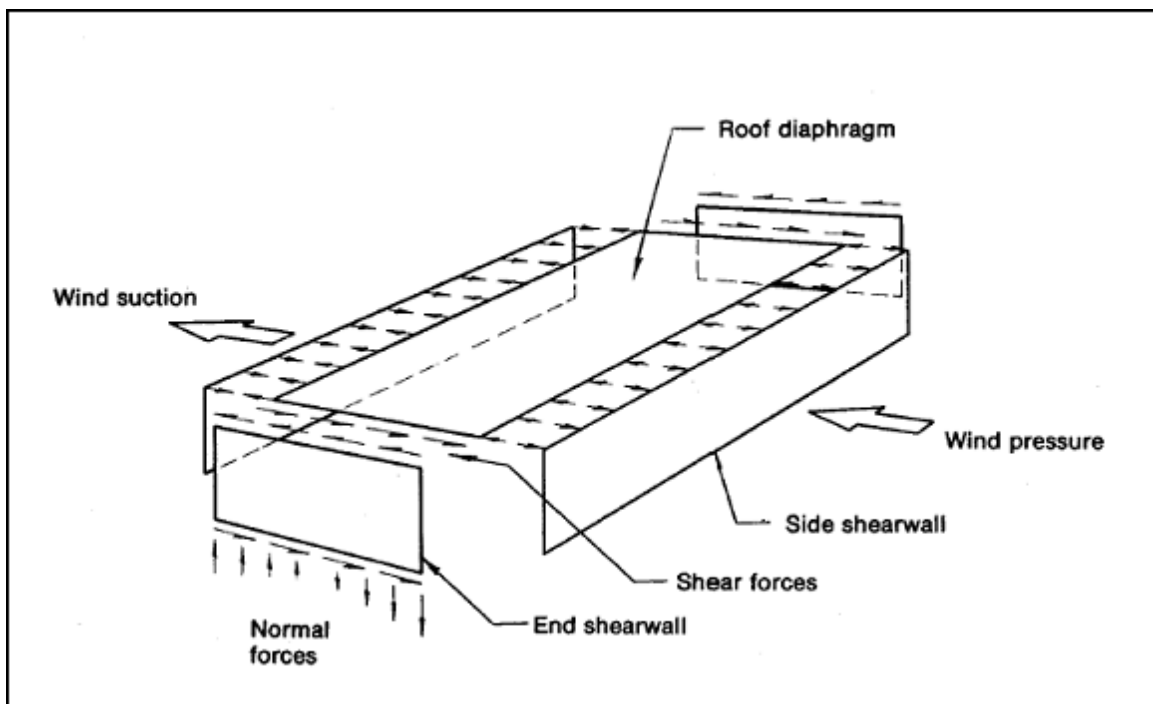


Figure 2.1: Lateral Force Resisting System of Light-Framed Building

A typical single section manufactured house is rectangular in plan and has a high length to width ratio. This shape creates a large area over which lateral wind load acts, but a relatively short width for resisting it. Lateral loads are primarily resisted by the shear walls and the ceiling diaphragm. When the lateral wind load acts on the sidewalls of a structure, simply supported between the roof and the foundation, it is transferred to

the horizontal ceiling diaphragm. This diaphragm, acting as a deep horizontal beam, transmits the load to end shear walls, which in turn transfer the load to the foundation as shown in *Figure 2.1*. In shear walls, load is transferred from the top plate to the sheathing, then from the upper portion of sheathing back to the studs so that it can cross the horizontal joints. Then the load is passed from the studs back into the sheathing and, finally from the sheathing to the bottom plate (Stricklin et al. 1996).

2.2 Testing

2.2.1 Manufactured Homes

Marshall (1977) conducted an experiment on full-scale manufactured homes to determine the wind load acting on them. The load-deflection characteristics of the full-scale home were determined by simulating the wind loads.

Nelson et al. (1985) tested the structural behavior of seven shear wall assemblies used in manufactured homes under simulated wind loads. They studied the response of the interior shear walls, along with adjacent structural elements as shown in the *Figure 2.2*. Parameters investigated were size and location of the shear walls, number of joists under the shear wall, and number of the panels glued to the framing. They found that shear walls located on the windward side of the assembly have higher racking strength and that shear walls typically failed at the connection of the shear wall to the floor on the windward side. A significant amount of load may be transferred into sidewalls due to slip between the shear wall and the sidewall.

Stewart et al. (1988) conducted full-scale tests on two manufactured (14 X 66 ft.) homes under simulated concentrated and uniformly distributed wind loads. The home was constructed according to standard procedure, while omitting all non-structural

components. The lateral load capacity of the home tested was found to be much greater than the design lateral pressure and the shear wall response was almost linear. They measured the racking resistance provided by transverse walls under lateral loading and noted that the shear wall and roof diaphragm system behaves as a stiff beam on an elastic foundation, with the end walls carrying the majority of the lateral loads. They concluded that the method that considers combined system stiffness and load sharing provided by the interaction of various structural components is the most appropriate for manufactured homes.

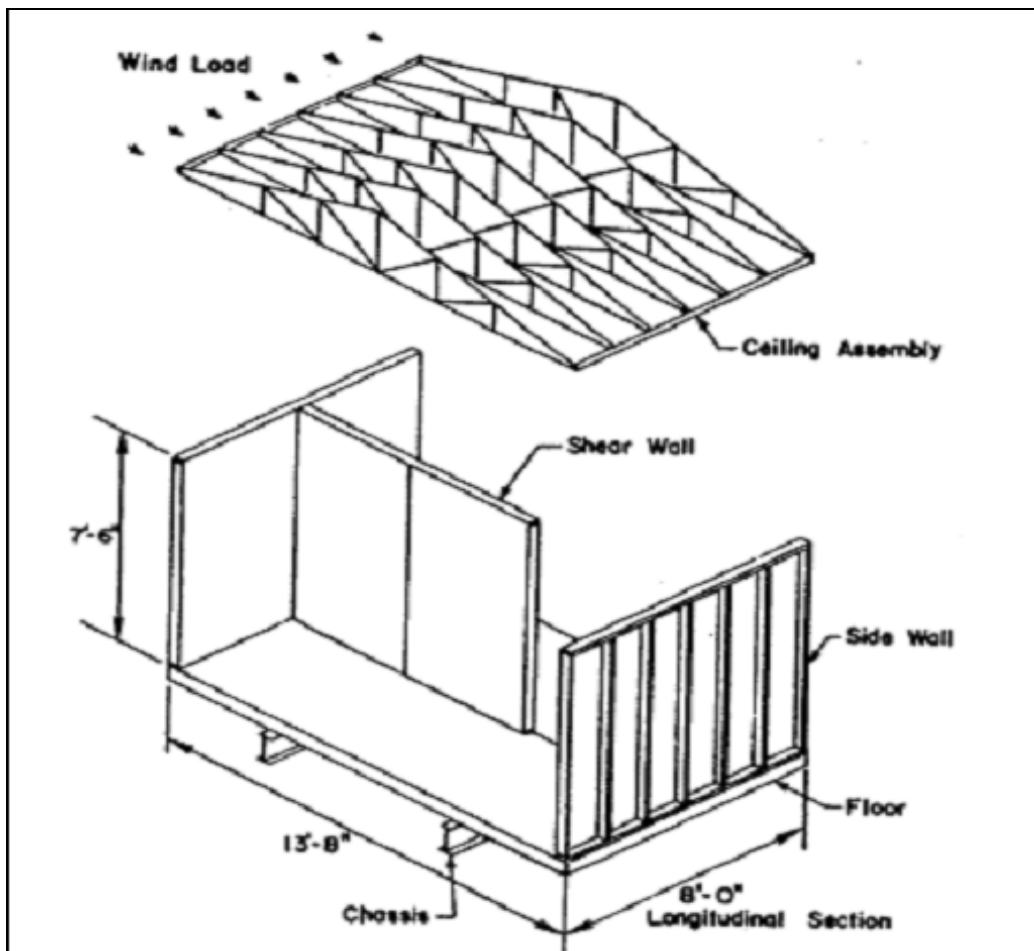


Figure 2.2: Test Setup (Nelson et al., 1985) For Testing Interior Shear Wall Along With Adjacent Structural Elements

Richins et al. (2000) performed a series of full-scale static load tests on a typical single-wide manufactured home subjected to simulated wind loads. Loads were applied using either a pressurized airbag for distributed loading or a hydraulic jack for concentrated loading. Results show nearly linear initial system response, but as the load increases, significant non-linear behavior was observed for concentrated and distributed loading. Interface slip and racking of the manufactured home was nearly insignificant. Permanent horizontal deformation was also observed due to slippage in the tie-down straps and horizontal displacement of the home on the foundation.

2.2.2 Light-Framed Structures

Boughton (1988) conducted tests on a full-scale wood house subjected to lateral wind load. Only the primary failure modes under lateral loads were determined and no attempt was made to measure the force distribution in the shear walls. He showed that the load does not always follow paths through the major structural components, and noted that the assumptions on load-sharing capabilities are, in some cases, unconservative. A comparison of his results with laboratory tests showed that the stiffness of the loading frame and the rigidity of the support system play a significant role in the determination of the ultimate load and failure mechanism.

Phillips et al. (1993) conducted tests on a full-scale single-story wood structure under lateral loading. Testing at various stages of construction were performed, which enabled the determination of the load-sharing characteristics of the different elements of the building, particularly among the walls and roof diaphragms. The home was tested under concentrated loads, and the portion of the load shared by various components, such as diaphragms, sidewalls, shear walls, etc., were determined. The roof diaphragm was

found to behave in almost a rigid manner, which affected the distribution of lateral load to shear walls. Load distribution among the shear walls was a function of stiffness and position within the building. The wall transverse to the loading direction carried between 8 % and 25 % of the applied lateral load.

Paevere et al. (2003) performed a series of experiments on a full-scale one-story L-shaped wood frame house. The main purpose of this test was to determine the load redistribution in a nonsymmetrical light-frame structure under lateral loading. They found that there is significant potential for sharing and redistribution of applied lateral load between main shear resisting walls of the light-frame house.

2.2.3 Shear Walls

Shear walls are the most important lateral force resisting structures in manufactured homes/light-frame structures. In the last two decades, significant progress has been made in the study of shear walls. New analytical techniques and numerical analysis methods, such as the finite element method, have been developed to predict shear wall behavior. Several researchers have studied the effect of the configurations, geometry, types of fasteners, etc., on the behavior of the shear walls, as described below.

2.2.3.1 Sheathing

Wolfe (1983) tested thirty shear walls and found that the racking resistance of a wall sheathed with two gypsum boards is equal to the sum of the individually tested gypsum boards. Walls tested with panels oriented horizontally were more than 40% stronger and stiffer than those with panels oriented vertically. He also concluded that gypsum wallboard could provide a significant contribution to the racking resistance when

subjected to monotonic loading. Patton-Mallory, et al (1984) tested a series of small-scale plywood and gypsum plasterboard clad timber frames under monotonic load. They found that the racking resistance of a double-sided wall was the sum of the resistance of the individual single-sided walls. They also found that the contribution of single sided gypsum sheathing is about 38% of the racking resistance of single sided plywood sheathing. Kallsner (1984) tested shear walls with fiberboard, plywood, particleboard, and plasterboard sheathing and noted the additive nature of individual sheathings in double-sided shear walls. Dolan (1989) tested 20 waferboard and 22 plywood sheathed shear walls. He observed no significant difference in the dynamic response for waferboard and plywood sheathed walls. For up to 50% of the ultimate static load, and for higher loads, plywood sheathed walls deflected more due to lower stiffness when compared to waferboard. Karacabeyli and Ceccotti (1996) tested a series of shear walls and found that OSB and gypsum sheathed shear walls have greater ultimate strength but lower ductility than walls with OSB on one side.

2.2.3.2 Effect Of Openings

Tuomi and McCutcheon (1974) experimentally investigated the effect of wall openings on the racking resistance of wood-frame walls and found that the presence of openings reduces the ability of a wall to resist racking load. Sugiyama (1981) proposed a simple method for determining the monotonic capacity of shear walls with openings based on the capacity of fully sheathed shear walls without openings. Patton-Mallory, et al (1985) found that the racking strength and stiffness of a wall was proportional to the effective wall length, which is defined as the total length of the wall less the total length

of the openings. This methodology is currently used in practice, but it overestimates the stiffness of the walls. Based on a simple equilibrium equation and the shear transfer method, Dean et al (1984) developed a design procedure for shear walls with rectangular openings. Yasumura (1986) developed a theoretical method on the basis of the non-linear load-slip relation of a nail to calculate the racking strength and stiffness of shear walls with openings. White (1995) found that as the length of the opening in a shear wall increases, its strength, initial stiffness, and maximum seismic base shear decreases. Also, shear walls with openings are stronger and stiffer than walls without openings for the same effective length and height. Also, as the length of the opening increases, the strength and the stiffness of the wall decreases. Johnson (1997) performed tests on long shear walls with various opening configurations and concluded that sheathing above and below the opening resists shear, validating Sugiyama's design method.

2.2.3.3 Aspect Ratio

Response of a shear wall depends on its aspect ratio and the ratio of its length to its height. Suzuki et al (1978) performed racking tests on shear walls of various lengths and concluded that the maximum shear load is almost linearly proportional to the wall length. Wolfe (1983) tested wall panels with one-sided gypsum sheathing having an aspect ratio between 1 and 3 and noted that racking strength increases as the length of the wall increases. Patton-Mallory et al. (1984) conducted small-scale tests on shear walls with sheathing on both sides and showed that the strength of the wall was proportional to the wall length. Naik et al. (1984) found that the lateral stiffness and strength of a shear wall is more dependent on the number of nails and nail spacing than on wall height. For

shear walls of short length, McDowall and Halligan (1989) found that the failure load varies linearly as a function of wall length. For walls of length greater than 1.2m (4 ft.), White (1995) found that maximum strength, initial stiffness, and maximum base shear increase linearly as the length of a shear wall increases for walls of the same height. Salenikovich (2000) concluded that strength, shear modulus, and ductility of the unrestrained (conventional) walls were dependent on the aspect ratio and the number of panels in the wall. Single-panel walls with higher aspect ratio were weaker but the more ductile.

2.2.3.4 Adhesives

Thurston and Flack (1980) investigated the effects of gluing the sheathing to the framing and found that glued sheathing provides an increased ultimate load capacity compared to the case without glue. They also found that the racking resistance of shear walls depends on the hold-down anchors at the bottom of end studs. Oliva and Wolfe (1988) tested fifty-nine shear walls and found that nail gluing of the gypsum to the framing increased stiffness and strength compared to nailing alone. They also found that the panel orientation has a significant effect on racking stiffness and strength, with panels oriented horizontally having higher values than those with panels oriented vertically. Dolan (1989) found that deflection of shear walls was significantly lowered by using adhesives. Filiatrault and Foschi (1990) determined the response of shear walls fastened with nails and with adhesives under various loadings. Test results showed that shear walls fastened with adhesive and nails behave almost linearly with very little ductility. Also, the initial stiffness of these walls is about 65% higher than the initial stiffness of a wall

fastened with nails only. Dolan and White (1992) also showed that walls with adhesives are stronger, stiffer, and less ductile than standard nailed walls. These walls thus are better suited for being used in high wind zones because, in those applications, the strength of the wall is more important than the ductility of the wall. Pellicane (1991) tested laterally loaded joints that were nailed or glued and nailed. The results showed that the use of adhesives along with nails greatly enhanced the load carrying capacity of the connection.

2.2.3.5 Large Sheathing Panels

Enjily and Griffiths (1996) tested shear walls with larger sheathing panels and concluded that racking strength is proportional to panel height. Lam et al. (1997) tested eleven shear walls, three with regular sized panels (1.2 X 2.4 m) and the remaining eight with oversized panels to study the effect of oversized panels. Under monotonic loading, they observed that shear walls with oversized panels had a substantial increase in both stiffness and lateral load carrying capacity. However, under cyclic loading, walls with regular sized panels were shown to dissipate more energy than the walls with oversized panels.

2.2.3.6 Overturning Restraints

White (1997) found that the shear force resisted by the anchorages located in close proximity to studs where sheathing panels meet is significantly larger than the average shear force resisted per anchorage. Heine (1997) found that walls with no tie-

down anchors to restrain overturning had lower stiffness and capacity than the walls with overturning restraint.

2.2.3.7 Stud Spacing

De Klerk (1985) tested twelve plywood and gypsum plasterboard clad timber frames and observed that the racking strength of timber walls can be increased by at least 15% if the stud spacing is reduced from 600 mm to 400 mm on center.

2.2.3.8 Panel Width

Kamiya (1986) concluded that strength and stiffness of a panel is proportional to its width. He observed that 1.2 X 2.4 m (4 X 8 ft.) sheathing panels, commonly used in North America, have higher stiffness and load capacity than 0.9 X 2.4 m (3 X 8ft.) sheathing panels, commonly used in Japan.

2.3 Modeling

Numerous models have been developed to predict the behavior of manufactured homes/light-frame structures and shear walls. With them, useful information is provided without carrying out costly experimental testing.

2.3.1 Entire Structure

Moody and Schmidt (1988, 1989) developed a structural model for predicting the lateral behavior of light-frame wood buildings. The model assumed the roof as a rigid diaphragm. Using the assumed structural properties of the component materials, the

model provided good agreement with data from three different houses tested in Japan. The model predicts the lateral translation and rotation of the rigid diaphragm that is restrained by the shear walls.

Kasal et al. (1994) used the ANSYS finite-element software to analyze the behavior of light-frame wood structures loaded by static loads and verified the results by conducting tests of a full-scale house. The roof and floor were considered to be linear, and they were represented by superelements. Quasi-superelements containing a truss and diagonal spring were used to represent the wall system, which was considered to be non-linear. Intercomponent connections were modeled as non-linear, one-dimensional elements similar to individual nail connectors. They found that the load shared by the shear walls was a function of shear wall stiffness, roof diaphragm action, and intercomponent stiffness. Deformations and reaction forces predicted by the model agreed closely with the experimental data.

Jablin and Schmidt (1996) developed a finite element modeling procedure for manufactured homes. For verification of the modeling procedure, numerical models were constructed to replicate two full-scale experimental tests. The model accurately predicted the total deflections of manufactured homes under uniform loading. For a concentrated loading sequence, the model accurately predicted the overall structural response, including the distribution of lateral loads to various shear walls. The difference between the racking deformation with and without interface slip shows that interface behavior must be included in the analysis of manufactured homes, as it was a significant part of the structural behavior.

Koerner et al. (2000) developed a finite element modeling technique for the analysis of manufactured homes and verified it with experimental results. The sensitivity of the model to different boundary conditions and material properties was examined. They concluded that interface slip and internal deformations are not affected by boundary conditions, but that they had a big influence on global displacements.

He et al. (2001) developed a non-linear finite element model to study the behavior of light-frame buildings under static loading. In the model, a mechanics-based representation of the load-deformation characteristics of individual panel to framing connections in the diaphragm systems was implemented. The model can predict the behavior of wood light-frame structures with good accuracy, even with a wide range of structural, material, and loading variation.

2.3.2 Shear Walls

2.3.2.1 Analytical Model

Tuomi and McCutcheon (1978) developed an analytical procedure for calculating the racking strength of shear walls based on the energy method, where externally applied load is resisted by the nails as they distort. They proposed that when a wall is subjected to a racking load, the nail connectors deform, with the framing distorting to a parallelogram and the sheathing remaining rectangular. The racking strength of the panel depends on the lateral strength of the fasteners and not on the framing. The load-deflection relationship for a single nail was assumed to be linear and hence this method is only valid for small deformations. The racking strength of the sheathed panel calculated by this method depends on the panel geometry, the number and spacing of nails, and the lateral

resistance of a single nail. The results obtained from this method were in close agreement with the experimental tests.

Easley et al. (1982) developed formulas for the analysis of shear walls based on the force and moment equilibrium for a panel. They assumed that both frame and sheathing deform as a parallelogram and the vertical nail force component is proportional to vertical distance from the centerline of the panel.

McCutcheon (1985) developed a method for calculating the racking deformation of wood-framed shear walls based on the same energy approach as Tuomi and McCutcheon (1978). It takes nonlinear nail behavior into consideration and can predict the racking performance up to moderate level of deformations. At higher loads, this method underestimates the displacement. Racking due to the shear deformations of the sheathing was also taken into account. It was assumed that the corner nails distort along the diagonal of the sheathing.

Gupta and Kuo (1985) used a strain energy method to predict the behavior of wood-framed shear walls. The stiffness of a shear wall mainly depends on the nail load-slip relationship and, secondarily, on the bending stiffness of the studs and the shear stiffness of the sheathing. Later, they developed a simple model for determining the lateral behavior of wood-framed shear walls with uplifting.

Akerlund (1987) developed a modeling method for shear walls based on the principle of equal internal and external energy. This method assumed a hinged frame of stiff framing members, stiff sheathing, a linear load-slip relation for a single nail, and rigid top and bottom plates.

Sugiyama and Matsumoto (1994) developed a conservative method to predict the behavior of shear walls with openings based on the sheathing area ratio. They assumed that only the nails along the perimeter of a shear wall contribute to the slip resistance, and slip resistance of nails at intermediate studs is negligible.

2.3.2.2 Finite Element Modeling

Itani and Cheung (1984) developed a nonlinear finite element model for single-skinned walls. Fastener flexibility between sheathing and framing was modeled by orthogonal springs. Falk and Itani (1988) developed a simplified form of the earlier model that accounted for the stiffness of fasteners connecting the sheathing to the framing. They reduced the number of degrees of freedom by replacing individual fastener elements for the sheathing to framing connection with a two-dimensional transfer element. This reduced the total number of degrees of freedom by 40%, and produced results nearly identical to those obtained using the previous model. Gutkowski and Castillo (1988) developed finite element software for the nonlinear analysis of single and double sheathed shear walls. Their model considered the nonlinear behavior of the sheathing gap. McCutcheon (1988) developed a computer program for predicting the behavior of shear walls to in-plane loads which agreed with the experimental data. Dolan (1989) developed numerical as well as mathematical models to predict the behavior of timber shear walls. Ge et al (1991) proposed a method that considered the contribution of wall areas above and below the openings to wall stiffness and its racking resistance, but it slightly overestimated the stiffness of shear walls with openings. Dolan and Foschi (1991) developed a method that includes the nonlinear behavior of the connectors

between sheathing and framing, bearing effects between the adjacent sheathing panels, the out-of-plane behavior of the sheathing panels. Results compared well with static shear wall tests performed by Dolan (1989). White and Dolan (1995) developed a finite element program, which was capable performing monotonic or dynamic analysis on timber shear walls, and compared the results with existing experimental data.

3. *FElt* OVERVIEW

3.1 Introduction

To develop the entire finite element code for modeling of a manufactured home would be a monumental task, well beyond the scope of this research. As the Desktop Design Tool should be self-contained, the decision was made not to use commercial finite element software, which would have unnecessary capabilities along with licensing considerations and issues of compatibility. Hence, an existing finite element program, *FElt* (Gobat and Atkinson, 2000), was obtained as a starting point and modified to contain all of the elements necessary for modeling manufactured homes.

3.2 *FElt* Overview

FElt, which stands for **F**inite **E**lement **l**earning **t**ool, is a self-contained finite element system. It is written in the “C” language and the source is available in the public domain. It contains all of the procedures for linear static structural analysis, transient structural analysis, modal analysis, and spectral analysis. In addition, pre- and post-processors are available.

An input file is required to execute *FElt*, which contains the complete description of everything that defines the structure: the nodes, the elements, analysis parameters, the constraints and the forces on the nodes, and material properties of the elements.

3.2.1 Existing Elements

*FEl*t has an extensive element library, and contains most of the elements needed to model a manufactured home. In its element library are the necessary routines for truss/spring elements, two and three-dimensional beam elements, Timoshenko beam elements, plate-bending elements, and others. These elements can be used directly to model the base frame and the tie-downs. However, to model the rest of the structure, modifications to existing elements must be made.

3.2.2 Modifications in *FEl*t

Several enhancements are required for the existing *FEl*t code to be applicable as the analysis module for the Desktop Design Tool for manufactured homes. The first modification to be made to *FEl*t is the addition of a four-node, orthotropic, flat shell element. The main purpose for adding this element is to model walls, floor, and roof/ceiling diaphragms. In addition, the loading capabilities within *FEl*t are somewhat limited. To properly model wind loading, the ability to consider pressure load on shell elements had to be added. Also, a new one-dimensional, four-node, line interface element to connect the sides of adjacent shell elements and to connect the sides of shell elements to beam elements had to be added. One purpose of the interface element is to allow the determination of forces between structural elements of the manufactured home and to include the effects of joint flexibility. In this capacity, the element serves to model interfaces along the ridgeline, and connections between wall-wall, wall-floor, wall-ceiling, etc. The other purpose for the interface element is to include the nail and glue flexibility when modeling the interaction between sheathing and studs in shear walls.

The first step in implementing each element was to develop a stiffness matrix subroutine. The formulation for the element stiffness matrix and necessary displacement-strain-stress relations are outlined in *Chapter 4* and *Chapter 5* for the shell and the interface elements, respectively. The element routine performs a number of error checks and then computes the element stiffness matrix and transforms it to global coordinates. After the global stiffness matrix is assembled, deflections are computed. These global deflections are passed to an element stress routine where stresses and forces are computed. These results are then passed to an output routine for printing.

4. SHELL ELEMENT FORMULATION

4.1 Introduction

Shells resist load through a combination of “in-plane” (membrane) force and bending moment. The mechanism for bending stresses in a shell is the same as that for bending stresses in a plate, with contribution from bending and twisting moments. Membrane stresses correspond to those of a plane stress application and act tangential to the shell mid-surface, producing mid-surface tangential forces per unit length. A flat shell element is obtained by superimposing the membrane stiffness of a plane stress element and the bending stiffness of an identical plate element at the local level. Coupling between the two for a shell occurs when the element is transformed and assembled. For the present application of modeling walls, floors, and roofs of manufactured homes, the shells are generally flat.

The derivation of a four-node shell element is well known (Cook, et al. 2002), but it is presented here for completeness.

4.2 Element Formulation

The shell element is a flat, four-node, isoparametric quadrilateral. A diagram of the element geometry and node numbering is given in *Figure 4.1*. The element is developed in a local coordinate system. There are five active degrees of freedom (DOF) at each node. These are displacements in the local x , y , and z directions and rotations about the local x and y -axes (u , v , w , θ_x , and θ_y respectively). A dummy degree of freedom (the so-called “drilling” degree of freedom), representing the rotation about the

local z -axis, is also included to give six DOF per node. This is necessary for the element to be compatible with other 3-D structural elements, such as beams, and to enable it to model the intersection of non-coplanar shells. *Figure 4.1* shows the DOF for the shell element.

The portion of the element that provides stiffness for membrane behavior is obtained from the usual plane stress formulation and the portion of the element that provides stiffness for bending behavior is obtained from a plate formulation. For plate bending, Mindlin plate theory is applied.

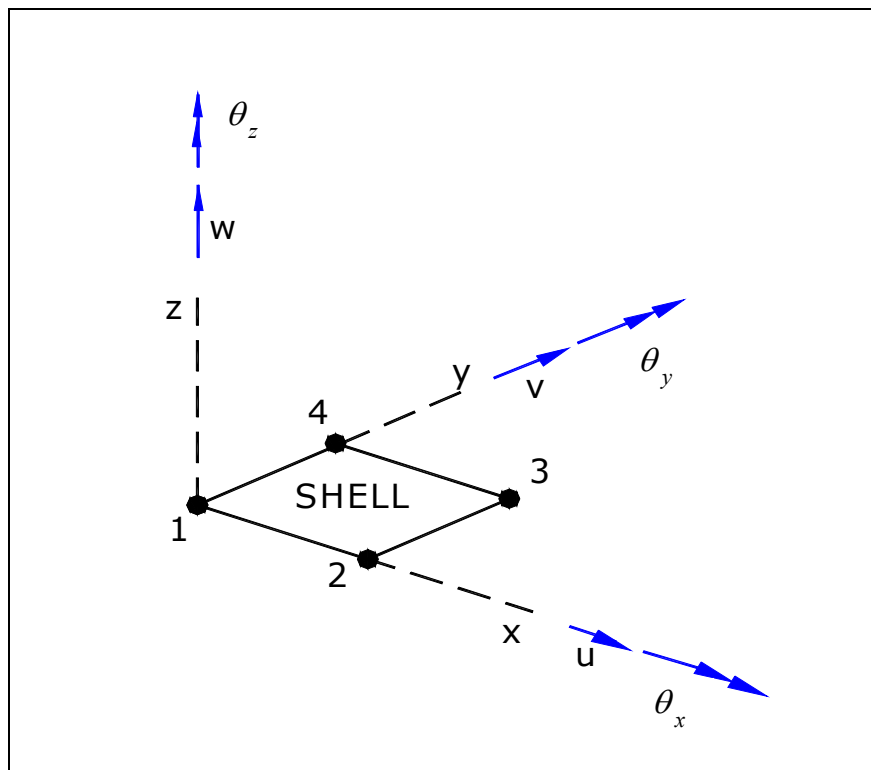


Figure 4.1: Geometry and Degrees of Freedom for Shell Element

4.2.1 Formulation of the Plane Stress Portion of the Element

To formulate the stiffness matrix for the plane stress component of the shell element, the shape functions (Lagrangian Polynomials) that define continuous

displacements in terms of the displacements at each node are developed. There are two degrees of freedom per node, u and v as shown in *Figure 4.2* that may be expressed in terms of shape functions as follows:

$$\begin{aligned} u &= \sum_{i=1}^4 N_i \cdot u_i \\ v &= \sum_{i=1}^4 N_i \cdot v_i \end{aligned} \quad (4.1)$$

Functions, N_i , are standard two dimensional shape functions in terms of isoparametric natural coordinates.

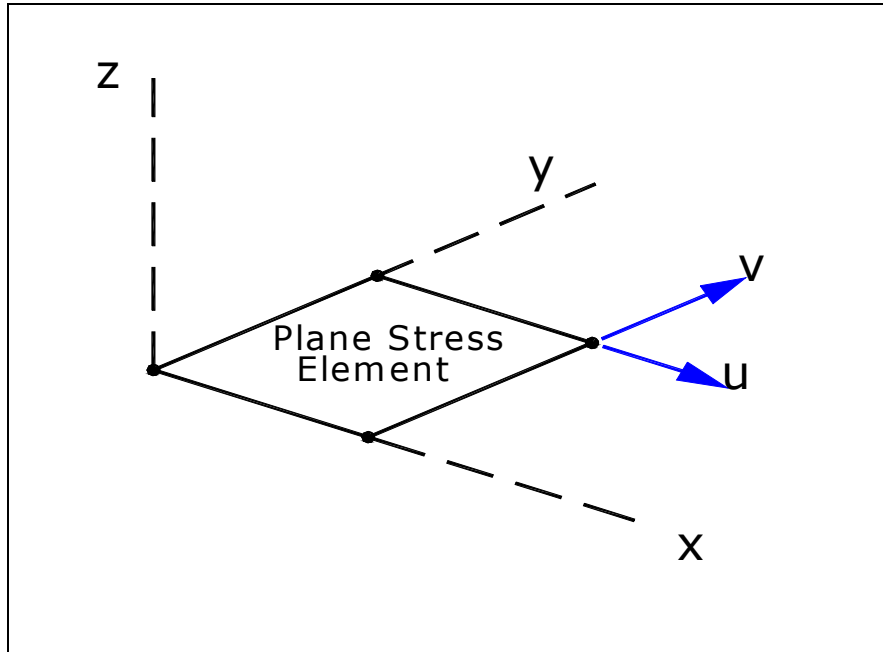


Figure 4.2: Degrees of Freedom per Node for the 4-Node Plane Stress Element

Strain components may be expressed in terms of displacements as

$$\begin{aligned} \varepsilon_x &= u_{,x} \\ \varepsilon_y &= v_{,y} \\ \gamma_{xy} &= u_{,y} + v_{,x} \end{aligned} \quad (4.2)$$

In matrix form, the strain and displacement components may be written as

$$\{\varepsilon\}_{3 \times 1} = \begin{Bmatrix} \varepsilon_x \\ \varepsilon_y \\ \gamma_{xy} \end{Bmatrix} \quad (4.3)$$

$$\{d\}^T = \{u_1 \quad v_1 \quad \dots \quad u_4 \quad v_4\}$$

Substitution of Equations (4.1) and (4.2) into (4.3) gives the expression for strains in terms of the nodal displacements in matrix form as

$$\varepsilon = \begin{Bmatrix} \varepsilon_x \\ \varepsilon_y \\ \gamma_{xy} \end{Bmatrix} = \begin{Bmatrix} u_{,x} \\ v_{,y} \\ u_{,y} + v_{,x} \end{Bmatrix} = \begin{Bmatrix} \sum N_{i,x} \cdot u_i \\ \sum N_{i,y} \cdot v_i \\ \sum N_{i,y} u_i + \sum N_{i,x} v_i \end{Bmatrix} \quad (4.4)$$

Derivatives of shape functions with respect to Cartesian coordinates are obtained by using the chain rule, applied through the Jacobian matrix, J , as described in section 4.2.3.1.

Thus, strain components in matrix form can be written as,

$$\{\varepsilon\}_{3 \times 1} = [B]_{M_{3 \times 8}} \cdot \{d\}_{8 \times 1} \quad (4.5)$$

where $[B]_M$ is a strain-displacement matrix.

$$[B]_M = \begin{bmatrix} N_{1,x} & 0 & N_{2,x} & 0 & N_{3,x} & 0 & N_{4,x} & 0 \\ 0 & N_{1,y} & 0 & N_{2,y} & 0 & N_{3,y} & 0 & N_{4,y} \\ N_{1,y} & N_{1,x} & N_{2,y} & N_{2,x} & N_{3,y} & N_{3,x} & N_{4,y} & N_{4,x} \end{bmatrix} \quad (4.6)$$

The stiffness matrix for the membrane portion of the element, K_M , is derived from strain energy, U , as follows,

$$U = \frac{1}{2} \cdot \int \{\sigma\}^T \cdot \{\varepsilon\} \cdot dV = \frac{1}{2} \cdot \int \{\varepsilon\}^T \cdot [E] \cdot \{\varepsilon\} \cdot dV \quad (4.7)$$

But, from Equation (4.4),

$$\{\varepsilon\}_{3 \times 1} = [B]_{M_{3 \times 8}} \cdot \{d\}_{8 \times 1} \quad (4.8)$$

Thus,

$$U = \frac{1}{2} \cdot \{d\}^T \cdot \left(\int [B]_M^T \cdot [E] \cdot [B]_M \cdot dV \right) \cdot \{d\} \quad (4.9)$$

Also, dV can be written as,

$$dV = t \cdot dA = t \cdot dx \cdot dy \quad (4.10)$$

where t is thickness of the element.

The Jacobian, $[J]$, relates length in natural coordinates (ξ, η) to length in cartesian co-ordinates (x, y),

$$dx \cdot dy = |J| \cdot d\xi \cdot d\eta \quad (4.11)$$

Strain energy, U , can then be written as,

$$U = \frac{1}{2} \cdot \{d\}^T \cdot \left(\int_{-1}^1 \int_{-1}^1 [B]_M^T \cdot [D]_M \cdot [B]_M \cdot |J| \cdot d\xi \cdot d\eta \right) \cdot \{d\} \quad (4.12)$$

where $[D]_M$ is the plane stress constitutive matrix in the global frame of reference,

In terms of material axes 1 and 2, $[D]_M'$ for orthotropic materials is given by,

$$[D]_M^V = t \cdot \begin{bmatrix} \frac{E_1}{(1-\nu_{12} \cdot \nu_{21})} & \frac{E_1 \cdot \nu_{21}}{(1-\nu_{12} \cdot \nu_{21})} & 0 \\ \frac{E_2 \cdot \nu_{12}}{(1-\nu_{12} \cdot \nu_{21})} & \frac{E_2}{(1-\nu_{12} \cdot \nu_{21})} & 0 \\ 0 & 0 & G_{12} \end{bmatrix} \quad (4.13)$$

Standard techniques for tensor transformation are used to transform $[D]_M^V$ in the material axes into $[D]_M$ in the local element axes, as follows.

$$[D]_M = [T]^T [D]_M^V [T] \quad (4.14)$$

where, $[T]$ is the strain transformation matrix, defined in *Section 4.2.3.2*.

Now, strain energy, U , can be written as,

$$U = \frac{1}{2} \cdot \{d\}^T \cdot [K]_M \cdot \{d\} \quad (4.15)$$

where, $[K]_M$ is the stiffness matrix, defined as:

$$[K]_M = \int_{-1}^1 \int_{-1}^1 [B]_M^T \cdot [D]_M \cdot [B]_M \cdot |J| \cdot d\xi \cdot d\eta \quad (4.16)$$

4.2.2 Formulation of the Plate Portion of the Element

Mindlin plate theory is used to derive the plate-bending portion of the element.

Assumptions made in Mindlin plate theory are as follows,

- i Displacements and rotations are small. Compared to thickness, transverse displacement is negligible.
- ii The material is linear and elastic.

- iii The normal stress component, σ_z , is considered negligible in comparison with σ_x , σ_y , and τ_{xy} .
- iv The middle surface is undeformed. That is, points on the middle surface ($z = 0$) move only in the z -direction as the plate deforms in bending.
- v A line that is straight and normal to the middle surface before loading is assumed to remain straight, but not necessarily normal to the middle surface after loading.

To formulate the stiffness matrix for the plate portion of the element, shape functions are developed from Lagrangian Polynomials. There are three degrees of freedom per node for plate bending, w , θ_x , and θ_y , as shown in *Figure 4.3*, and they may be expressed in terms of shape functions as follows:

$$\begin{aligned}
 w &= \sum_{i=1}^4 N_i \cdot w_i \\
 \theta_x &= \sum_{i=1}^4 N_i \cdot \theta_{xi} \\
 \theta_y &= \sum_{i=1}^4 N_i \cdot \theta_{yi}
 \end{aligned} \tag{4.17}$$

Plate element displacements, u , v , and w , in terms of nodal DOF, are given by,

$$\begin{aligned}
 v &= -z \cdot \theta_x \\
 u &= z \cdot \theta_y \\
 w &= w
 \end{aligned} \tag{4.18}$$

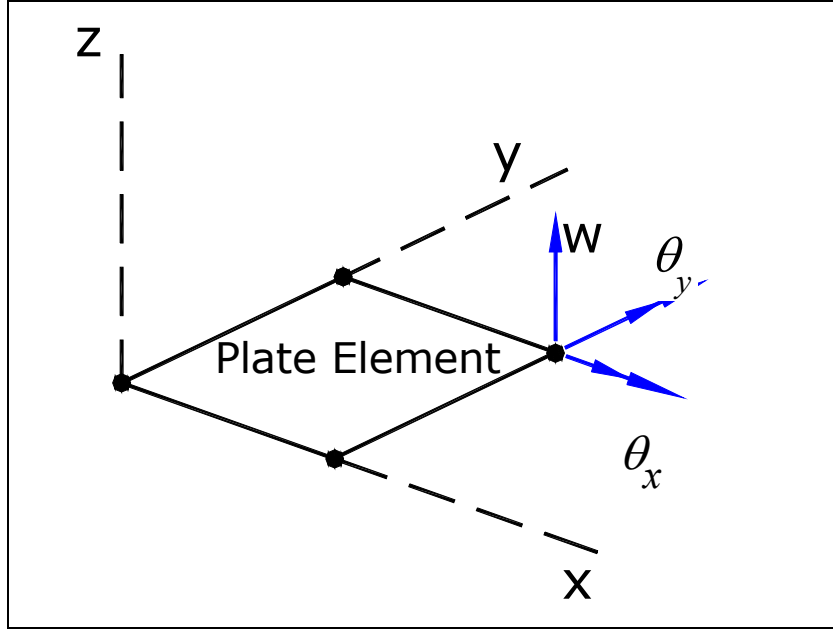


Figure 4.3: Degrees of Freedom per Node for the 4-Node Plate Element

The expressions for strain components may be given in terms of displacements as

$$\begin{aligned}
 \varepsilon_x &= u_{,x} = z \cdot \theta_{y,x} \\
 \varepsilon_y &= v_{,y} = -z \cdot \theta_{x,y} \\
 \gamma_{xy} &= u_{,y} + v_{,x} = z \cdot \theta_{y,y} - z \cdot \theta_{x,x} \\
 \gamma_{yz} &= w_{,y} + v_{,z} = w_{,y} - \theta_x \\
 \gamma_{zx} &= w_{,x} + u_{,z} = w_{,x} + \theta_y
 \end{aligned} \tag{4.19}$$

In matrix form, the strains and displacements may be written as

$$\{\varepsilon\} = \begin{Bmatrix} \varepsilon_x \\ \varepsilon_y \\ \gamma_{xy} \\ \gamma_{yz} \\ \gamma_{zx} \end{Bmatrix} \tag{4.20}$$

$$\{d\}^T = \{w_1 \quad \theta_{x_1} \quad \theta_{y_1} \quad \dots \quad w_4 \quad \theta_{x_4} \quad \theta_{y_4}\}$$

The expression for strain components in terms of the nodal displacements is given in matrix form as

$$\{\varepsilon\} = \begin{Bmatrix} \varepsilon_x \\ \varepsilon_y \\ \gamma_{xy} \\ \gamma_{yz} \\ \gamma_{zx} \end{Bmatrix} = \begin{Bmatrix} z \cdot \theta_{y,x} \\ -z \cdot \theta_{x,y} \\ z \cdot \theta_{y,y} - z \cdot \theta_{x,x} \\ w_{,y} - \theta_x \\ w_{,x} + \theta_y \end{Bmatrix} = \begin{Bmatrix} z \cdot \left(\sum_{i=1}^4 N_i \cdot \theta_{y_i} \right)_{,x} \\ -z \cdot \left(\sum_{i=1}^4 N_i \cdot \theta_{x_i} \right)_{,y} \\ z \cdot \left[- \left(\sum_{i=1}^4 N_i \cdot \theta_{x_i} \right)_{,x} + \left(\sum_{i=1}^4 N_i \cdot \theta_{y_i} \right)_{,y} \right] \\ \left(\sum_{i=1}^4 N_i \cdot w_i \right)_{,y} - \sum_{i=1}^4 N_i \cdot \theta_{x_i} \\ \left(\sum_{i=1}^4 N_i \cdot w_i \right)_{,x} + \sum_{i=1}^4 N_i \cdot \theta_{y_i} \end{Bmatrix} \quad (4.21)$$

Gradients with respect to Cartesian coordinates are obtained by using chain rule through the use of the Jacobian matrix, J , as described in *Section 4.2.3.1*. Thus, strains in matrix form can be written as:

$$\{\varepsilon\}_{5 \times 1} = [B]_{PLATE \ 5 \times 24} \cdot \{d\}_{24 \times 1} \quad (4.22)$$

where $[B]_{PLATE}$ is a strain-displacement matrix, defined as,

$$[B]_{PLATE} = \begin{bmatrix} 0 & 0 & zN_{1,x} & 0 & 0 & zN_{2,x} & 0 & 0 & zN_{3,x} & 0 & 0 & zN_{4,x} \\ 0 & -zN_{1,y} & 0 & 0 & -zN_{2,y} & 0 & 0 & -zN_{3,y} & 0 & 0 & -zN_{4,y} & 0 \\ 0 & -zN_{1,x} & zN_{1,y} & 0 & -zN_{2,x} & zN_{2,y} & 0 & -zN_{3,x} & zN_{3,y} & 0 & -zN_{4,x} & zN_{4,y} \\ N_{1,y} & -N_1 & 0 & N_{2,y} & -N_2 & 0 & N_{3,y} & -N_3 & 0 & N_{4,y} & -N_4 & 0 \\ N_{1,x} & 0 & N_1 & N_{2,x} & 0 & N_2 & N_{3,x} & 0 & N_3 & N_{4,x} & 0 & N_4 \end{bmatrix}$$

The $[B]_{PLATE}$ matrix may be divided into a transverse shear portion, $[B]_S$, and a bending portion, $[B]_B$.

$$[B]_{PLATE} = [B]_S + z \cdot [B]_B \quad (4.23)$$

where $[B]_S$ and $[B]_B$ are defined as,

$$[B]_S = \begin{bmatrix} 0 & 0 & 0 & 0 & 0 & 0 & 0 & 0 & 0 & 0 & 0 & 0 \\ 0 & 0 & 0 & 0 & 0 & 0 & 0 & 0 & 0 & 0 & 0 & 0 \\ 0 & 0 & 0 & 0 & 0 & 0 & 0 & 0 & 0 & 0 & 0 & 0 \\ N_{1,y} & -N_1 & 0 & N_{2,y} & -N_2 & 0 & N_{3,y} & -N_3 & 0 & N_{4,y} & -N_4 & 0 \\ N_{1,x} & 0 & N_1 & N_{2,x} & 0 & N_2 & N_{3,x} & 0 & N_3 & N_{4,x} & 0 & N_4 \end{bmatrix}$$

and

$$[B]_B = \begin{bmatrix} 0 & 0 & N_{1,x} & 0 & 0 & N_{2,x} & 0 & 0 & N_{3,x} & 0 & 0 & N_{4,x} \\ 0 & -N_{1,y} & 0 & 0 & -N_{2,y} & 0 & 0 & -N_{3,y} & 0 & 0 & -N_{4,y} & 0 \\ 0 & -N_{1,x} & N_{1,y} & 0 & -N_{2,x} & N_{2,y} & 0 & -N_{3,x} & N_{3,y} & 0 & -N_{4,x} & N_{4,y} \\ 0 & 0 & 0 & 0 & 0 & 0 & 0 & 0 & 0 & 0 & 0 & 0 \\ 0 & 0 & 0 & 0 & 0 & 0 & 0 & 0 & 0 & 0 & 0 & 0 \end{bmatrix}$$

Thus, the strain-displacement relationship is written as

$$\{\varepsilon\}_{5 \times 1} = ([B]_S + z \cdot [B]_B) \cdot \{d\}_{24 \times 1} \quad (4.24)$$

The stiffness matrix for the plate portion of the element, K_p , is derived from strain energy, U , as follows:

$$U = \frac{1}{2} \cdot \int \{\sigma\}^T \cdot \{\varepsilon\} \cdot dV = \frac{1}{2} \cdot \int \{\varepsilon\}^T \cdot [E] \cdot \{\varepsilon\} \cdot dV \quad (4.25)$$

But, from the strain-displacement relationship, $\{\varepsilon\} = [B]_{PLATE} \cdot \{d\}$

Hence, Equation (4.25) gives

$$U = \frac{1}{2} \cdot \{d\}^T \cdot \left(\int [B]_{PLATE}^T \cdot [E] \cdot [B]_{PLATE} \cdot dV \right) \cdot \{d\} \quad (4.26)$$

$$U = \frac{1}{2} \cdot \{d\}^T \cdot [K_P] \cdot \{d\}$$

where,

$$[K]_P = \iiint \left([B]_{PLATE}^T \cdot [E] \cdot [B]_{PLATE} \right) \cdot dx \cdot dy \cdot dz \quad (4.27)$$

Substitution of Equation (4.23) into (4.27) gives,

$$[K]_P = \iiint \left([B]_S + z \cdot [B]_B \right)^T \cdot [E] \cdot \left([B]_S + z \cdot [B]_B \right) \cdot dx \cdot dy \cdot dz \quad (4.28)$$

In the above Equation, [E] is the elasticity matrix and it is given by

$$[E]_{5 \times 5} = \begin{bmatrix} E_{PS} & 0 \\ 0 & E_{TS} \end{bmatrix} \quad (4.29)$$

where, E_{PS} is for the plane stress portion and E_{TS} is for the transverse shear portion.

In terms of Material Axes 1 and 2, $[E_{PS}]$ and $[E_{TS}]$ for orthotropic materials is given by

$$[E_{PS}]_{3 \times 3} = \frac{E}{1 - \nu^2} \cdot \begin{bmatrix} \frac{E_1}{(1 - \nu_{12} \cdot \nu_{21})} & \frac{E_1 \cdot \nu_{21}}{(1 - \nu_{12} \cdot \nu_{21})} & 0 \\ \frac{E_2 \cdot \nu_{12}}{(1 - \nu_{12} \cdot \nu_{21})} & \frac{E_2}{(1 - \nu_{12} \cdot \nu_{21})} & 0 \\ 0 & 0 & G_{12} \end{bmatrix} \quad (4.30)$$

$$[E_{TS}] = \begin{bmatrix} \frac{G_{23}}{1.2} & 0 \\ 0 & \frac{G_{31}}{1.2} \end{bmatrix} \quad (4.31)$$

Standard techniques for tensor transformation are used to transform $[E_{PS}]$ and $[E_{TS}]$ in the material axes into $[E_{PS}]$ and $[E_{TS}]$ in the local element axes, as follows.

$$[E_{PS}] = [T_{PS}]^T \cdot [E_{PS}] \cdot [T_{PS}] \quad (4.32)$$

$$[E_{TS}] = [T_{TS}]^T \cdot [E_{TS}] \cdot [T_{TS}] \quad (4.33)$$

where $[T_{PS}]$ and $[T_{TS}]$ are given in *Section 4.2.3.2*.

The factor of 1.2 is inserted to give equivalent strain energy for the assumption of constant shear strain instead of the actual parabolic distribution.

The stiffness matrix for the plate portion of the element is decoupled into bending, $[K]_B$, and transverse shear, $[K]_S$, portions.

$$[K]_P = \iiint ([B]_S^T \cdot [E]_{TS} \cdot [B]_S \cdot dx \cdot dy \cdot dz) + \iiint z^2 \cdot ([B]_B^T \cdot [E]_{PS} \cdot [B]_B \cdot dx \cdot dy \cdot dz) \quad (4.34)$$

For a homogenous plate, integration in the z – direction can be performed analytically.

$$\int_{-t/2}^{t/2} z^2 \cdot dz = \frac{t^3}{12} \quad (4.35)$$

Substituting Equation (4.35) into (4.34) results in following:

$$[K]_P = \iint \left([B]_S^T \cdot [D]_S \cdot [B]_S \cdot dx \cdot dy \right) + \iint \left([B]_B^T \cdot [D]_B \cdot [B]_B \cdot dx \cdot dy \right) \quad (4.36)$$

where $[D]_B$ and $[D]_S$ are given by:

$$[D]_B = \left(\frac{t^3}{12} \right) \cdot [E_{PS}] \quad (4.37)$$

and

$$[D]_S = t \cdot [E_{TS}] \quad (4.38)$$

The Jacobian, $[J]$, relates length in natural (ξ, η) coordinates to length in cartesian coordinates (x, y) ,

$$dx \cdot dy = \det J \cdot d\xi \cdot d\eta \quad (4.39)$$

Thus, in isoparametric natural co-ordinates (ξ, η) , Equation (4.34) can be written as,

$$[K]_P = \int_{-1}^1 \int_{-1}^1 \left([B]_S^T \cdot [D]_S \cdot [B]_S \cdot \det J \cdot d\xi \cdot d\eta \right) + \int_{-1}^1 \int_{-1}^1 \left([B]_B^T \cdot [D]_B \cdot [B]_B \cdot \det J \cdot d\xi \cdot d\eta \right)$$

where $\det J$ is the determinant of the Jacobian.

$$\begin{aligned}
[K]_S &= \int_{-1}^1 \int_{-1}^1 \left([B]_S^T \cdot [D]_S \cdot [B]_S \cdot \det J \cdot d\xi \cdot d\eta \right) \\
[K]_B &= \int_{-1}^1 \int_{-1}^1 \left([B]_B^T \cdot [D]_B \cdot [B]_B \cdot \det J \cdot d\xi \cdot d\eta \right)
\end{aligned} \tag{4.40}$$

Thus,

$$[K]_P = [K]_S + [K]_B \tag{4.41}$$

4.2.2.1 Shear Locking of Plate Element

When a Mindlin plate element becomes thin, it becomes extremely stiff to the point of “locking”. This is a well-known phenomenon (Cook, et al. 2002), and it is caused by an unreasonable growth of strain energy from transverse shear strain as the element thickness becomes small. Because w and θ degrees of freedom are interpolated by polynomials of the same order, terms of $w_{,x}$ and θ do not match. Thus, as the element becomes thin and the transverse shear strain terms, such as $(w_{,x} - \theta)^2$, should approach zero, they cannot due to spurious quadratic terms. By using reduced integration, the quadratic terms vanish. Thus, reduced integration prevents locking, but it can introduce zero-energy modes (i.e., modes of element deformation for which there is no strain energy).

A standard technique (Cook, et al., 2002) to remove shear locking and unwanted zero-energy modes is to use selective reduced integration. As K_S and K_B are calculated separately, a different order of integration is used for K_S (1 x 1 – reduced integration) and K_B (2 x 2 – full integration).

4.2.3 Formulation of Shell Element

The final stiffness matrix for the shell element $[K]_{\text{SHELL}}$ is developed as a combination of stiffness coefficients for the plate element, $[K]_P$, with the stiffness coefficients for the plane stress element, $[K]_M$. With the combination of plane stress and plate bending stiffness to form the shell element, no stiffness is provided for rotation degrees of freedom about the local z -axis (the so-called “drilling” degrees of freedom). This lack of stiffness leads to a singular system stiffness matrix for coplanar elements if not corrected. A standard remedy is to insert a small stiffness, K_0 , for the “drilling” degrees of freedom (Zienkiewicz and Taylor, 1991) as shown below.

$$[K]_O = \alpha \cdot E \cdot V \cdot \begin{bmatrix} 1 & -0.33 & -0.33 & -0.33 \\ -0.33 & 1 & -0.33 & -0.33 \\ -0.33 & -0.33 & 1 & -0.33 \\ -0.33 & -0.33 & -0.33 & 1 \end{bmatrix} \quad (4.42)$$

where,

α = an arbitrary parameter, chosen to be 0.3.

E = Elastic Modulus of the material, and

V = Element Volume

The final stiffness matrix for the shell element, $[K]_{\text{SHELL}}$, shown in *Figure 4.4*, is given by,

$$[K]_{\text{SHELL}(24 \times 24)} = [K]_{P(12 \times 12)} + [K]_{M(8 \times 8)} + [K]_{O(4 \times 4)} \quad (4.43)$$

The assembled element shell stiffness matrix, $[K]_{SHELL}$, is in local coordinates and must be transformed into global coordinates before assembling into the system, as described in *Section 4.2.3.3*.

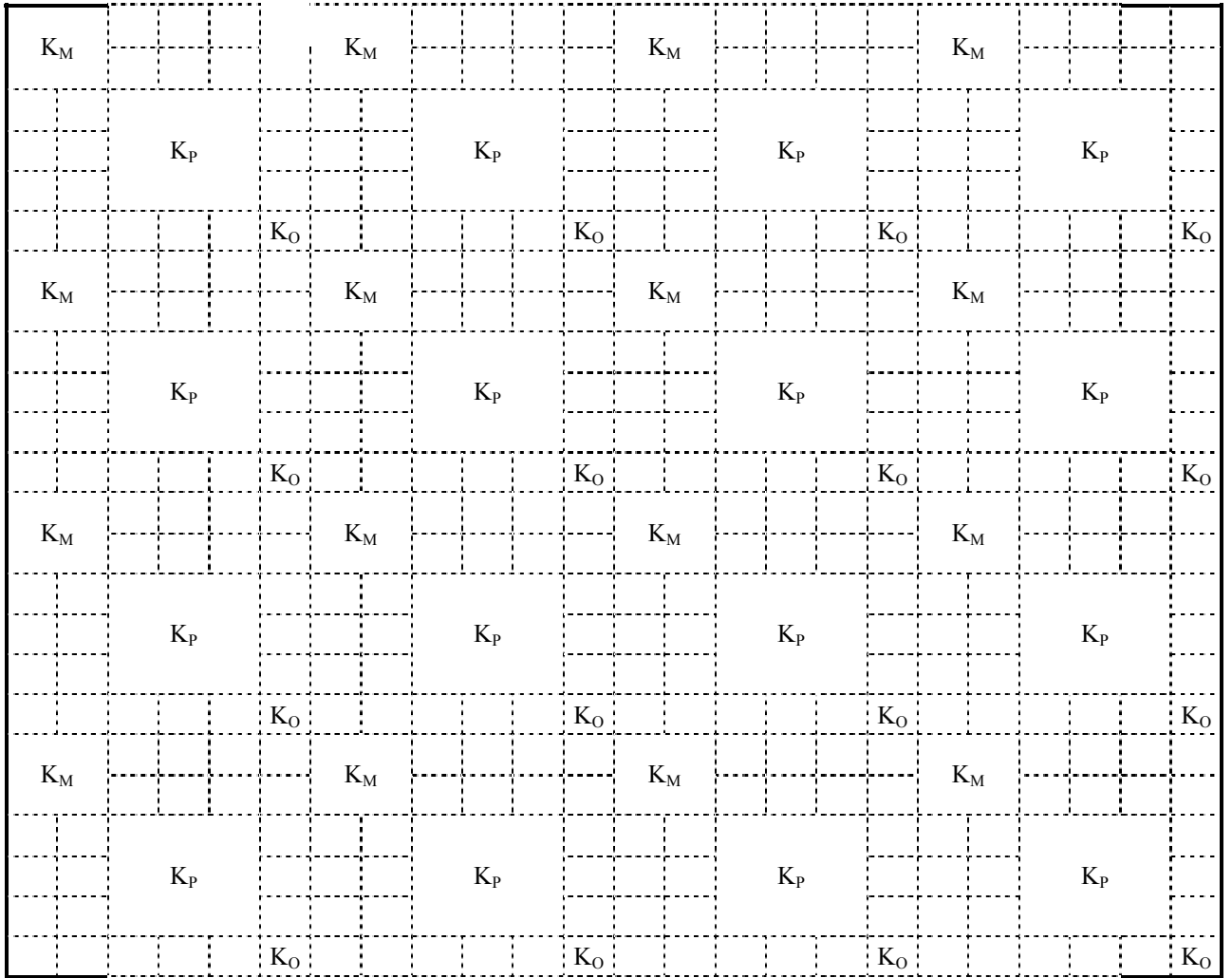


Figure 4.4: Stiffness Matrix for Shell Element, $[K]_{SHELL}$

4.2.3.1 Transformation from Isoparametric Natural Coordinates (ξ, η) to Cartesian Coordinates (x, y)

Lagrangian polynomials are standard two dimensional shape functions in terms of isoparametric natural coordinates.

$$\begin{aligned}
N_1 &= \frac{1}{4}(1-\eta)(1-\xi) \\
N_2 &= \frac{1}{4}(1-\eta)(1+\xi) \\
N_3 &= \frac{1}{4}(1+\eta)(1+\xi) \\
N_4 &= \frac{1}{4}(1+\eta)(1-\xi)
\end{aligned} \tag{4.44}$$

Natural coordinates are related to Cartesian coordinates by a mapping. Gradients with respect to Cartesian coordinates ($N_{,x}$ and $N_{,y}$) are obtained by using the chain rule and through the use of the Jacobian matrix, $[J]$ (Cook, et al., 2002).

Using the chain rule, $N_{,x}$ and $N_{,y}$ can be written as,

$$N_{,x} = \frac{\partial N}{\partial x} = \frac{\partial \xi}{\partial x} \cdot \frac{\partial N}{\partial \xi} + \frac{\partial \eta}{\partial x} \cdot \frac{\partial N}{\partial \eta} \tag{4.45}$$

$$N_{,y} = \frac{\partial N}{\partial y} = \frac{\partial \xi}{\partial y} \cdot \frac{\partial N}{\partial \xi} + \frac{\partial \eta}{\partial y} \cdot \frac{\partial N}{\partial \eta}$$

In matrix form,

$$\begin{Bmatrix} N_{,x} \\ N_{,y} \end{Bmatrix} = \begin{bmatrix} \xi_{,x} & \eta_{,x} \\ \xi_{,y} & \eta_{,y} \end{bmatrix} \cdot \begin{Bmatrix} N_{,\xi} \\ N_{,\eta} \end{Bmatrix} \tag{4.46}$$

As this relationship is not available, the inverse may be written:

$$\begin{Bmatrix} N_{,\xi} \\ N_{,\eta} \end{Bmatrix} = \begin{bmatrix} x_{,\xi} & y_{,\xi} \\ x_{,\eta} & y_{,\eta} \end{bmatrix} \cdot \begin{Bmatrix} N_{,x} \\ N_{,y} \end{Bmatrix} \tag{4.47}$$

The Jacobian, $[J]$, is defined as:

$$[J]_{2 \times 2} = \begin{bmatrix} x_{,\xi} & y_{,\xi} \\ x_{,\eta} & y_{,\eta} \end{bmatrix} = \begin{bmatrix} N_{1,\xi} & N_{2,\xi} & N_{3,\xi} & N_{4,\xi} \\ N_{1,\eta} & N_{2,\eta} & N_{3,\eta} & N_{4,\eta} \end{bmatrix} \cdot \begin{bmatrix} x_1 & y_1 \\ x_2 & y_2 \\ x_3 & y_3 \\ x_4 & y_4 \end{bmatrix} \quad (4.48)$$

where x_i, y_i are the co-ordinates of node i .

Then,

$$\begin{Bmatrix} N_{,x} \\ N_{,y} \end{Bmatrix} = [J]_{2 \times 2}^{-1} \cdot \begin{Bmatrix} N_{,\xi} \\ N_{,\eta} \end{Bmatrix} \quad (4.49)$$

4.2.3.2 Orthotropic Material Transformation

The matrix of elastic constants for an orthotropic material, when its Material Axes 1 and 2, as shown in Figure 4.5, do not coincide with its local axes x and y , needs to be rotated from material axes to local axes. Material axes are oriented at an angle θ with the local x and y -axes. Angle θ is measured counterclockwise from the x -axis to the 1-axis.

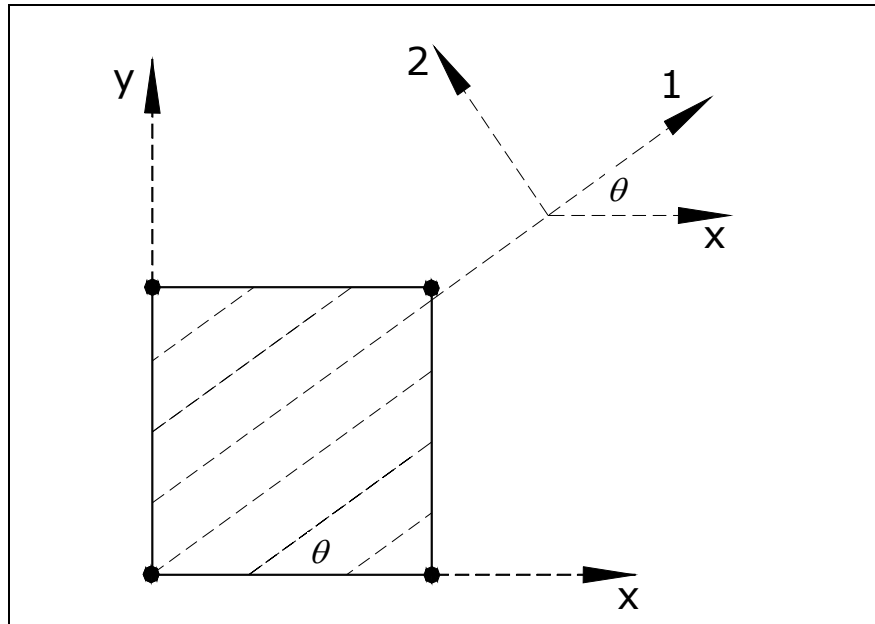


Figure 4.5: Orientation of Orthotropic Material Axes

A strain transformation matrix applicable to the strain components of both plane stress, $[T]$ and bending portions, $[T_{PS}]$, (Belegundu and Chandrupatla, 1997) is given by

$$[T]_{3 \times 3} = [T_{PS}]_{3 \times 3} = \begin{bmatrix} \cos^2 \theta & \sin^2 \theta & \sin \theta \cdot \cos \theta \\ \sin^2 \theta & \cos^2 \theta & -\sin \theta \cdot \cos \theta \\ -2 \cdot \sin \theta \cdot \cos \theta & 2 \cdot \sin \theta \cdot \cos \theta & \cos^2 \theta - \sin^2 \theta \end{bmatrix} \quad (4.50)$$

Similarly, the strain transformation matrix, $[T_{TS}]_{2 \times 2}$ for the transverse shear component is given by

$$[T_{TS}]_{2 \times 2} = \begin{bmatrix} \cos \theta & \sin \theta \\ -\sin \theta & \cos \theta \end{bmatrix} \quad (4.51)$$

4.2.3.3 Element Transformation from Local Coordinates (x, y) to Global Coordinates (X, Y)

The assembled shell stiffness matrix, $[K]_{\text{SHELL}}$, is derived in local co-ordinates and must be transformed into global co-ordinates, $[K]_{\text{GLOBAL}}$ by using rotation matrix $[R]$. To derive the rotation matrix, local axes must be defined, in accordance with the following convention.

The local x -axis is always assumed to coincide with the side containing Nodes 1 and 2. The unit vector along that side is designated as \hat{V}_x . The orientation of the local z -axis, \hat{V}_z , is computed by taking the cross product of the unit vectors defining the local x -axis, \hat{V}_x , and the unit vector along Nodes 1 and 4, \hat{V}_0 .

$$\hat{V}_z = \hat{V}_x \times \hat{V}_0$$

Then, the orientation of the local y -axis, \hat{V}_y , is computed by taking the cross product of the unit vectors defining the local axis, z , \hat{V}_z , and x -axis, \hat{V}_x .

$$\hat{V}_y = \hat{V}_z \times \hat{V}_x$$

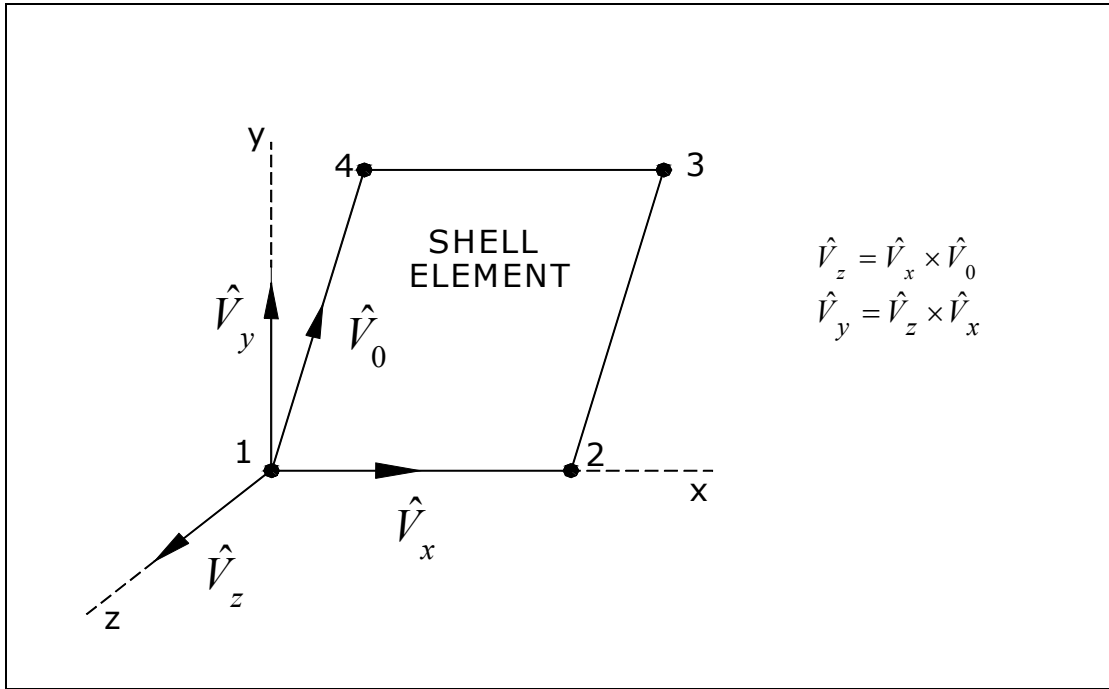


Figure 4.6: Orientation of Local Axes

Once the orientations of the three local axes are known, the direction cosines l , m , and n for each direction are defined. They are then formed into a rotation matrix, $[R]$, as shown below,

$$[R] = \begin{bmatrix} l_1 & m_1 & n_1 \\ l_2 & m_2 & n_2 \\ l_3 & m_3 & n_3 \end{bmatrix} \quad (4.52)$$

where Subscripts 1, 2, and 3 define are the direction cosines for the local x, y, and z-axes, respectively.

Then, the shell stiffness matrix in global coordinates is given by

$$[K]_{GLOBAL(24 \times 24)} = [R]_{24 \times 24}^T \cdot [K]_{SHELL(24 \times 24)} \cdot [R]_{24 \times 24} \quad (4.53)$$

5. INTERFACE ELEMENT FORMULATION

5.1 Introduction

The interface element, as discussed earlier, is used to model the interface between walls, walls and floors, and walls and the roof assembly in a manufactured home. The interface element thus allows the determination of forces between structural elements of the manufactured home and it is also used to include the effects of joint flexibility. The floor, walls, ceiling, and roof are modeled using shell elements. *Figure 5.1* shows the layout of the interface element and how the interface elements are used along with shell elements.

5.2 Element Geometry

The interface element is a four-node line element and it connects the sides of adjacent shell or beam elements. As each side of a shell element is defined by two nodes, the connector element is defined by four nodes, as shown in *Figure 5.1*.

Although the element is shown as two lines, it occupies only a single line in space. Stiffness is smeared, with units of stiffness per length, having components that pertain to four degrees of relative displacement between the lines. The smeared spring provides the resistance between relative deflections and rotation of the two halves of the element, as shown in *Figure 5.1*. This figure shows only springs in the local x direction, but there are also similar springs restraining relative displacement in local y and z directions and relative rotation about the y -axis, respectively.

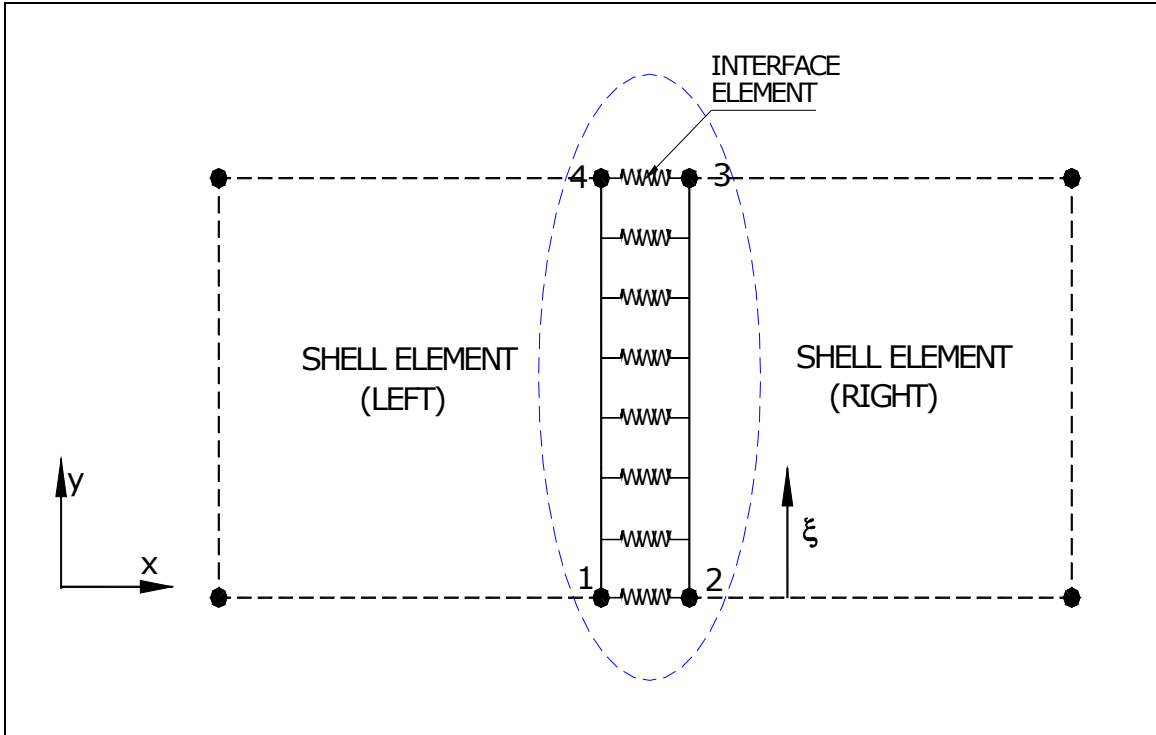


Figure 5.1: Interface Element Geometry

5.3 Element Formulation

The element is developed in a local coordinate system. There are four active degrees of freedom (DOF) at each node. These are displacements in the local x , y , and z directions and a rotation about the local y -axis, u , v , w , and θ_y , respectively. DOF for the interface element are shown in *Figure 5.2*. To make the interface element compatible with similar DOF's in the shell element, two dummy DOF's, the rotation about the x and z -axes, are also considered. The interface element provides no resistance to these DOF's. Rather, resistance against these two rotations is provided by the attached shell elements or any other attached element.

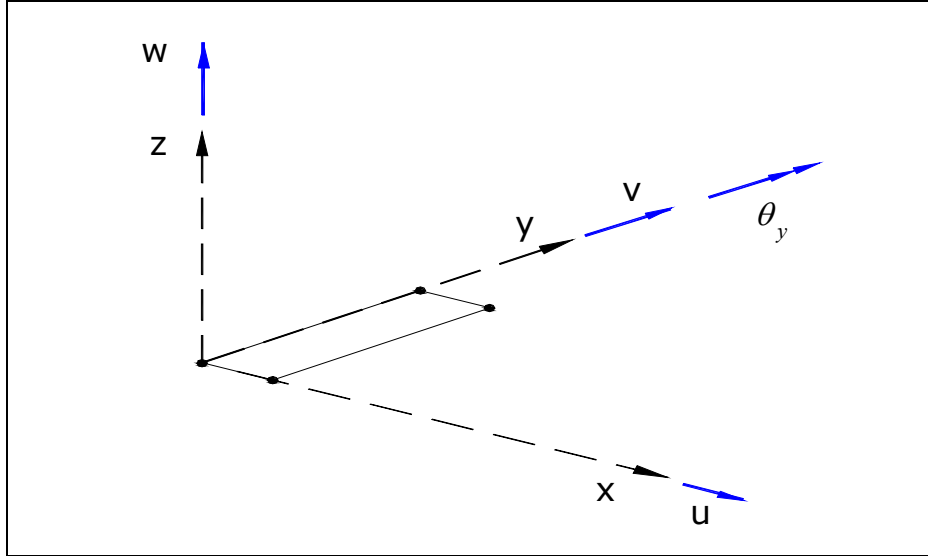


Figure 5.2: Degrees of Freedom per Node for an Interface Element

To formulate the stiffness matrix for the interface element, the shape functions (Lagrangian Polynomials) that define continuous displacements in terms of the displacements at each node are developed. These functions must be compatible with the shape functions for the shell element and other elements used along with the interface element. Lagrangian polynomials are standard linear shape functions in terms of isoparametric natural coordinates and are given by:

$$\begin{aligned} N_1 &= \frac{1}{2}(1-\xi) \\ N_2 &= \frac{1}{2}(1+\xi) \end{aligned} \quad (5.1)$$

The two shell elements to be connected are designated as Shell Element Left (L) and Shell Element Right (R) as shown in *Figure 5.1*. Displacement in the global x -direction on the respective edges is given in terms of linear shape functions as

$$U_L(\xi) = N_1(\xi) \cdot u_1 + N_2(\xi) \cdot u_4 \quad (5.2)$$

$$U_R(\xi) = N_1(\xi) \cdot u_2 + N_2(\xi) \cdot u_3$$

Then, the relative displacement (stretch) in the global x -direction, ΔU , between the left and right sides is given as

$$\begin{aligned} \Delta U(\xi) &= U_L(\xi) - U_R(\xi) \\ &= N_1 \cdot u_1 + N_2 \cdot u_4 - N_1 \cdot u_2 - N_2 \cdot u_3 \\ &= N_1 \cdot u_1 - N_1 \cdot u_2 - N_2 \cdot u_3 + N_2 \cdot u_4 \\ &= [N_1 \quad -N_1 \quad -N_2 \quad N_2] \cdot \begin{Bmatrix} u_1 \\ u_2 \\ u_3 \\ u_4 \end{Bmatrix} \end{aligned} \quad (5.3)$$

Similarly, the relative displacement in the global y and z -directions and rotation, ΔV , ΔW , and $\Delta \theta$ between the left and right sides are given as

$$\begin{aligned} \Delta V(\xi) &= [N_1 \quad -N_1 \quad -N_2 \quad N_2] \cdot \begin{Bmatrix} v_1 \\ v_2 \\ v_3 \\ v_4 \end{Bmatrix} \\ \Delta W(\xi) &= [N_1 \quad -N_1 \quad -N_2 \quad N_2] \cdot \begin{Bmatrix} w_1 \\ w_2 \\ w_3 \\ w_4 \end{Bmatrix} \\ \Delta \theta(\xi) &= [N_1 \quad -N_1 \quad -N_2 \quad N_2] \cdot \begin{Bmatrix} \theta_1 \\ \theta_2 \\ \theta_3 \\ \theta_4 \end{Bmatrix} \end{aligned} \quad (5.4)$$

The expression for stretch components in terms of the displacement components can be written as

$$\begin{aligned}
 \delta_x &= \Delta U(\xi) \\
 \delta_y &= \Delta V(\xi) \\
 \delta_z &= \Delta W(\xi) \\
 \delta_\theta &= \Delta \theta(\xi)
 \end{aligned} \tag{5.5}$$

In matrix form, the stretch and displacement components may be written as

$$\{\delta\}_{6 \times 1} = \begin{Bmatrix} \Delta U(\xi) \\ \Delta V(\xi) \\ \Delta W(\xi) \\ \Delta \theta_x(\xi) \\ \Delta \theta_y(\xi) \\ \Delta \theta_z(\xi) \end{Bmatrix} \tag{5.6}$$

$$\{d\}_{24 \times 1}^T = \left\{ u_1 \quad v_1 \quad w_1 \quad \theta_{x_1} \quad \theta_{y_1} \quad \theta_{z_1} \quad \dots \quad u_4 \quad v_4 \quad w_4 \quad \theta_{x_4} \quad \theta_{y_4} \quad \theta_{z_4} \right\}$$

Substituting Equations (5.3) and (5.4) into Equation (5.6), the stretch is obtained in terms of the nodal displacements in matrix form as

$$\{\delta\}_{6 \times 1} = [B]_{6 \times 24} \cdot \{d\}_{24 \times 1} \tag{5.7}$$

where [B] is the stretch-displacement matrix, and it is given as,

$$B_{6 \times 24} = \begin{bmatrix} N_1 & 0 & 0 & 0 & 0 & 0 & -N_1 & 0 & 0 & 0 & 0 & 0 & -N_2 & 0 & 0 & 0 & 0 & 0 & N_2 & 0 & 0 & 0 & 0 & 0 \\ 0 & N_1 & 0 & 0 & 0 & 0 & 0 & -N_1 & 0 & 0 & 0 & 0 & 0 & -N_2 & 0 & 0 & 0 & 0 & 0 & N_2 & 0 & 0 & 0 & 0 \\ 0 & 0 & N_1 & 0 & 0 & 0 & 0 & 0 & -N_1 & 0 & 0 & 0 & 0 & 0 & -N_2 & 0 & 0 & 0 & 0 & 0 & N_2 & 0 & 0 & 0 \\ 0 & 0 & 0 & N_1 & 0 & 0 & 0 & 0 & 0 & -N_1 & 0 & 0 & 0 & 0 & 0 & -N_2 & 0 & 0 & 0 & 0 & 0 & 0 & N_2 & 0 \\ 0 & 0 & 0 & 0 & N_1 & 0 & 0 & 0 & 0 & 0 & -N_1 & 0 & 0 & 0 & 0 & 0 & -N_2 & 0 & 0 & 0 & 0 & 0 & 0 & N_2 \\ 0 & 0 & 0 & 0 & 0 & N_1 & 0 & 0 & 0 & 0 & 0 & -N_1 & 0 & 0 & 0 & 0 & 0 & -N_2 & 0 & 0 & 0 & 0 & 0 & N_2 \end{bmatrix}$$

Now that the relationship between stretch and displacement has been fully developed, the stiffness relationships can be established. Traction, f , between the two halves of the element is given by

$$f = [k] \cdot \{\delta\} \quad (5.8)$$

where $[k]$ is the spring stiffness matrix and, in local coordinates, it can be written as

$$[k]_{LOCAL} = \begin{bmatrix} k_x & 0 & 0 & 0 \\ 0 & k_y & 0 & 0 \\ 0 & 0 & k_z & 0 \\ 0 & 0 & 0 & k_{\theta_y} \end{bmatrix} \quad (5.9)$$

where k_x , k_y , k_z , and k_{θ_y} are the spring stiffness values for a unit length of interface (i.e., force/length/length). As this matrix is diagonal, the values of the spring coefficients have no effect on one another. For instance, the stiffness resisting the local x -relative displacement has no effect on the resistance to local y -relative displacement.

5.3.1 Stiffness Matrix Derivation

Now that all the necessary relationships have been defined, the stiffness matrix for the *interface* element, $[K]$, is derived from strain energy, U , as follows,

$$U = \frac{1}{2} \int \{f\}^T \cdot \{\delta\} = \frac{1}{2} \int ([k]_{GLOBAL} \cdot \{\delta\})^T \cdot \{\delta\} = \frac{1}{2} \int \{\delta\}^T \cdot [k]_{GLOBAL} \cdot \{\delta\} \quad (5.10)$$

But, from the stretch-displacement relationship, $\{\delta\} = [B] \cdot \{d\}$

Thus, strain energy, U, is

$$U = \frac{1}{2} \cdot \{d\}^T \cdot \left(\int [B]^T \cdot [k]_{GLOBAL} \cdot [B] \cdot dS \right) \cdot \{d\} \quad (5.11)$$

Strain energy, U, can then be written as,

$$U = \frac{1}{2} \cdot \{d\}^T \cdot [K] \cdot \{d\} \quad (5.12)$$

where $[K]$ is the global stiffness matrix for the element and it is given by,

$$[K]_{24 \times 24} = \int [B]_{24 \times 6}^T \cdot [k]_{GLOBAL} \cdot [B]_{6 \times 24} \cdot dS \quad (5.13)$$

where $[k]_{GLOBAL}$ is the spring stiffness matrix in the global coordinates. The spring stiffness matrix in the local coordinates, $[k]_{LOCAL}$, is transformed to $[k]_{GLOBAL}$ using the rotation matrix, $[R]$ as described in *Section 5.3.1*.

$$[k]_{GLOBAL} = [R]^T \cdot [k]_{LOCAL} \cdot [R] \quad (5.14)$$

The Jacobian, $[J]$, generally relates length in natural (ξ, η) coordinates to length in cartesian coordinates (x, y). Along a line, the differential length, $dS = \sqrt{J_{11}^2 + J_{12}^2 + J_{13}^2} \cdot d\xi$. Then,

$$[K]_{24 \times 24} = \int_{-1}^1 [B]^T \cdot [k]_{GLOBAL} \cdot [B] \cdot \sqrt{J_{11}^2 + J_{12}^2 + J_{13}^2} \cdot d\xi \quad (5.15)$$

where J_{11} , J_{22} , and J_{33} can be written as,

$$\begin{bmatrix} J_{11} & J_{12} & J_{13} \end{bmatrix} = \begin{bmatrix} N_{1,\xi} & N_{2,\xi} \end{bmatrix} \cdot \begin{bmatrix} x_1 & y_1 & z_1 \\ x_2 & y_2 & z_2 \end{bmatrix} \quad (5.16)$$

Finally, force per unit length at the nodes, $\{f\}$, that is traction between the two halves can be written as,

$$\begin{aligned} \{f\}_{LOCAL(4X1)} &= [k]_{LOCAL(4X4)} \cdot [R]_{4x6} \cdot \{\delta\} \\ \{f\}_{LOCAL(4X1)} &= [k]_{LOCAL(4X4)} \cdot [R]_{4x6} \cdot [B]_{6X24} \cdot \{d\}_{GLOBAL24X1} \end{aligned} \quad (5.17)$$

Integration is carried out numerically, using Gauss quadrature and two integration sampling points per element.

5.3.2 Element Transformation

The spring stiffness matrix $[k]$ is given by the user. In local coordinates, it can be written as:

$$[k]_{LOCAL} = \begin{bmatrix} k_x & 0 & 0 & 0 \\ 0 & k_y & 0 & 0 \\ 0 & 0 & k_z & 0 \\ 0 & 0 & 0 & k_{\theta_y} \end{bmatrix}$$

where k_x , k_y , k_z , and, k_{θ_y} are the spring stiffness coefficients for a unit length of interface, that is, in units of force/length/length. To compute the stiffness matrix for the interface element, this spring stiffness matrix is transformed from local to global co-ordinates, using a matrix of direction cosines.

The local y -axis is always assumed to lie along the length of the element and the local x -axis is defined normal to this axis (i.e., stretch direction) in the local x - y plane, as

specified by the user. The orientation of the local z-axis, \hat{V}_z , is computed by taking the cross product of the unit vector defining the local x-axis, \hat{V}_x , and unit vector defining the local y-axis, \hat{V}_y .

$$\hat{V}_z = \hat{V}_x \times \hat{V}_y$$

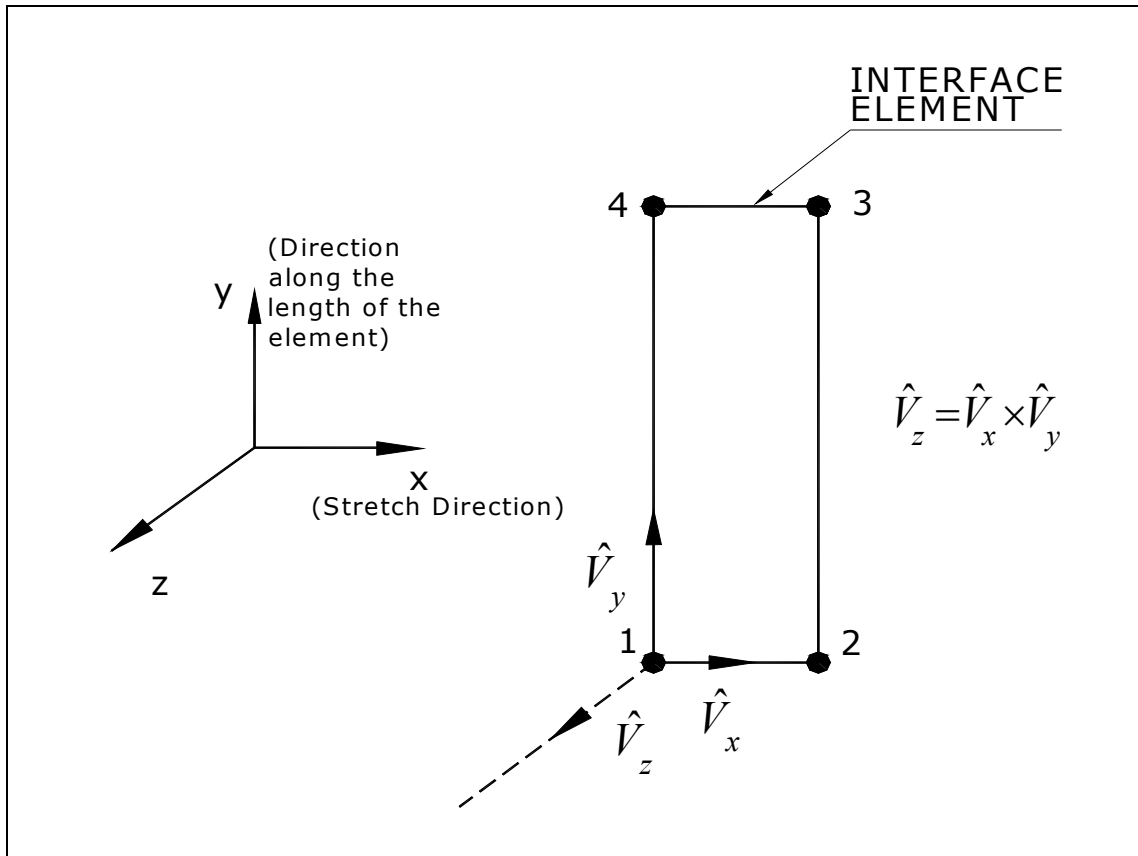


Figure 5.3: Orientation of the Local Axes

The orientations of the three local axes define the direction cosine. They are then formed into a rotation matrix, $[R]$, as shown below,

$$[R]_{4 \times 6} = \begin{bmatrix} l_1 & m_1 & n_1 & 0 & 0 & 0 \\ l_2 & m_2 & n_2 & 0 & 0 & 0 \\ l_3 & m_3 & n_3 & 0 & 0 & 0 \\ 0 & 0 & 0 & l_2 & m_2 & n_2 \end{bmatrix} \quad (5.18)$$

where l_1 , l_2 , and l_3 are the direction cosines for the local x and global X , Y , and Z -axes respectively. Similarly, the values of m and n are defined as the direction cosines for the local y and z -axes with respect to the global axes.

6. SHEAR WALLS

6.1 Introduction

The main purpose of shear walls is to provide resistance to lateral forces imposed by wind and seismic loadings. A shear wall has three main components: framing (plates and studs), sheathing (plywood or oriented strand board), and fasteners (nails or staples), which connect the sheathing to the framing. Studs resist the vertical load and they are connected to the bottom plate and the top plate to complete the frame. The framing provides the majority of the transverse bending resistance while contributing little to in-plane shear stiffness. The sheathing provides shear strength and stiffness, which is also highly dependent upon the fasteners that connect it to the frame.

6.2 Full-Scale Shear Wall Testing (NIST)

6.2.1 Introduction

The National Institute of Standards and Technology (NIST) tested four shear wall specimens, constructed with different configurations. Three of them were chosen to represent different sections of exterior walls, and the fourth one represents an interior wall of a typical manufactured home. The main purpose of these tests was to observe the behavior of shear walls under extreme loads. Results obtained from these tests were used to verify and calibrate the finite element modeling techniques described previously. In addition, the data provides useful insights into the stiffness and strength of shear walls with different configurations. Test configurations conformed to ASTM E564-00 standards. The following sections describe the test specimens and configurations.

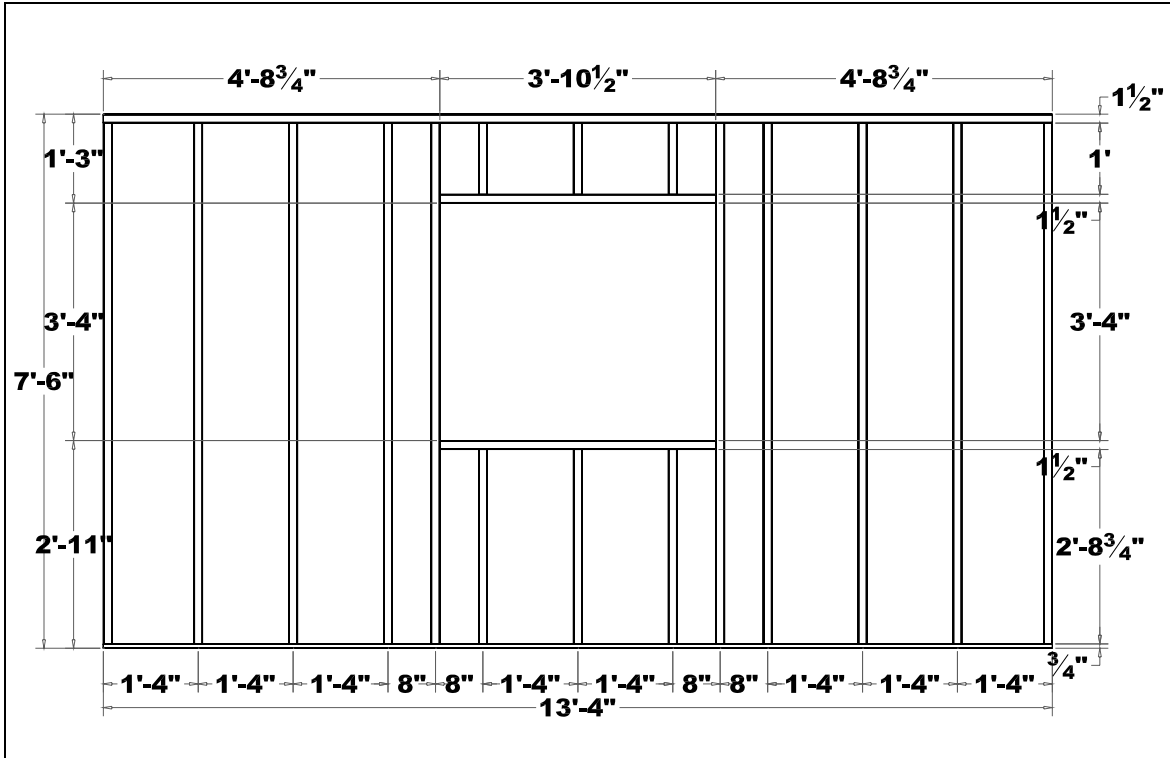


Figure 6.3: Framing Dimensions of the Wall Specimens with a Window Opening

All four specimens had 5/16 inch thick gypsum board cladding on the inside face. The outer face of the gypsum board had a layer of decorative wallpaper applied to it, and the gypsum board was attached to the studs with both glue and staples. The glue appeared to have been applied to the full length of the framing members. The staples were located approximately every 6 inches along the edges of the gypsum board, and every 12 inches along the interior studs. Additional staples were placed near the corners of each panel. The typical edge dimensions of the wall are shown in *Figure 6.4*.

The first three specimens also had a layer of 7/16 inches thick oriented strand board (OSB) cladding on the outside face, as shown in *Figure 6.4*. The OSB had an American Plywood Association (APA) rating for roofs, walls, and floors in Exposure Category 1, with stud spacing of 24 inches or 16 inches. The OSB was attached after the

base of the walls had been anchored to the test fixture. The OSB was attached with 6d nails, 8 inches on center along the edges of the OSB and 10 inches on center along the interior studs.

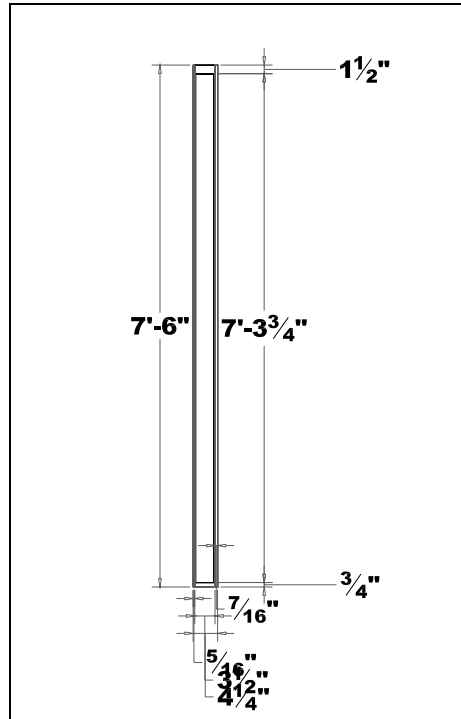


Figure 6.4: Edge Dimensions of the Specimen

A steel load beam was bolted to the top plate of each specimen with twelve 3/8 inch-diameter by 4 inch-long lag bolts, spaced 16 inches on center. The bottom plate of each specimen was anchored to the rigid steel foundation beam with twelve 1/2 inch-diameter bolts, spaced 16 inches on center. The foundation beam was bolted to the laboratory strong floor, as shown in *Figure 6.5*. 3/4 inch-thick spacer plates were placed between the specimen base plate and the foundation beams, and between the specimen top plate and the loading beam. The purpose of these spacers was to ensure that the foundation and loading beams did not prevent the cladding from rotating as the wall deformed.

The lateral loads were applied with a servo-hydraulic actuator connected between the steel load beam and a stiff frame. The actuator had a 6-inch stroke and a 10-kip capacity, and it was attached to a steel load beam, which was in turn bolted to the top plate of the wall. The loading beam was braced laterally, so as to prevent motion perpendicular to the plane of the wall. The actuator applied a constant deformation at a rate of 0.5 inches per minute.

To prevent out-of-plane motion of the test specimens, four braces were placed between the loading beam and frames located near each end of the specimen. These braces, shown in *Figure 6.5*, allowed the load beam to move laterally and vertically, but not perpendicular to the plane of the wall.

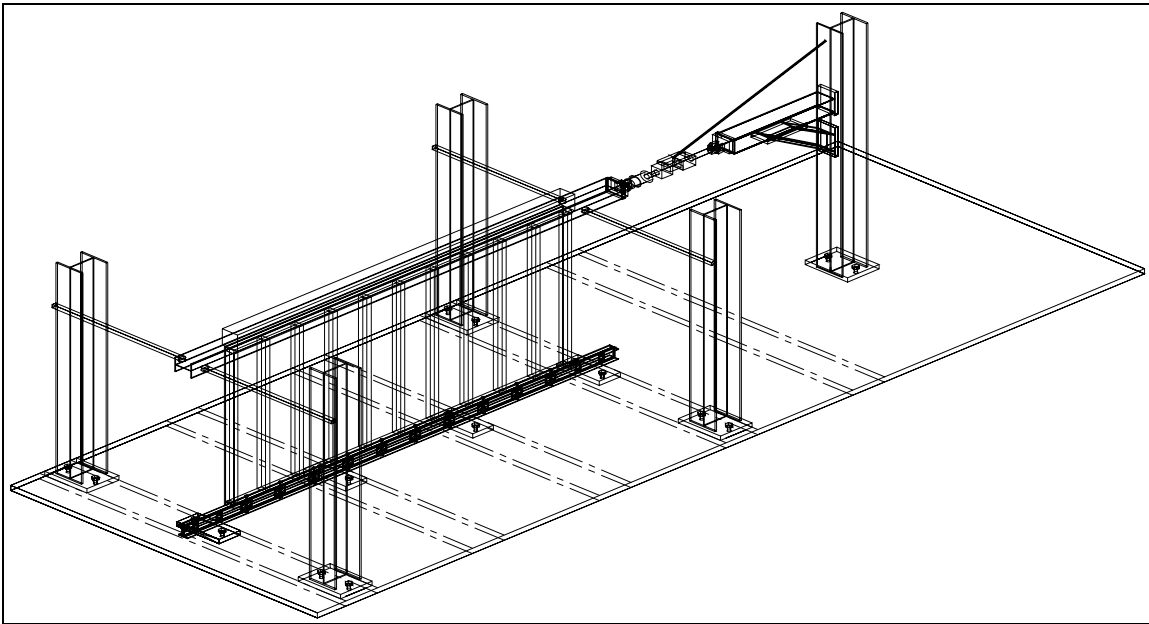


Figure 6.5: Wall Test Setup

The actuator stroke was measured with a linear variable differential transformer (LVDT) mounted inside the actuator's base. Force applied by the actuator was measured with a strain-gage-based load cell. Sixteen displacement sensors were used to measure

the lateral and vertical motion of each specimen as shown in *Figures 6.6, 6.7, and 6.8*. A seventeenth displacement sensor was used to verify there was no out-of-plane deflection. The sensors are named based on the direction measured (horizontal or vertical), their location (Actuator end or far (free) end of the wall/(1) base of the wall, (2) middle (1/2 height), or (3) top of the wall) and to what component the sensor was attached (the Wall studs, the Gypsum board cladding, or the OSB cladding). The out-of-plane sensor (WFOOP) was located at the far end, at 1/2 the height of the wall, and on the OSB side of the wall.

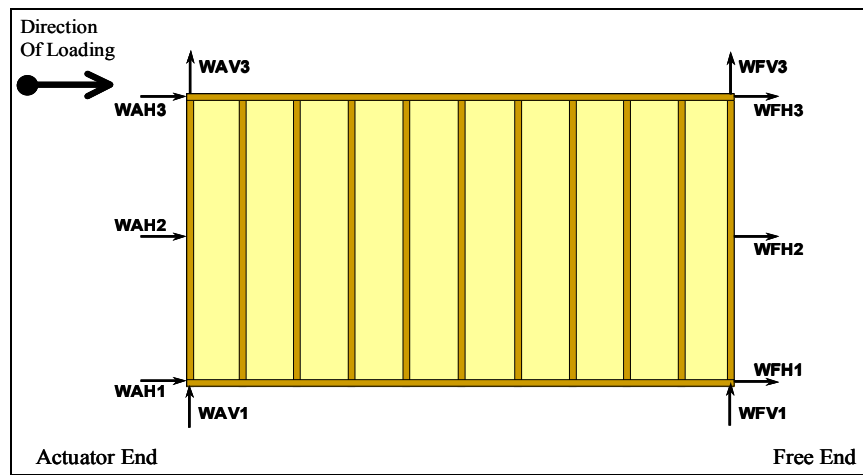


Figure 6.6: Locations of Sensors Connected to the Wall Framing

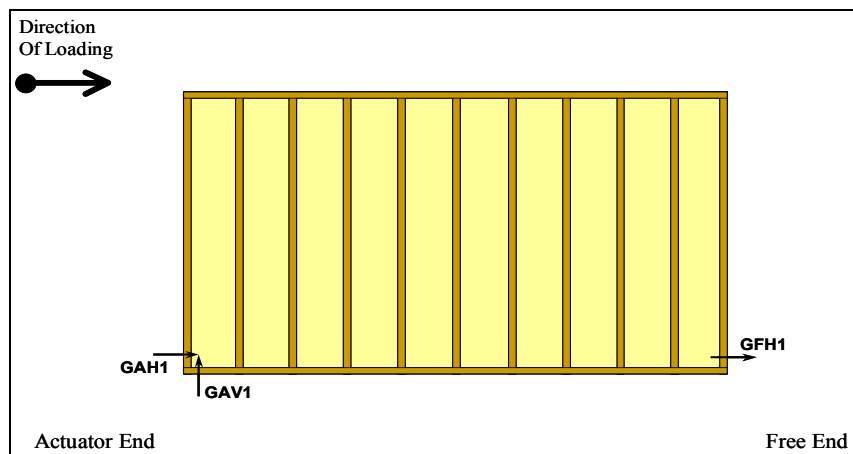


Figure 6.7: Locations of Sensors Connected to the Gypsum Board Cladding

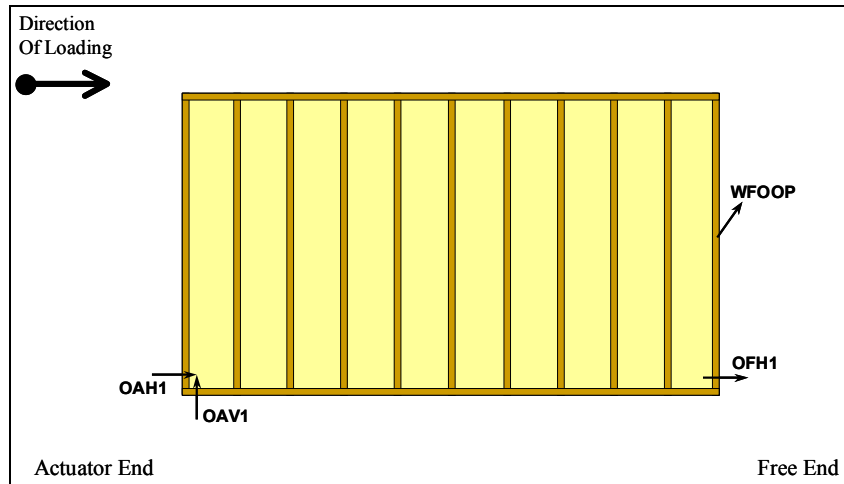


Figure 6.8: Locations of Sensors Connected to the OSB Cladding

6.2.3 Experimental Results

Figure 6.9 shows the horizontal displacement at the far end at the top of the wall framing for all four test specimens. For this research, only the portion deemed to be linear (0.1 inch of racking displacement) of the load versus racking displacement curve of the walls was taken into consideration.

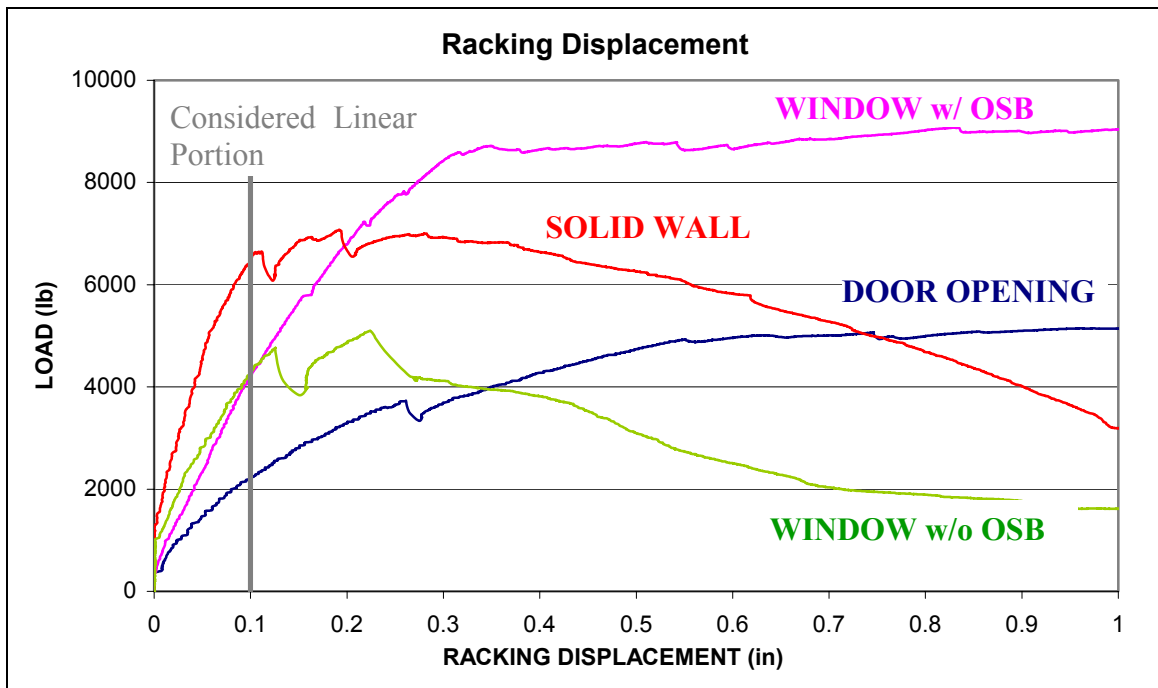


Figure 6.9: Load v/s Racking Displacement

6.3 Modeling of Shear Walls Using Orthotropic Shell Element

The shear walls tested by NIST were modeled using *FEIt* to derive the equivalent in-plane material properties for orthotropic flat shell elements, which are then used to model walls, floors and roof/ceiling systems in manufactured homes.

Sheathing and studs of shear walls are modeled using orthotropic flat shell elements and the top plate framing is modeled using beam elements, as shown in *Figures 6.10, 6.11 and, 6.12*. Door posts and lintels around door openings (Wall-2) are modeled with beam elements. Window posts, the lintel, and the window sill around window openings (Wall-3 and Wall-4) are also modeled using beam elements. The bottom plate is not modeled because all the nodes along the base of all four shear walls were pinned. A horizontal concentrated unit load was applied at the top of the wall. The thickness of the orthotropic flat shell element was assumed to be the combined thickness of the entire wall. In-plane material properties, such as modulus of elasticity in the x - and y -directions (E_x and E_y), are derived as shown in *Appendix A*. The shear modulus, G_{xy} , for the combined OSB and Gypsum sheathing, along with the studs, was derived from these shear wall tests. *Table 6.1* shows the material properties used for the shear walls.

Table 6.1: Properties of Orthotropic Shell Element

Wall Sheathing	E_x (psi)	E_y (psi)	G_{xy} (psi)	t (in)
OSB and Gypsum Sheathing (Both Sides: Wall-1, Wall-2, and Wall-3)	34074	92647	7750	4.25
Gypsum Sheathing (Single Side: Wall-4)	20860	103278	11300	3.8125

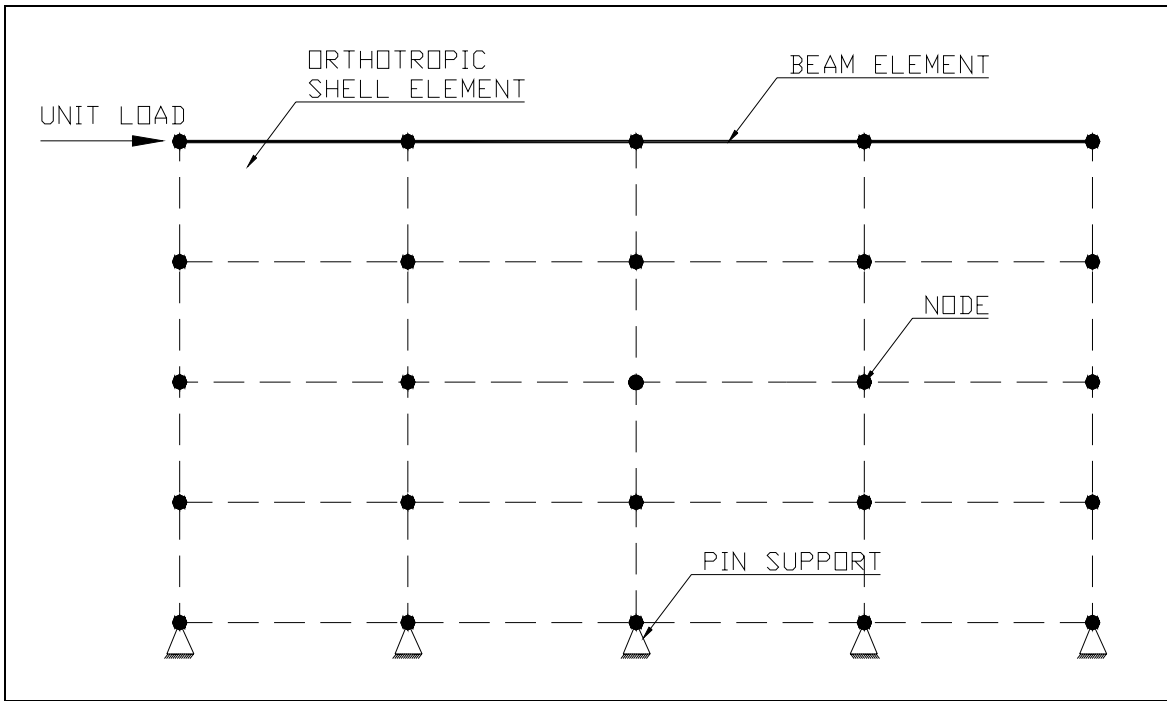


Figure 6.10: Finite Element Model of Wall-1 using Orthotropic Shell Element

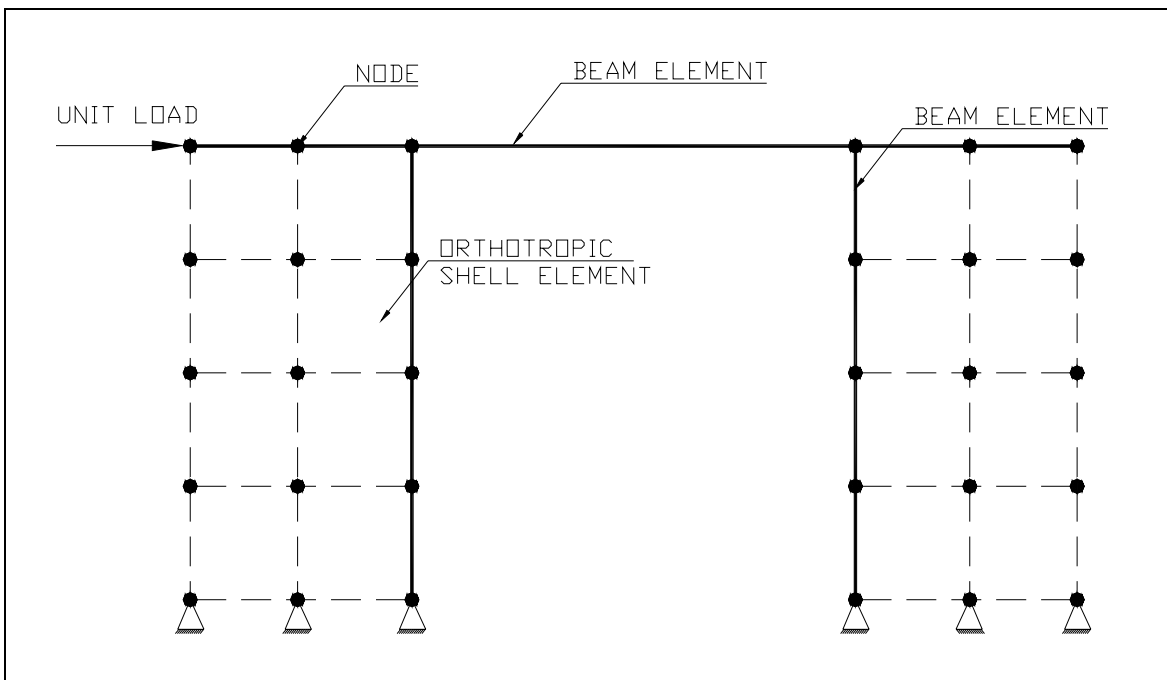


Figure 6.11: Finite Element Model of Wall-2 using Orthotropic Shell Element

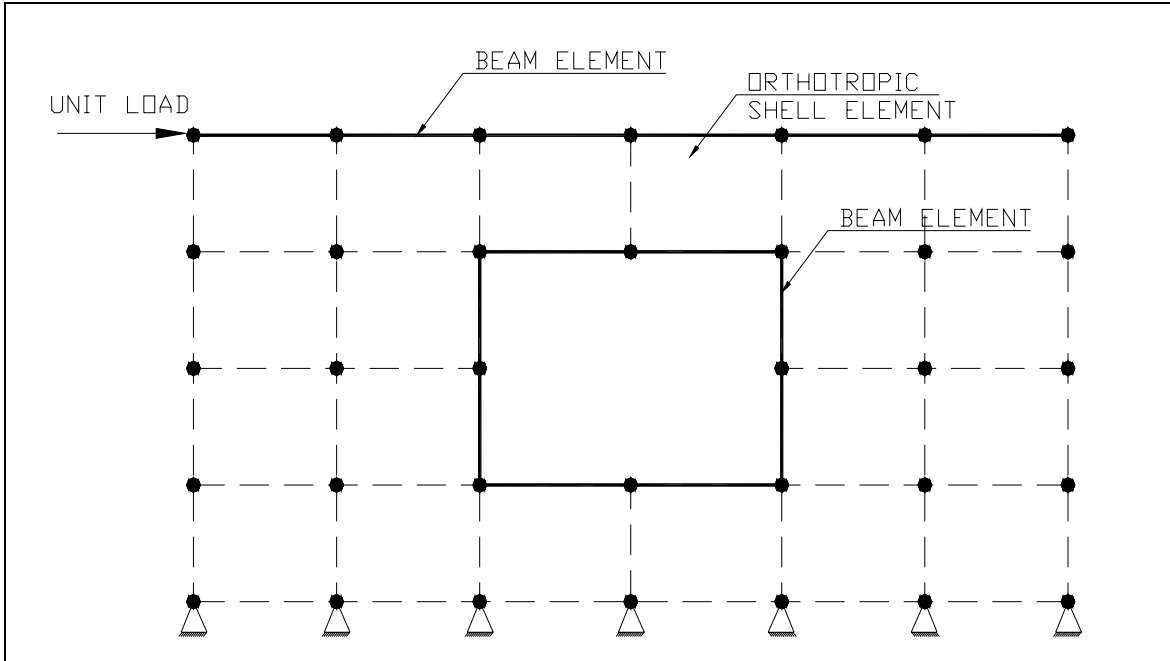


Figure 6.12: Finite Element Model of Wall-3 and Wall-4 using Orthotropic Shell Element

6.3.1 Results

For the walls with exterior (OSB) and interior (Gypsum) sheathing, the combined shear modulus, G_{xy} , for the entire shear wall was calibrated from Wall-1. These properties were then verified by using them to model Wall-2 and Wall-3. Racking displacements obtained from the finite element models for Wall-2 and Wall-3 are compared with test results in *Table 6.2*. From the results obtained for Wall-2 and Wall-3, it can be seen that the finite element model for shear walls using orthotropic shell elements is relatively flexible. Wall-2 and Wall-3 are the shear walls with a door and window cut out. These models do not account for the gluing and nailing of the sheathing along the edge of the opening, which increases the stiffness of the shear walls. Hence, the model is more flexible than the actual test specimens.

For the wall with gypsum sheathing only, the shear modulus, G_{xy} , for the entire wall was calibrated from Wall-4. There was no other data available to verify this calibrated model.

Table 6.2: Comparison of Racking Displacement for Unit Load for Orthotropic Shell Model

Shear Wall	<i>FEl</i> t Model (in x 10 ⁻⁵)	NIST Test (in x 10 ⁻⁵)	% Difference
Wall with Door Opening (Wall-2)	6.488	4.348	33
Wall with Window Opening sheathed on both sides (Wall-3)	3.464	2.602	25

6.3.2 Drawbacks to the Model with Orthotropic Shells

The main purpose for modeling shear walls with orthotropic shells was to obtain equivalent material properties. Using these modified properties for orthotropic shells, the walls in the manufactured home can be modeled with great simplicity, keeping the required number of elements comparatively small. The drawback of this method is that, to derive these material properties, some experimental data is always required. Also, walls with door and window cut-outs modeled with orthotropic shells are relatively flexible compared to test data.

A preferred modeling technique is one in which only the properties of the studs, sheathings, and nails are required, eliminating the need for calibrating with full-size tests. Hence, these shear walls are also modeled using some enhanced simplified techniques, as shown in the following section. This will verify the capability of *FEl*t program to model shear walls in detail.

6.4 Enhanced Model

In this model, all the individual components of the shear walls are modeled separately. Sheathing on each side (interior and exterior) is modeled using isotropic 4-node flat shell elements. Framing members, such as studs (only along the sheathing perimeter), top plate, bottom plate, door posts, lintels, and window sills are modeled using a 2-node beam element. OSB sheathing is nailed to the framing members while gypsum board is glued to the framing members. These connections are modeled with an interface element. *Figures 6.13, 6.14, 6.15, 6.16, 6.17, 6.18, and 6.19* show the enhanced finite element model of all four types of shear walls. A horizontal concentrated static unit load was applied at the top of the walls. Nodes common to the top plate and studs are modeled as moment release nodes, while the nodes along the bottom plate are pinned.

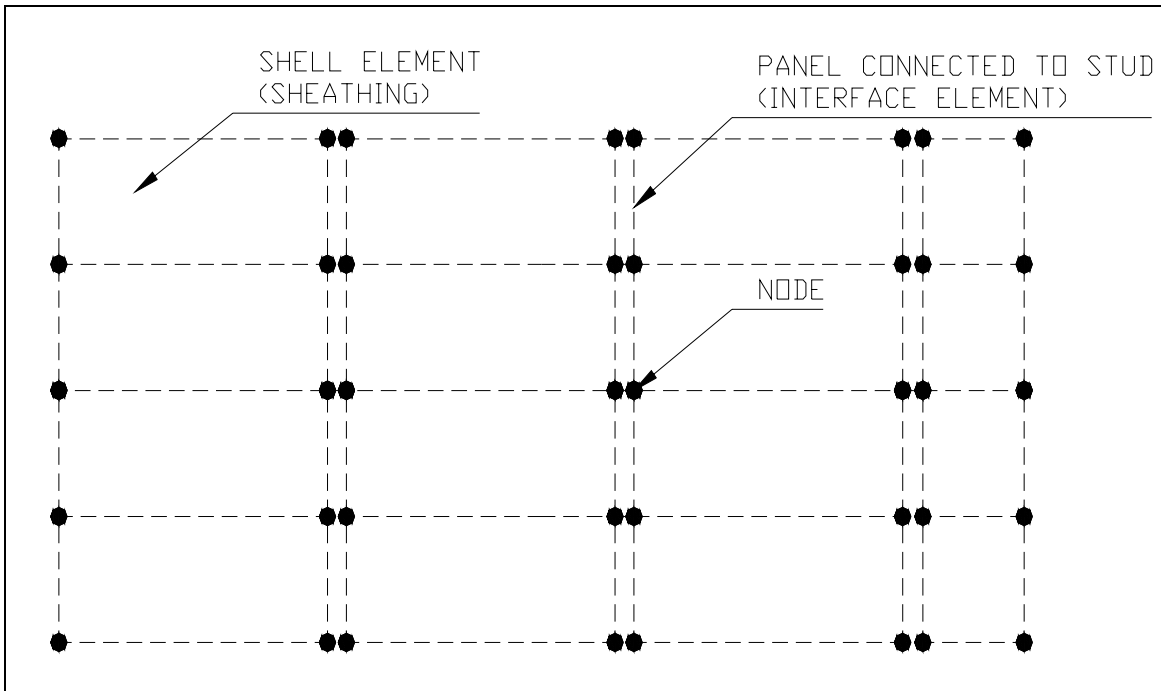


Figure 6.13: Enhanced Model of Wall-1 Representing Sheathing (Interior or Exterior)

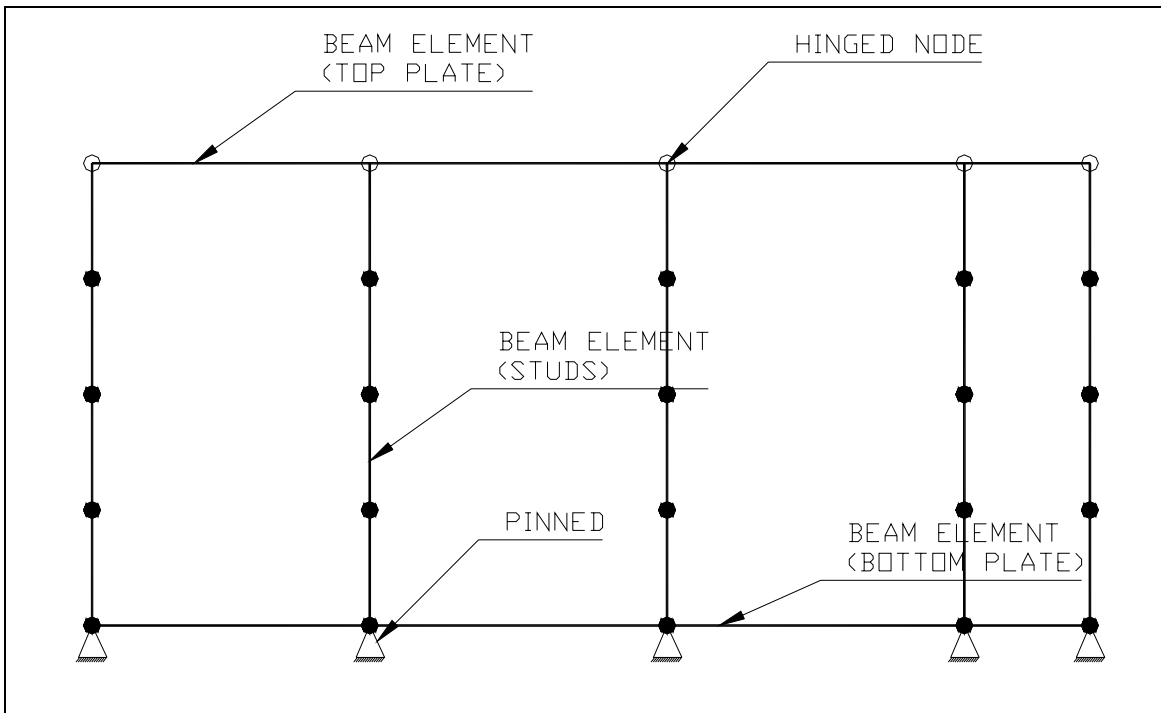


Figure 6.14: Enhanced Model of Wall-1 Representing Framing Members

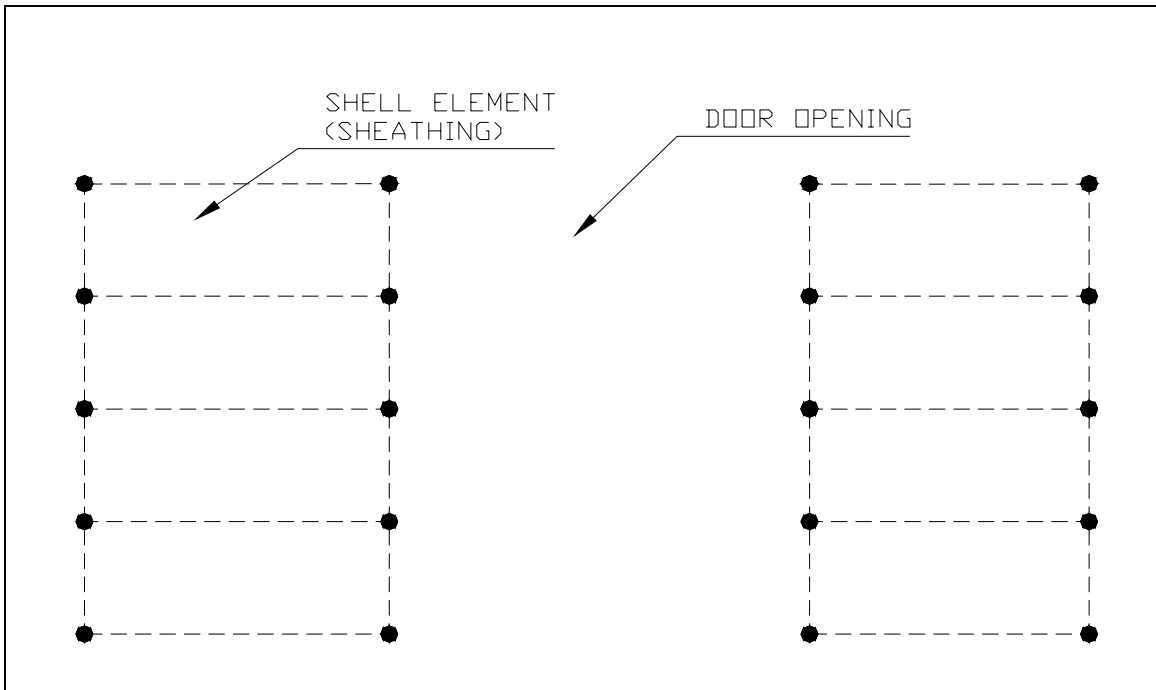


Figure 6.15: Enhanced Model of Wall-2 Representing Sheathing

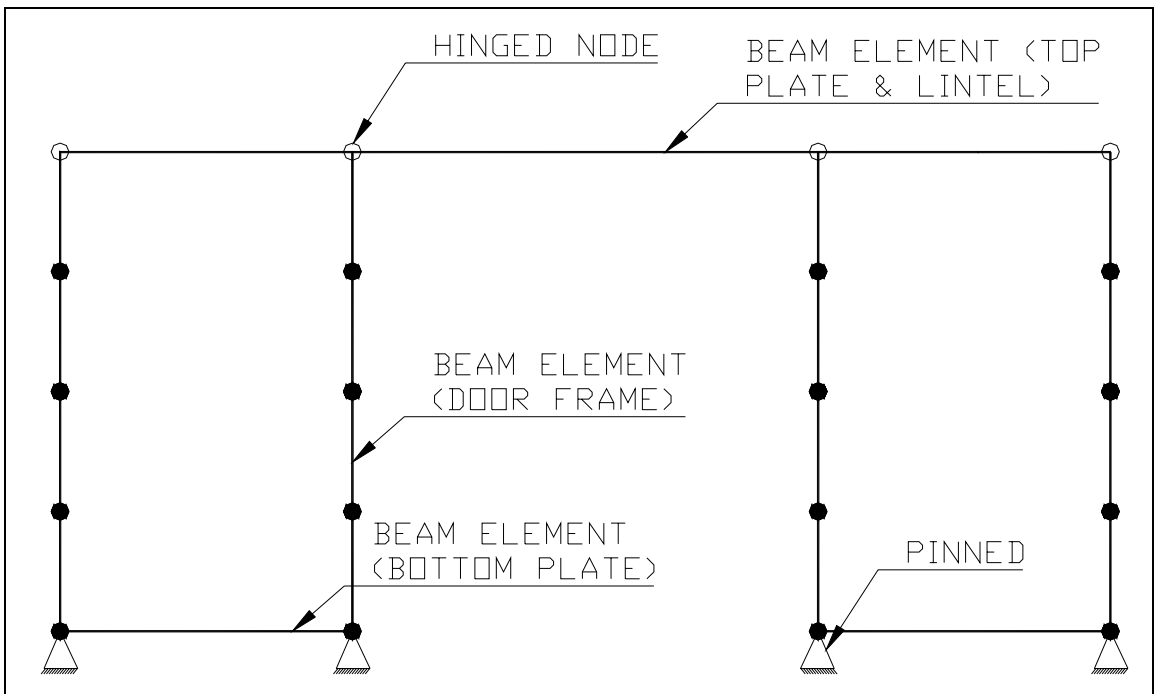


Figure 6.16: Enhanced Model of Wall-2 Representing Framing Members

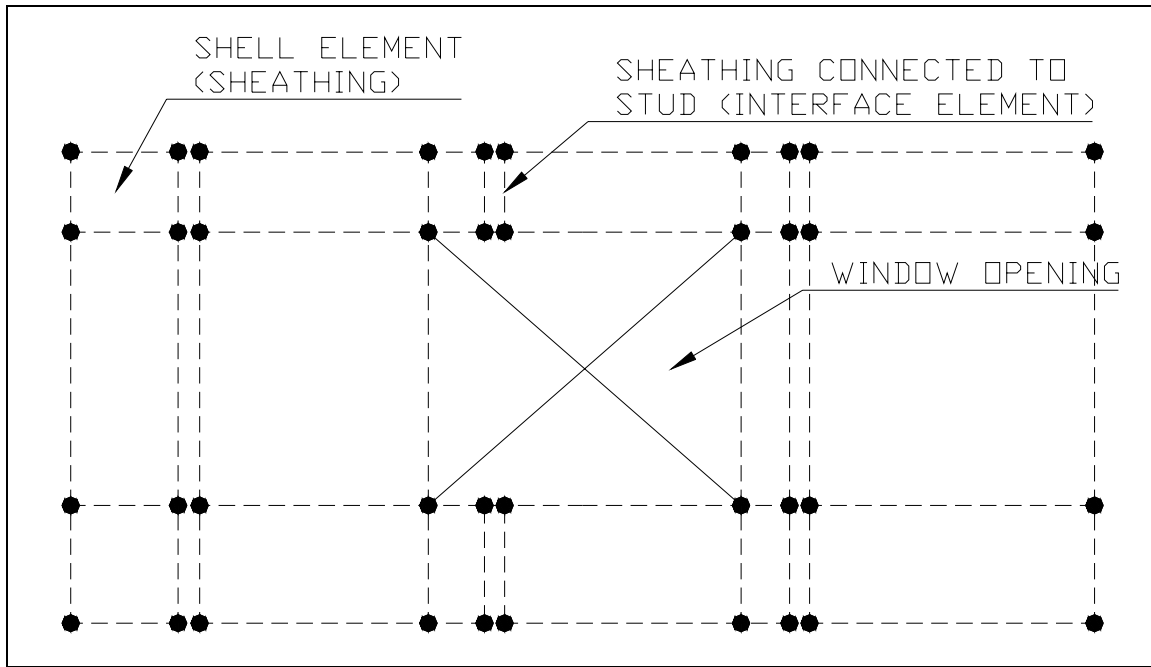


Figure 6.17: Enhanced Model of Wall-3 and Wall-4 Representing Sheathing

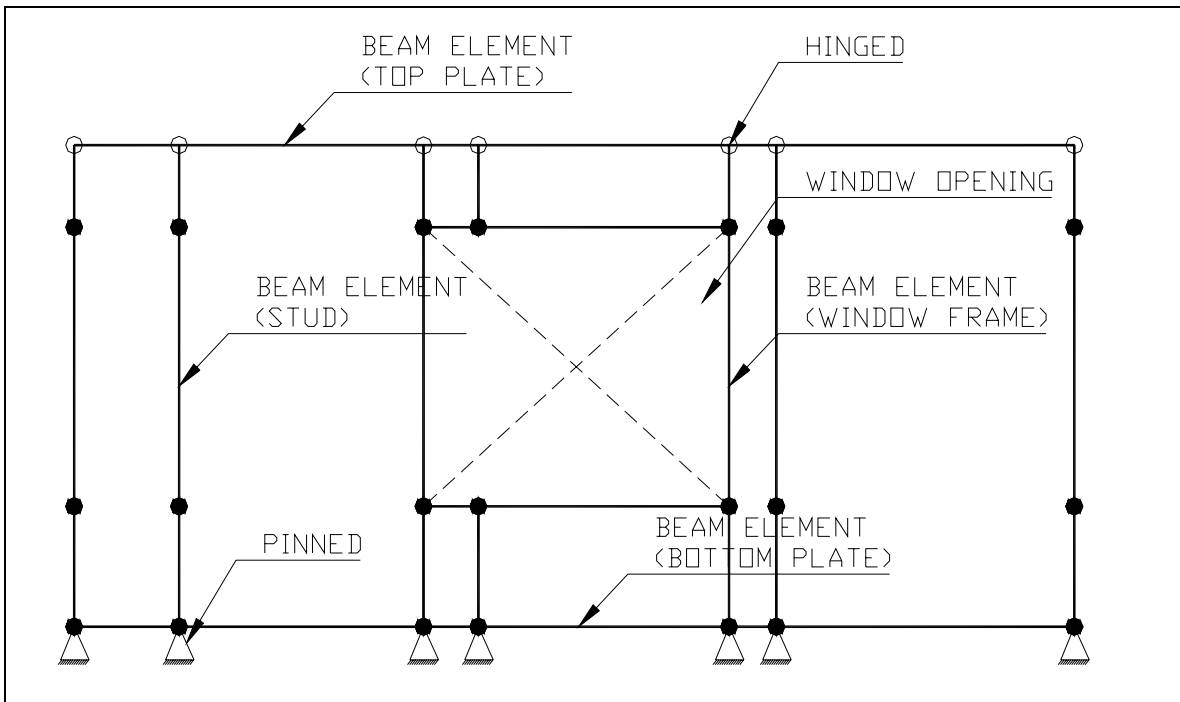


Figure 6.18: Enhanced Model of Wall-3 and Wall-4 Representing Framing Members

Material properties for OSB (7/16 inch thick) and gypsum board (5/16 inch thick) used in the analysis were derived from the Allowable Stress Design (ASD) Manual for Engineered Wood Construction (2001) and Gypsum Board Typical Mechanical and Physical Properties, Gypsum Association (GA-235-01), respectively. Properties of the framing members (Spruce-Pine-Fir) were taken from the National Design Specification (NDS) Design Values for Wood Construction Supplement (2001). Stiffness of the nails was derived from the works of Dolan (1989) and McCutcheon (1985). Due to a lack of information on the adhesive used to glue gypsum to the wall framing, its stiffness was derived from the test carried out on the single-sheathed wall with the window opening (Wall-4). A reasonable value of stiffness of the adhesive was found to be 10,000 lb/in/in, which was further verified by results of the enhanced model for Wall-1, Wall-2, and Wall-3. *Tables 6.3 and 6.4* show the material properties for the various components of the shear wall.

Table 6.3: Properties of Components in the Enhanced Model

Wall Component	E (psi)	ν	t (inch)	A (in ²)	I (in ⁴)
OSB	1.49e5	0.28	7/16	-	-
Gypsum	2.55e5	0.30	5/16	-	-
Stud	1.2e6	-	-	5.25	0.9844
Top Plate	1.2e6	-	-	5.25	0.9844
Bottom Plate	1.2e6	-	-	2.63	0.1230

Table 6.4: Properties of Nails (6d common)

Orientation of Framing Grain	Orientation of Sheathing Grain	K (lb/in)
Parallel	Parallel	2472
Parallel	Perpendicular	2800

6.4.1 Results

Racking displacements obtained from the enhanced model for Wall-1, Wall-2, and Wall-3 agree well with test results as shown in *Table 6.5*. However, the test data is highly dependent upon the range of racking displacement considered. Test data selected for the comparison was displacement magnitude up to 0.1-inch, for which all of the four walls behave linearly.

Table 6.5: Comparison of Racking Displacement for Unit Load for Enhanced Model

Shear Wall	FELT (in x 10 ⁻⁵)	NIST Test (in x 10 ⁻⁵)	% Difference
Solid Wall (Wall-1)	1.761	1.799	2.15
Wall with Door Opening (Wall-2)	4.493	4.418	1.67
Wall with Window Opening sheathed on both sides (Wall-3)	2.562	2.586	0.93

Figures 6.19, 6.20, 6.21, and 6.22 show the comparison of the wall stiffness values obtained from experimental tests and finite element models, using both orthotropic shells and the enhanced model. The orthotropic shell model for Wall-2 and Wall-3 was shown to be relatively flexible compared to experiment. Wall-2 and Wall-3 are the shear walls with a door and window cut-out. As previously mentioned, a possible explanation is that these models do not account for the gluing and nailing of the sheathing along the edge of the openings, which increases the stiffness of the shear walls. In the orthotropic shell model, these connections are not modeled and, hence, the model is overly flexible. In the enhanced model, however, the connections along the panel edge and framing members are considered. Results obtained from the enhanced model agree well with the test results. Stiffness values for the shear walls sheathed on both sides, Wall-1, Wall-2, and Wall-3, are almost equal to those of these walls obtained from the experimental tests.

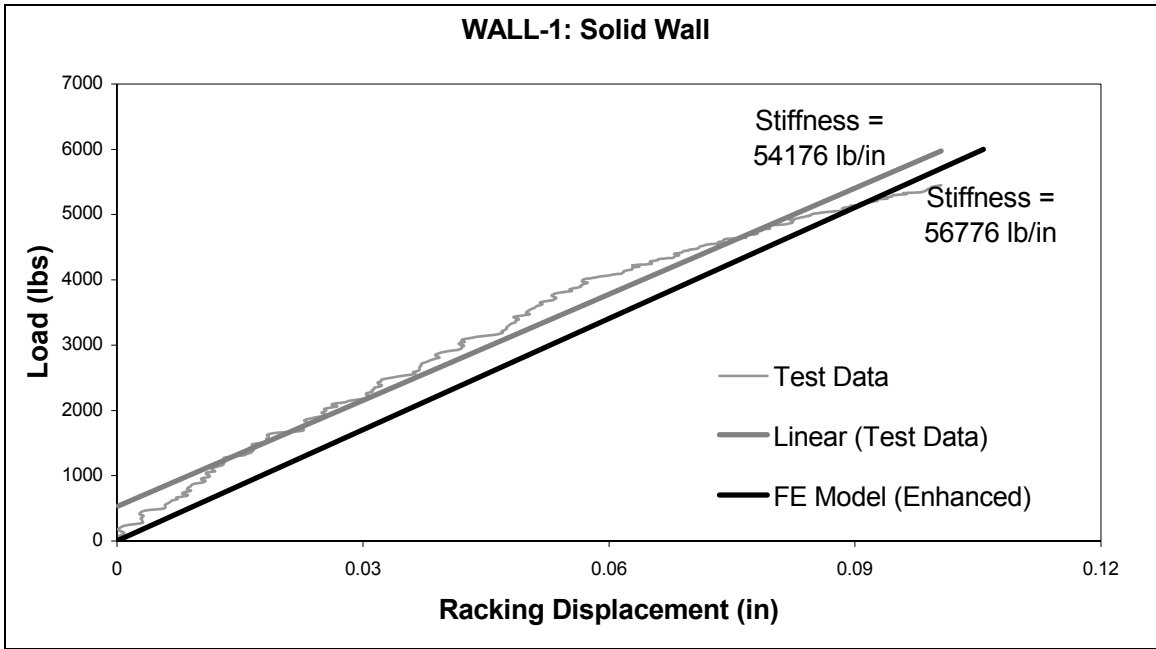


Figure 6.19: Wall Stiffness from the FE Model and Experimental Test for the Solid Wall (Wall-1)

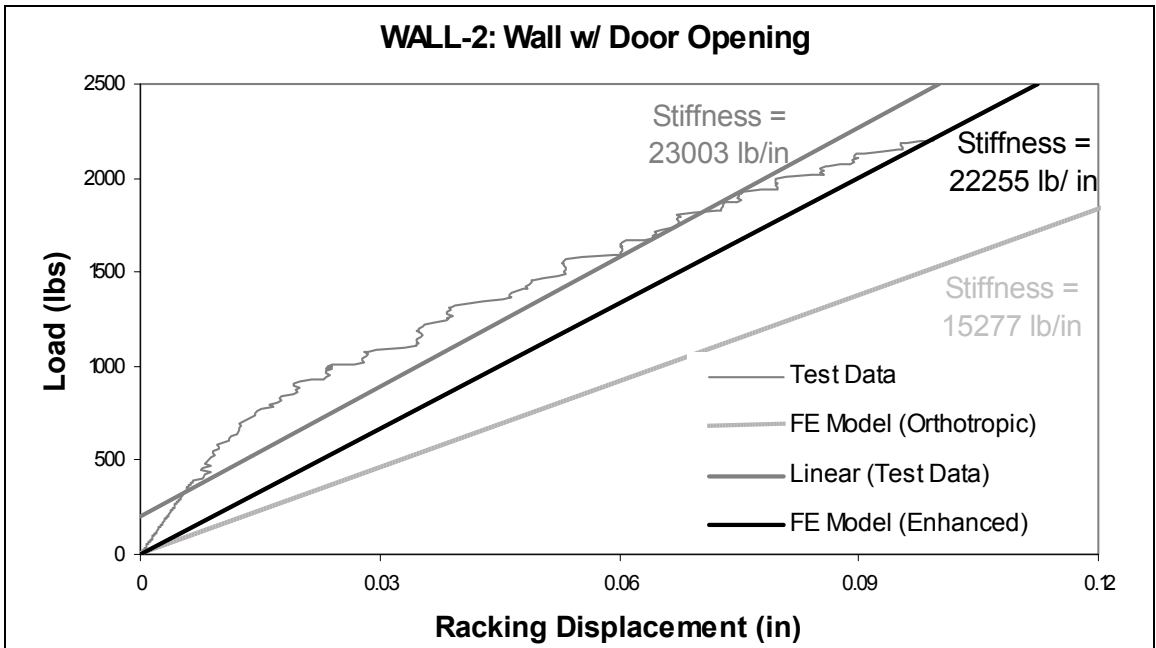


Figure 6.20: Wall Stiffness from FE Models and Experimental Test for the Wall w/ Door Opening (Wall-2)

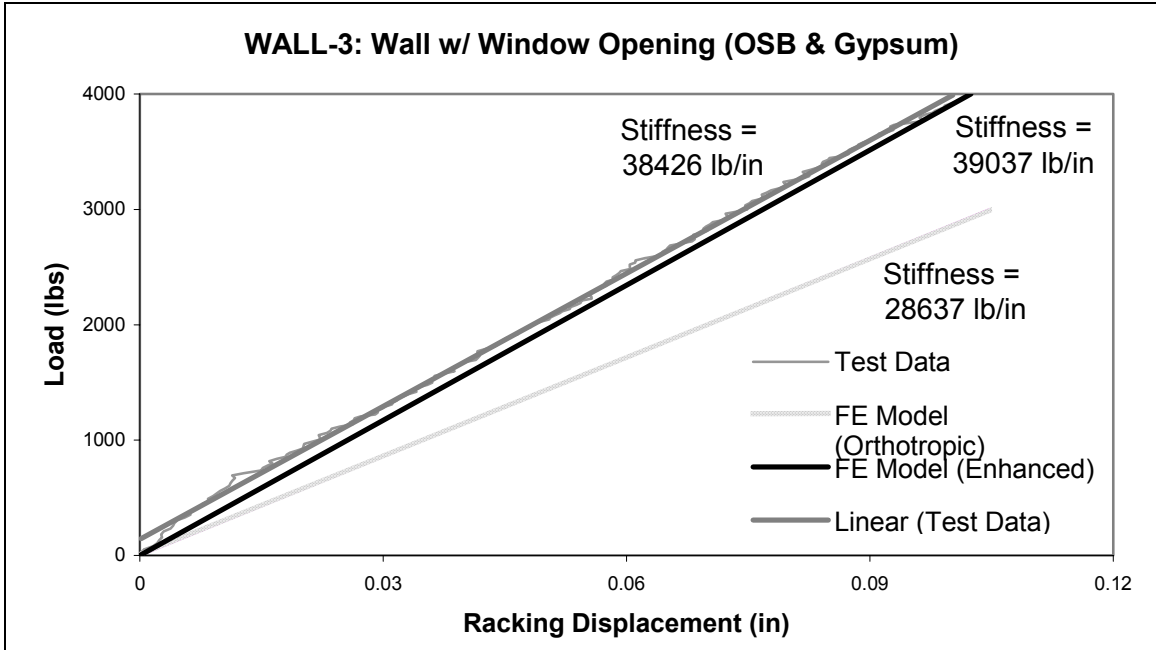


Figure 6.21: Wall Stiffness from FE Models and Experimental Test for the Wall w/ Window Opening Sheathed on Both Sides (Wall-3)

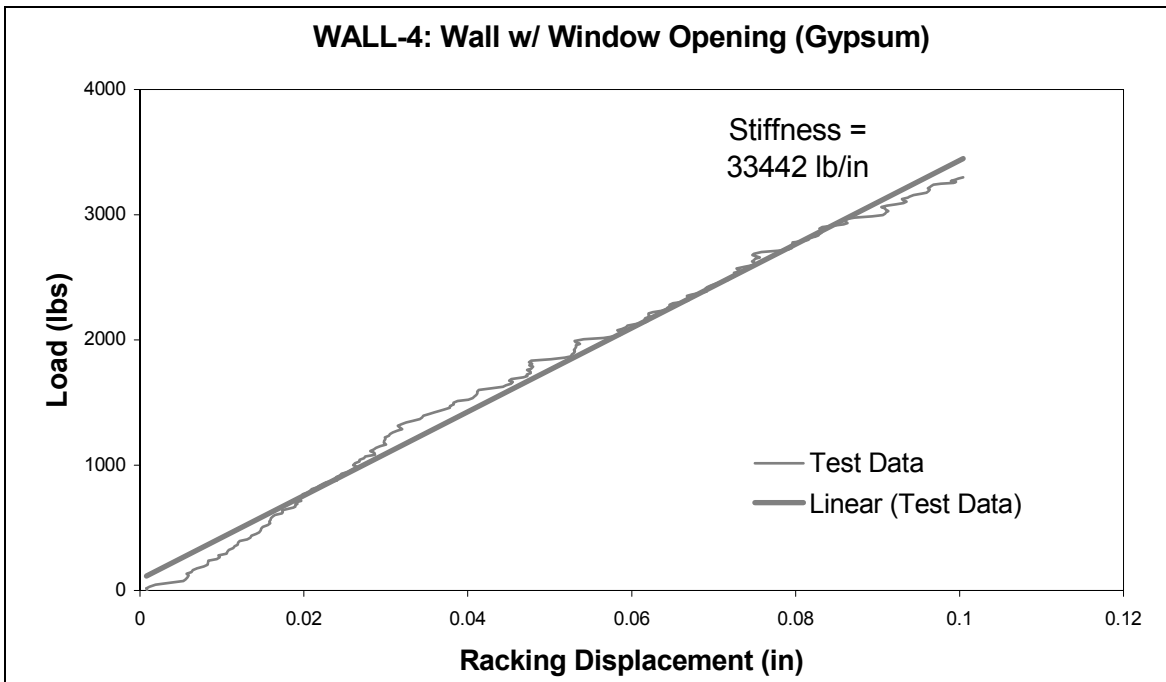


Figure 6.22: Wall Stiffness from the FE Model and Experimental Test for the Wall w/ Window Opening Sheathed on Only One Side (Wall-4)

7. DOUBLE-SECTION MANUFACTURED HOME

7.1 Introduction

Hurricane Andrew and other catastrophic events have caused large amount of damage to manufactured homes. The vulnerability of these homes to high winds is a widely shared perception and it is of significant concern as more than 10% of the US population resides in this type of housing. To improve understanding of the structural behavior and improve durability, much research is being conducted on these types of structures. Results from investigations of damage to manufactured homes clearly demonstrate the need for a verified, three-dimensional system-based analysis model. The information provided by full-scale tests, advances understanding of the structural behavior, leading to improved simulation of manufactured homes subjected to high winds.

7.2 Full-Scale Testing of Double-Section Manufactured Home

7.2.1 Introduction

Engineers from the Idaho National Engineering and Environmental Laboratory (INEEL), Mid-America Manufacturing Technology Center (MAMTC), and EDM International Inc. (EDM), along with students from the University of Wyoming (UW), and Idaho State University (ISU) performed a series of seven full-scale lateral load tests on a double-section manufactured home at a field test site in Wyoming, primarily to address the need to improve the ability of these homes to withstand high winds. The main purpose of the tests was to determine the displacements and forces on the home and its structural components, which are to be used in the development and validation of the

finite element modeling techniques described here. A brief description of the tests is given in the following section. For a detailed description, refer to Richins et al. (2003).

7.2.2 Double-Section Manufactured Home Description

The home used as a test specimen was a double-section unit manufactured by Kit Manufacturing Co. (Kit), Model 75-SW-23 (26ft. 8in. X 60ft.). The two halves of the double-section home were constructed independently in the factory, and assembled at the site. The home was structurally complete, with ducting, insulation, plumbing, electrical systems, roofing, siding, interior walls, etc., but without interior trim and most appliances. The materials and construction methods of the test home are representative of many homes currently produced by the manufactured housing industry. A floor plan of the tested home is shown in *Figure 7.1*, while a section view is shown in *Figure 7.2*. The installation system, shown in *Figure 7.3*, was designed in such a way that there was no significant displacement of the ground anchors or stretching of the tie-down straps.

7.2.3 Loading

A structurally complete double-section manufactured home was tested for simulated wind loads. The tests were designed to approach the design-level lateral load of the home (30 lb/ft²), but not lead to failure. To apply distributed loading (airbag loading), a strong wall was constructed and load was applied between it and the west sidewall of the home. The uniformly distributed load was applied over the entire longitudinal wall using a pressurized airbag. *Figure 7.4* shows the location of pressure load with respect to shear walls.

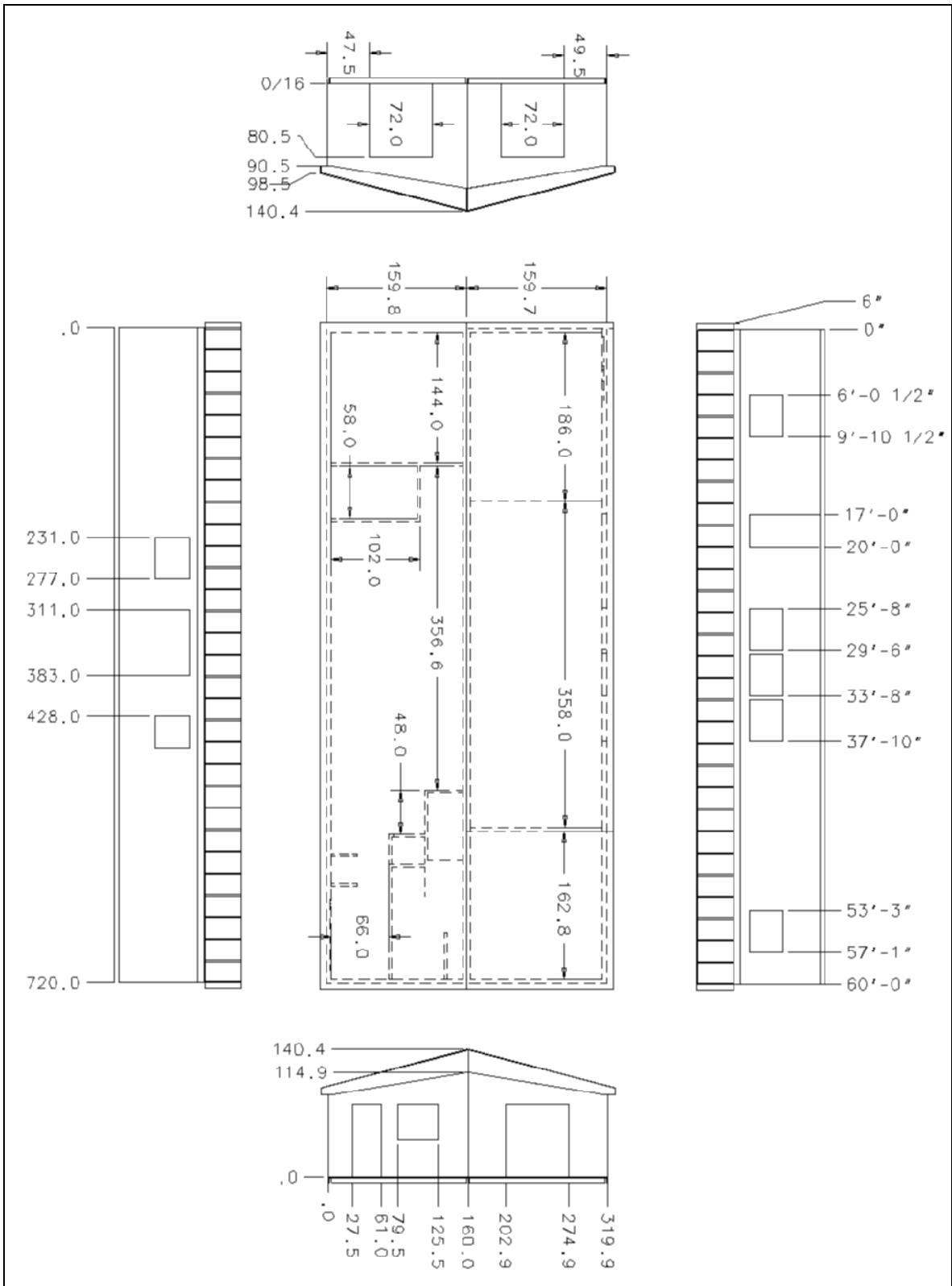


Figure 7.1: Typical Layout of Double-Section Manufactured Home

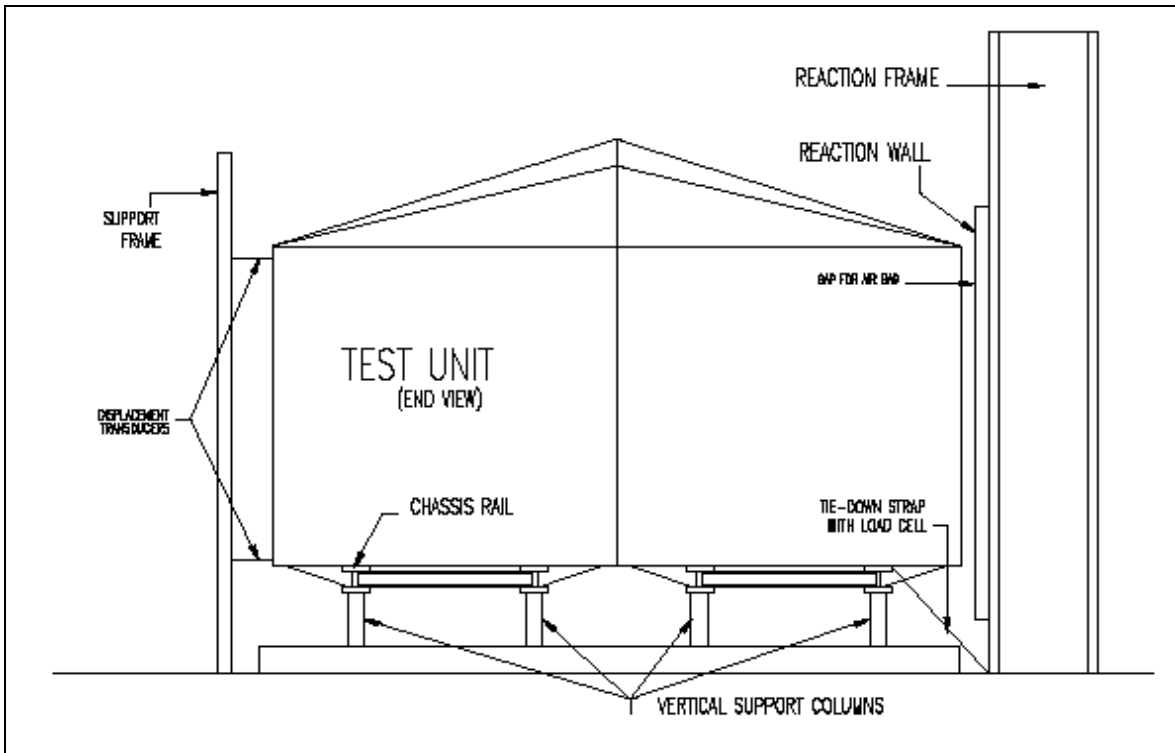


Figure 7.2: Section View of the Manufactured Home

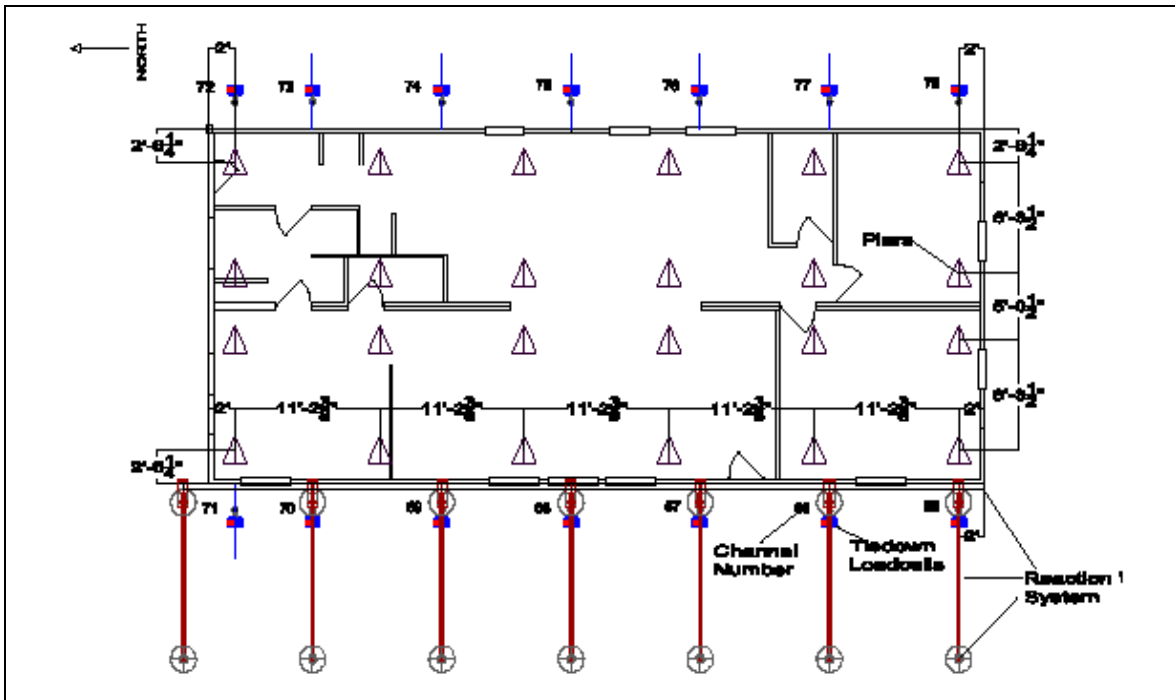


Figure 7.3: Test Home Installation Showing Piers, Tie-down Load Cells, and Reaction Wall with Braces

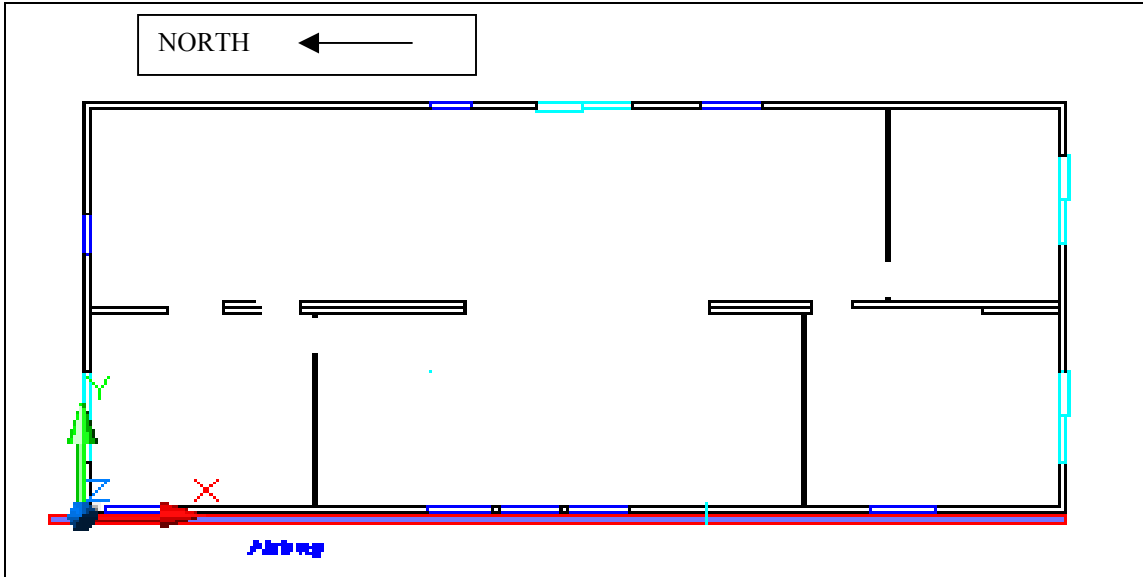


Figure 7.4: Location of the Point and Uniformly Distributed Airbag Loads

7.2.4 Data Acquisition

For each test, data were recorded as functions of time, including items such as the applied loads, tension in tie-down straps, load transfer across the marriage line, global displacements with respect to a fixed frame, internal shear wall racking, shear displacement along the marriage line, and interface slip.

Verification of finite element results is limited to this particular test because this is the only full-scale test known that has been performed on a double-section manufactured home. No material property data were recorded for the materials and the components used to build the home.

7.3 Modeling of Double-Section Manufactured Homes

7.3.1 Introduction

Construction of the test specimen and various components is described thoroughly in this section. The finite element model does not precisely represent all design aspects of

the home, but instead it is intended to be a simplified representation of its overall response under wind loading. The selection of material properties, the elements used to model various components, the boundary conditions, and the loading of the model are also discussed.

7.3.2 Model Description

The model was constructed with the floor frame resting on the steel chassis, the wall systems connected to the floor, and the roof system attached to the walls. *Figure 7.5* shows the finite element model for the double section manufactured home.

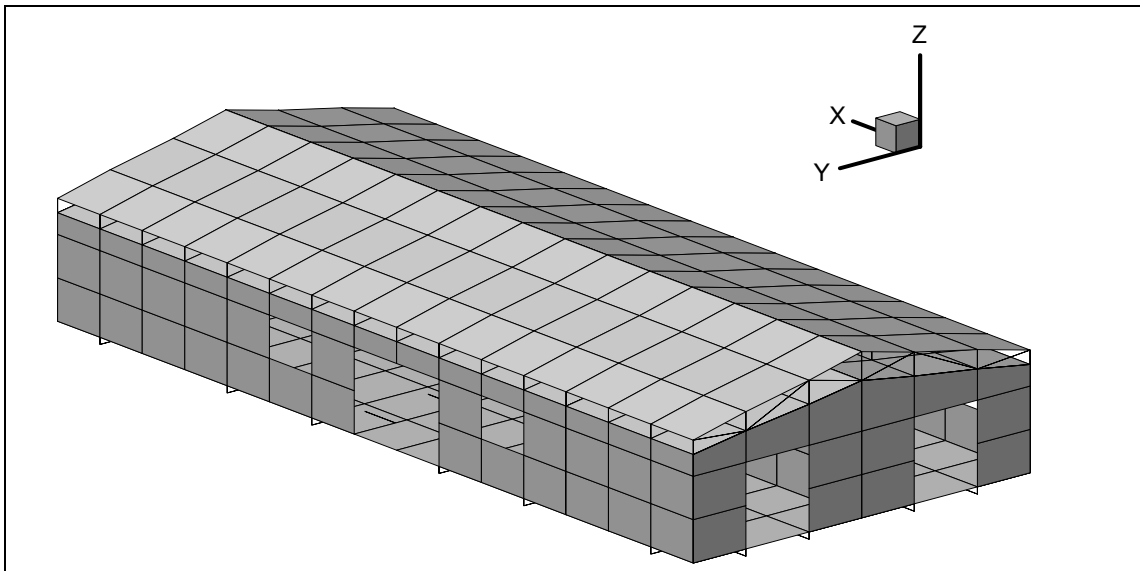


Figure 7.5: Finite Element Model of Double Section Manufactured Home

7.3.2.1 Foundation System

The foundation system includes the chassis, tie down springs, and chassis support points represented by nodal restraints. *Figure 7.6* shows the foundation system for both halves of the homes.

The chassis was made of a carbon steel frame and it supports the floor. The chassis was constructed of two longitudinal main beams running along the full length of the home. Six lateral members connected these two main beams, followed by outriggers to the outside edge of the home. The main beams of the chassis were M 12x10 sections, and the laterals and outriggers were C 6x8.2 sections. The properties for the steel members were taken from the American Institute of Steel Construction's Load and Resistance Factor Design manual (AISC, 2001). The properties used for the chassis members are listed in *Table 7.1*.

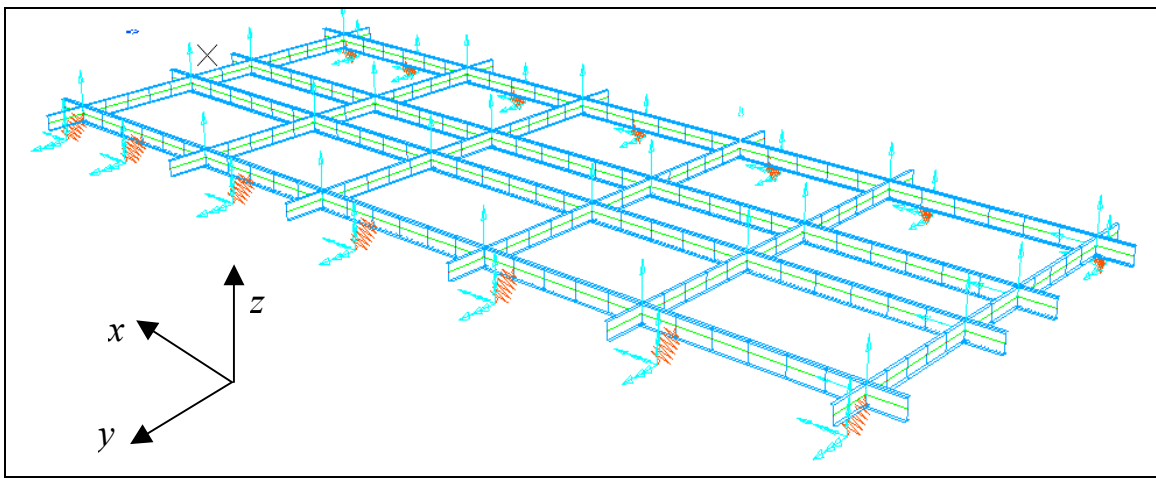


Figure 7.6: Foundation System: Chassis, Tie-Down Springs and Piers

The two chassis assemblies for the two halves were constructed independently and there is no connection between them along the mating plane. Outriggers appear to touch along the mating plane (Figure 7.6), but, in fact, they are distinct and do not transfer force or moment across the mating plane. In the model, these cross-sections were modeled as rectangular sections with corresponding geometric properties. Longitudinal

main beams, laterals, and outriggers were modeled using two-node (6-degrees of freedom per mode) 3D-beam elements.

The chassis was supported on piers, which were located at the junction of the main beams and the laterals. These piers were modeled with node restraints. All piers were restrained in the x , y , and z -direction (vertical).

Tie-downs were used to prevent the horizontal (side-to-side) motion and provide stability along the y -direction. Each tie-down strap was attached to the longitudinal main beams on one end, and to anchors embedded in a concrete pad or compacted soil at the other end. There were fourteen tie-down straps, lying in the Y - Z plane at a 45° angle, as shown in *Figure 7.6*. Two-node spring elements were used to simulate these tie-down straps, with one node fixed to ground. After executing the analysis, if a tie-down strap was found to be in compression, it was removed and the model was executed again, since these straps are assumed to be capable of resisting tension only. This process was repeated until all the spring elements were in tension. A large stiffness, such as 1×10^6 lbs/in. was assumed for these springs.

Table 7.1: Chassis Properties

Member	A (in ²)	Iz (in ⁴)	Iy (in ⁴)	J (in ⁴)	G (psi)	E (psi)	ν
Main Beam (M 12x 10)	2.95	61.7	1.03	0.029	1.12E+07	2.90E+07	0.3
Laterals and Outriggers (C 6 x 8.2)	2.39	13.1	0.687	0.074	1.12E+07	2.90E+07	0.3

7.3.2.2 Floor System

The floor system included the floor joists and rim joists on which floor sheathing was laid. The floor is connected to the chassis by means of frame clips.

The floor of the home was made of nominal 2 x 6 inch joists placed 24 inches on-center, and they were oriented across the home. The floor decking was assumed to be 5/8 inch thick.

Floor sheathing and joists were modeled with equivalent 4-node orthotropic flat shell elements as shown in *Figure 7.7*. Material properties for the floor were obtained from the literature (Schmidt, 1999), estimated by “smearing” the joists into an equivalent uniform layer of material. The floor was then analyzed as an orthotropic flat shell, consisting of a sheathing layer and a joist layer, using classical lamination theory. The properties used are presented in *Table 7.2*. The grid size was nominally 48 X 48 inches, modified to align with the geometric features such as the chassis and door openings. The two halves of the floors are joined with interface elements to consider the force transfer due to the lateral loading.

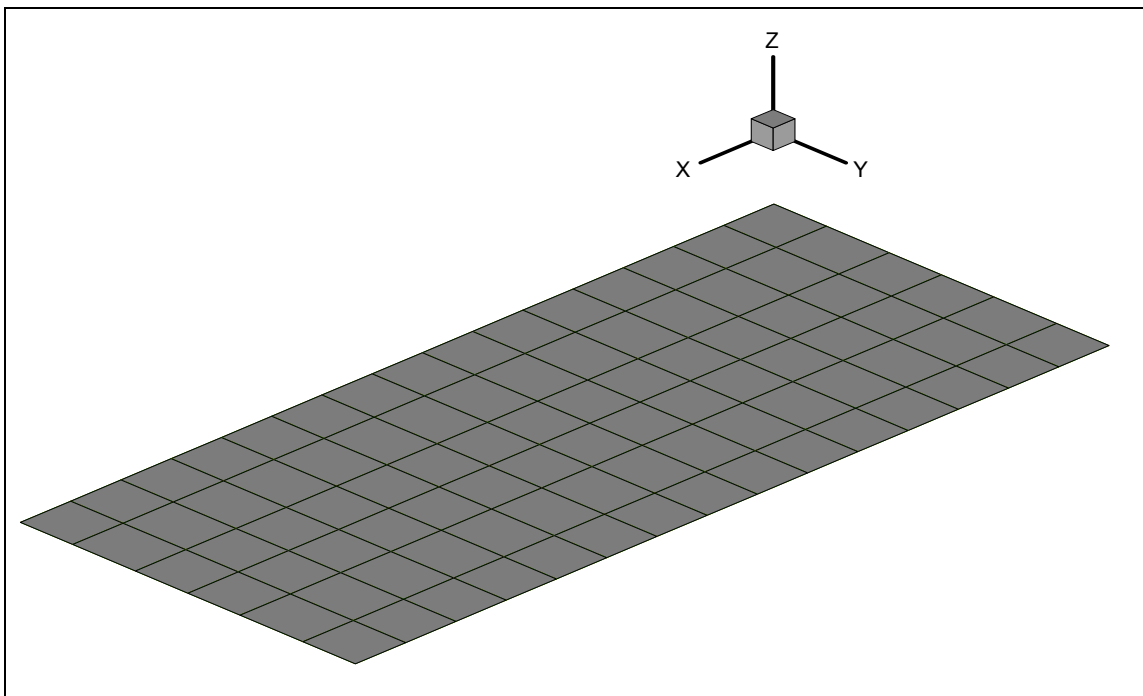


Figure 7.7: Layout of Floor Elements

The floor was connected to the chassis by means of frame clips. These frame clips were provided at the locations where the main longitudinal beams and laterals cross and at points where rim joists rest on the outside edge of the outriggers. Due to centerline-to-centerline modeling, there was a 9-inch offset between the chassis beam node and a floor node at each clip. To account for this vertical offset between the centerline of chassis longitudinal beams and the centerline of the floor joists, rigid links were used to connect them at points along the main beams and outrigger beam ends. These rigid links were modeled using two-node 3-D beam elements to simulate the floor to chassis connection (clips) and were assumed to be very stiff.

Table 7.2: Floor Properties

Member	E_x (psi)	E_y (psi)	G_{xy} (psi)	t (in)
Floor	1.54E+06	1.13E+06	94200	0.625

7.3.2.3 Wall System

The exterior and interior walls were constructed with 2 x 4 inch studs, 16-inches on-center. Exterior walls were sheathed with OSB on the exterior side and gypsum board on the interior side, whereas interior walls were sheathed with gypsum board on both sides. Minor partitions that do not span at least half the width of single section were not included in the model. Walls were modeled using 4-node orthotropic flat shell elements with dimensions of roughly 36 x 48 inches. Element locations and sizes were modified to accommodate geometric features like windows and doors, and elements were aligned with floor and roof nodes. The properties used, as derived in the previous chapter, are presented in *Table 7.3*. *Figure 7.8* shows the layout of the interior and exterior walls with respect to the floor.

Table 7.3: Wall Properties

Member	E_x (psi)	E_y (psi)	G_{xy} (psi)	t (in)
Exterior Walls	3.41e4	9.27e4	7.75e3	4.25
Interior Walls	2.09e4	1.03e5	2.26e4	3.82

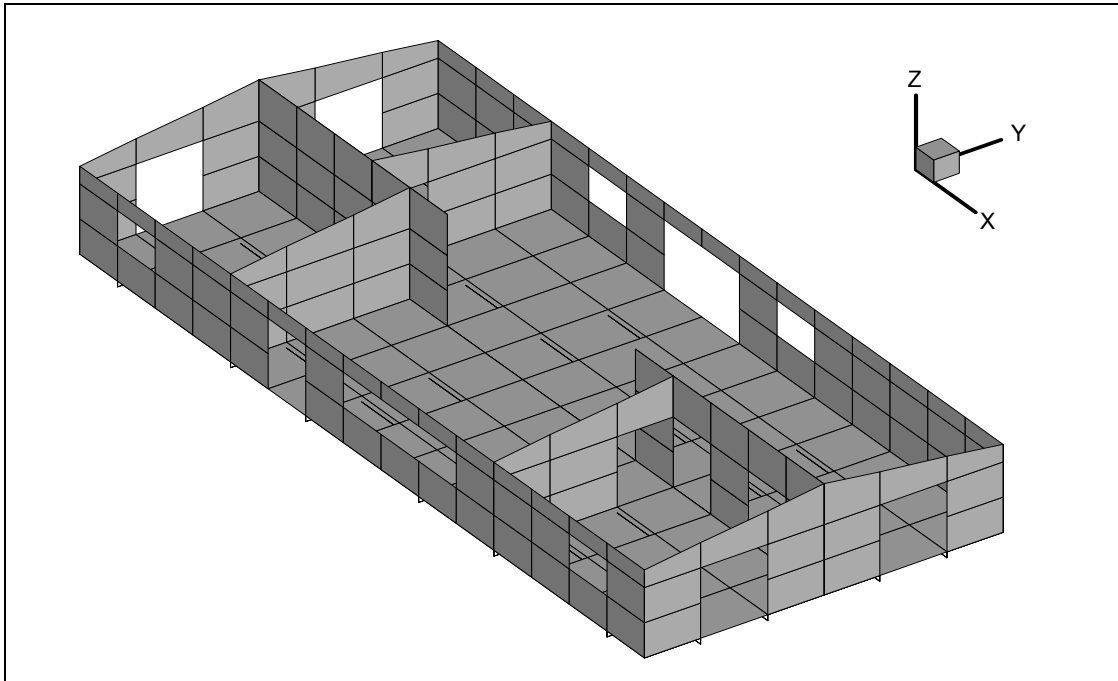


Figure 7.8: Layout of Interior and Exterior Walls

7.3.2.4 Roof System

The roof system was comprised of trusses, spaced at 48-inch intervals, sandwiched between OSB sheathing on the top and gypsum board sheathing on the bottom. OSB roof sheathing, along with the top chords of trusses, and gypsum board ceiling, along with the bottom chords of the trusses, were modeled using the 4-node orthotropic flat shell element. Remaining truss members were modeled using truss elements. The two halves were connected along the top of the trusses using interface elements. Interface elements at the lower edge of the ridge beam do not represent actual

connectors, but they were necessary to account for the compressive force transferred from lateral loading. *Figures 7.9, and 7.10* show the assembly of the roof system. Material properties for roof sheathing were assumed to be the same as those from the exterior walls and, for the ceiling, they were assumed to have the magnitude of those for the half inner walls. Material properties for the components of the roof system are given in *Table 7.4*.

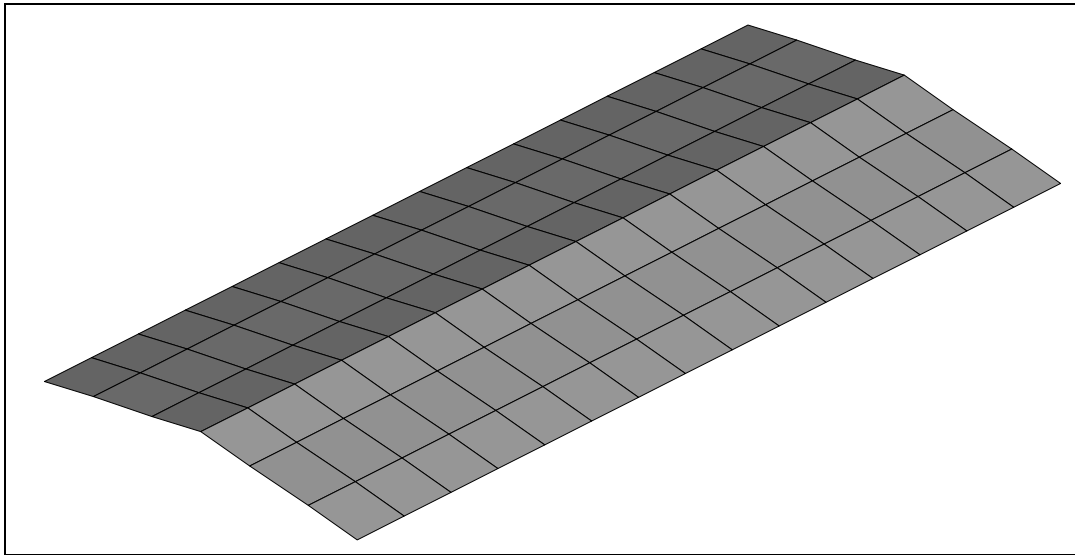


Figure 7.9: Layout of Ceiling

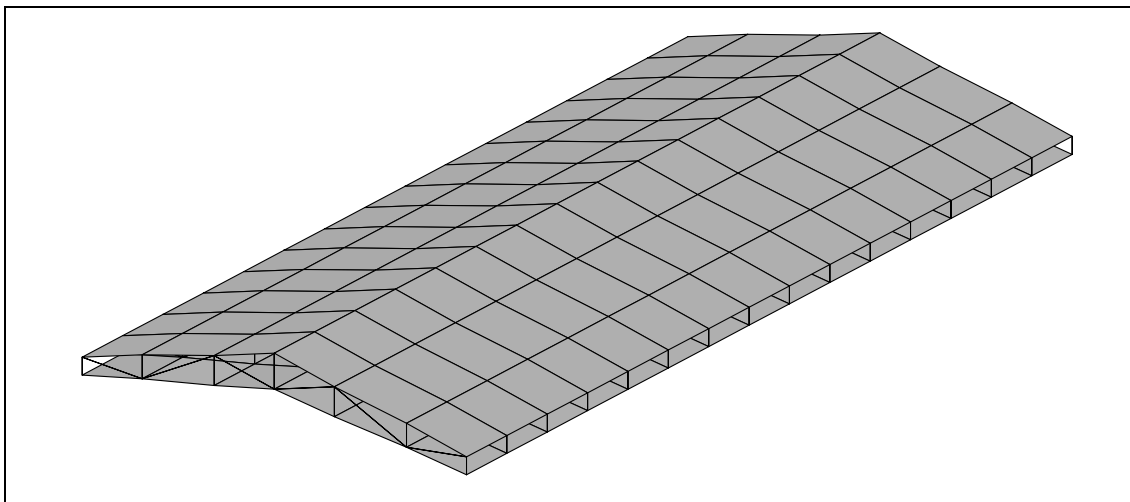


Figure 7.10: Complete Roof System with Ceiling, Trusses, and Roof Sheathing

Table 7.4: Roof Properties

Member	E_x (psi)	E_y (psi)	G_{xy} (psi)	t (in)	Area (in ²)
Roof Sheathing	3.41e4	9.27e4	7.75e3	4.25	-
Ceiling	2.09e4	1.03e5	1.13e4	3.82	-
Truss	1.2e6	-	-	-	10.5

7.3.2.5 Interfaces

All of the connections between floor-to-shear wall, shear wall-to-wall, and shear wall-to-ceiling, were modeled using the interface element. These interface elements were all assumed to have the same stiffness, as taken from the literature (Schmidt, 1999). 3/8 inch diameter lag bolts (12 inch spacing) were used to connect the two halves of the structure at the floor, ceiling, and roof levels. These connections were also modeled using interface elements and their properties (National Design Specification for Wood Construction, 2001) are tabulated in *Table 7.5*. *Figure 7.11* shows the location of the interface elements.

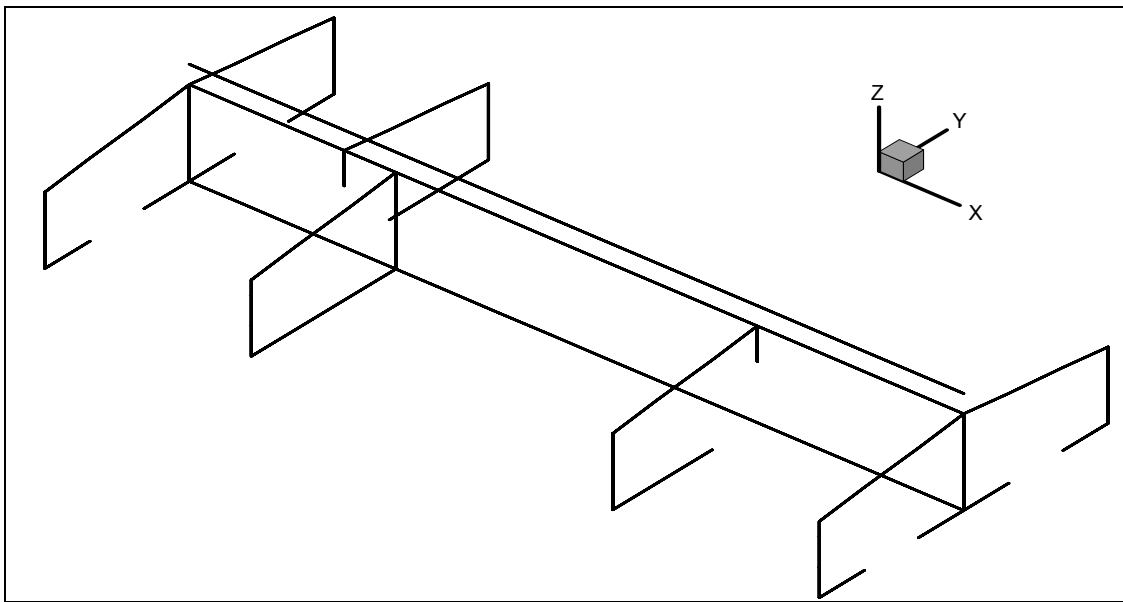


Figure 7.11: Layout of Interface Elements

Table 7.5: Interface Properties

Member	K_x (lb/in/in)	K_y (lb/in/in)	K_z (lb/in/in)	K_θ (lb/rad/in)
Interface	25000	1600	1600	250
Interface (3/8 inch Lag-Bolts)	3445	3445	3445	-

Figure 7.12 shows the location of the various displacement transducers and shear walls in the manufactured home.

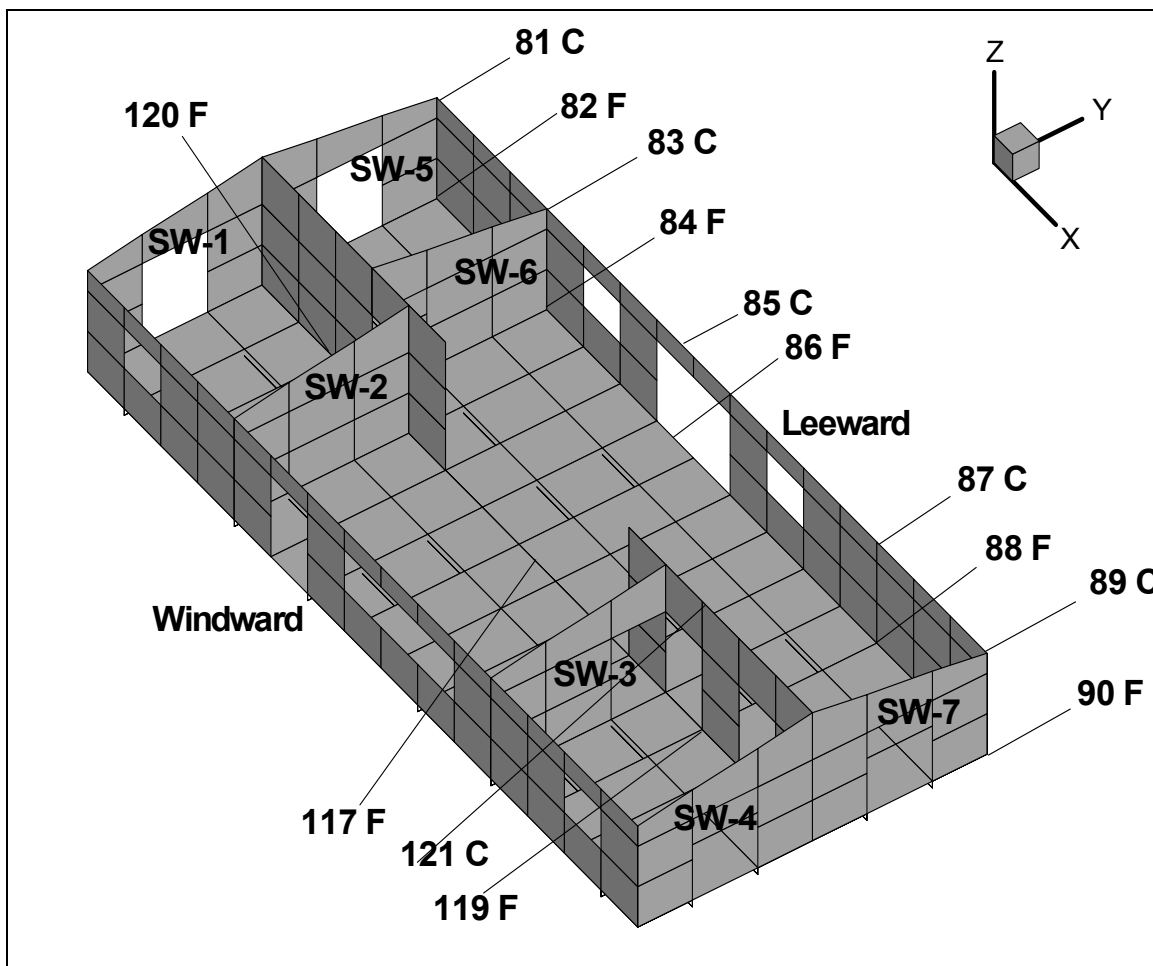


Figure 7.12: Location of Channels and Shear Walls

7.4 Results

7.4.1 Load – Deflection Behavior

Contours of the deflection response of the double-section manufactured home subjected to wind loading (uniform distributed load) are shown in *Figure 7.13*. Self-weight of the structure was considered, thus resisting the overturning of the structure.

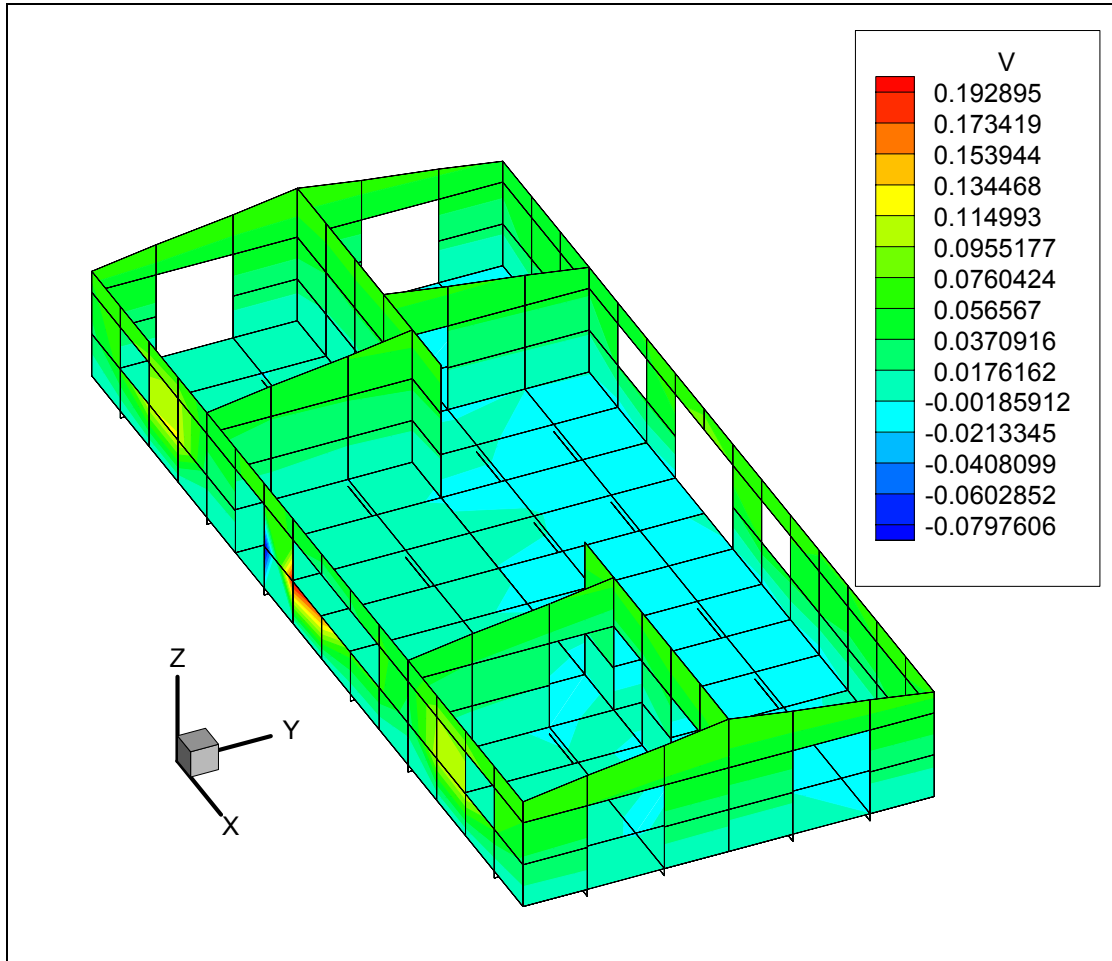


Figure 7.13: Deflection (y-direction) of Double-Section Manufactured Home when Subjected to Pressure Load

Global displacements along the top and bottom of the leeward wall are compared with experimental results in *Table 7.6*. It can be seen that the global displacements predicted by the finite element model are very small as compared to experimental results.

However, global displacements during the actual test were much higher due to rigid body translation of the structure that resulted from an almost total lack of lateral support at the foundation, other than very flexible tie-downs. Also, no interface slip was considered in the model between the diaphragms and longitudinal walls. Finally, the stiffness of floor and roof diaphragms in the model were estimated using values obtained from the literature. Actual values may be somewhat different. Thus, only relative displacements obtained from the finite element model can be compared.

Table 7.6: Global Displacements for Air Bag Test (Uniformly Distributed Load)

Channel Number	Experimental (in)	FE Model (in)
81 - Ceiling	0.2	0.06
82 - Floor	0.2	0
83 - Ceiling	0.2	0.0577
84 - Floor	0.19	-0.00016
85 - Ceiling	0.2	0.071
86 - Floor	0.18	-0.006
87 - Ceiling	0.18	0.0515
88 - Floor	0.15	-0.001
89 - Ceiling	0.15	0.056
90 - Floor	0.14	-0.0015

The racking displacements of the shear walls with interface slip are also compared in *Table 7.7*. The values obtained from the models are of the same order of magnitude but somewhat different, as compared to those from the experiment. The displacement of all shear walls in the model were nearly the same, while those that were measured were quite small for the interior walls. There are two possible reasons. First, the effect of interior

partitions, not designated as shear walls, was not included. Their stiffness may have caused a corresponding reduction in displacement for the interior of the structure. The second possibility is that there were differences in the interface properties between those used in the model and those in the actual structure, or differences in the behavior of the roof and floor diaphragms. One should note that the interface properties that were used were obtained from the literature, and are not necessarily representative of the construction of this structure.

Table 7.7: Racking Displacements of the Shear Walls

Shear Wall (SW) Channel Number	104 (SW-1)	112 (SW-2)	114 (SW-3)	108 (SW-4)	103 (SW-5)	110 (SW-6)
Experimental (in)	0.01	0.005	0.005	0.024	0	-0.002
FE Model (in)	0.0643	0.0653	0.0591	0.0685	0.0696	0.0681

The shear displacements along the mating line were also compared with experimental results and are tabulated in *Table 7.8*. Shear displacement along the mating line highly depends on the stiffness of the interface element connecting the two halves and again, those values come from literature. However, the results are in fairly close agreement.

Table 7.8: Shear Displacements Along the Mating Line

Displacement Transducer	121 C	120 F	118 C	117 F	119 F
Experimental (in)	0.001	0.0003	0.0004	0.0003	0.001
FE Model (in)	0.00035	0.00025	0.00015	0.00027	0.0014

7.4.2 Force Response

The forces transmitted through the various shear walls were also examined to evaluate the load distribution behavior of the model under a uniform loading. Table 7.9 shows the comparison of the percentage of the total load carried by each shear wall as calculated using the tributary area method versus the finite element model. In the finite element model, the load carried by each wall is proportional to the stiffness of the wall. All the interior shear walls have higher stiffness values than those of the exterior shear walls and thus carry a majority of the load. However, the interior leeward shear wall (SW-6) carries very small load as compared to other interior shear walls (SW-2 and SW-3). This shear wall (SW-6) is not as stiff as the other interior shear wall (SW-2) because it has a door opening. Also, the connection between the windward wall and other two interior shear walls (SW-2 and SW-3) acts as an overturning anchorage, whereas the leeward side shear wall (SW-6) is not similarly anchored due to a door opening near the mating line. Similar results were observed by Heine (1997). Another possible reason for this result may be the shear lag effect due to compression of the ceiling diaphragm. The ceiling diaphragm is not considered to be rigid, as is assumed with the tributary area method.

Table 7.9: Percentage of Forces in Each Shear Walls

Shear Wall (SW)	SW-1	SW-2	SW-3	SW-4	SW-5	SW-6	SW-7
Tributary Area Method (%)	6.9	30.5	21	6.9	6.9	21	6.9
Finite Element Model (%)	10.6	33.8	30	4.3	3.5	5.8	12

Shear forces along the mating line at floor, ceiling and roof sheathing levels are less than 150 lbs/ft. These forces are negligible and they agree well with the test results.

8. CONCLUSIONS AND RECOMMENDATIONS

8.1 Conclusions

A simplified method for predicting the behavior of shear walls is developed. This method accurately, within 3 %, predicts the in-plane stiffness properties of shear walls within manufactured homes without any need for full scale testing of structural systems or detailed modeling.

An interface element was developed and implemented to model interface flexibility and evaluate forces between components of manufactured homes. The interface properties used in this model were obtained from literature, and they do not necessarily resemble the construction of this structure. Taking this into consideration, the numerical results for displacement and force distribution show good agreement with the experimental results.

A finite element model for the linear analysis of a manufactured home has been developed. The model is highly dependent upon the material properties assumed for the floor, ceiling, walls, and interface. The results, in comparison with full-scale tests, are promising in that the model correctly predicts the overall behavior of the structure. Accuracy can be increased with further component testing and refinement of properties, especially for floor and roof diaphragms and interfaces.

In summary, the major conclusions of this study are:

1. An analysis module for linear structural analysis of manufactured homes has been developed and its ability to simulate overall structural behavior has been demonstrated.

2. The interface element can be used to determine one of the major results desired from the analysis module, which is the force at connections between shear walls and diaphragms and across the mating line.
3. A simplified analysis method was developed that accurately predicts the essential stiffness properties of shear walls within manufactured homes without the need to perform detailed tests or highly refined finite element models. Although not tried, the use of this method to analyze the behavior of the full-scale structure should provide a more realistic model than one using orthotropic shell elements. This is an item of further research.

8.2 Recommendations

The work completed in this study is only the first step to developing an effective design tool. More experimental and numerical work is recommended to improve the understanding of the behavior of a manufactured home, as listed below.

- For the connections, nail withdrawal is not modeled, as that would be a nonlinear effect. The analysis module is only valid for the linear analysis of manufactured homes.
- If only orthotropic shells are used to model the structure, the method cannot be used for the design of individual members because it does not take into account any localized effects. When walls, floor, ceiling, and roof diaphragms are modeled as orthotropic shells, the load distribution from the shear walls to the floor joists is not the same as observed in reality. For example, in-plane load within the shear wall is transmitted to the floor diaphragm as a distributed load

when modeled with shell elements, whereas in actual practice the studs in the wall apply a series of nearly point loads. Also, vertical loads acting on the structure are transmitted through individual framing members and not smeared as through a shell. The enhanced finite element method proposed here should address these limitations, but this remains an item of future research.

- In the finite element model of the double section manufactured home, all of the piers were modeled as pin supports. In reality, very little lateral support is provided by the piers, and the use of roller supports, or roller supports with some elastic restraint, is more appropriate than the pinned supports that were used.
- To develop an accurate model, the properties of the interface elements should be determined more precisely for the structure under consideration. Additional material and component tests should also be performed to develop a database of material properties for the Desktop Design Tool. Full-scale tests should be conducted under both simulated and actual loading conditions for full verification of the model. Uplift forces on the structure should be included to properly model wind effects. The behavior of floor and ceiling diaphragms should be investigated, along with variations in the support conditions.
- Further numerical work should accompany the experimental work mentioned previously to increase understanding of structural behavior. The first step is to conduct a thorough sensitivity study to determine the effects of changes in interface, wall, floor, and ceiling properties on the response of the structure. This will provide the insight as to which properties are most critical in affecting the response of the structure.

Literature Cited

- Akerlund, S., “Behavior of Wood-Framed Shear Walls,” *Journal of Structural Engineering*, Vol. 113, No. 11, pp. 2306-2309, 1987.
- American Plywood Association, “Hurricane Andrew: Structural Performance of Buildings in Southern Florida,” *APA Report T92-21*, 1992.
- Andreason, K.R., “Design Consideration for Wind and Earthquake Resisting Wood Panel Diaphragm,” *Proceedings of International Conference on Timber Engineering*, Seattle, WA, Sept. 19-22, Vol. 2, pp. 339-343, 1988.
- Bach, L., Wong, P.C., and Cheng, J., “Short and Long Term Stiffness of Stressed Skin Panels with OSB Flanges,” *Proceedings of International Conference on Timber Engineering*, Seattle, WA, Sept. 19-22, Vol. 2, pp. 344-351, 1988.
- Boughton, G.N., “Full Scale Structural Testing of Houses Under Cyclonic Wind Loads,” *Proceedings of International Conference on Timber Engineering*, Seattle, WA, Sept. 19-22, Vol. 2, pp. 82-88, 1988.
- Breyer, D.E., Fridley, K.J., and Cobeen, K.E., “*Design of Wood Structures – ASD*,” 4th Edition, McGraw-Hill, New York, 1999.
- Bulleit, W.M., “Markov Model for Wood Structural Systems,” *Journal of Structural Engineering*, Vol. 113, No. 9, pp. 2023-2031, 1987.
- Cook, R.B., Malkus, D.S., and Plesha, M.E., “*Concepts and Applications of Finite Element Analysis*,” 4th Edition, John Wiley and Sons, New York, 2002.
- Dean J.A., and Moss, P.J., “A Design of Rectangular Openings in Shear Walls and Diaphragms,” *Proceedings of the Pacific Timber Engineering Conference*, Vol. II, Auckland, New Zealand, pp. 513-518, 1984.

- De Klerk, D., “The Effect Of Stud Spacing on the Racking Strength of Timber Frame Walls,” *CSIR Special Report Hont 405*, National Timber Research Institute, Counsel for Scientific and Industrial Research, Pretoria, South Africa, 1985.
- Dolan, J. D., “*The Dynamic Response of Timber Shear Walls*,” Ph.D. Dissertation, University of British Columbia, Vancouver, Canada, 1989.
- Dolan, J.D., and Foschi, R.O., “Structural Analysis Model for Static Loads on Timber Shear Walls,” *Journal of Structural Engineering*, Vol. 117, No. 3, pp. 851-861, 1991.
- Douglas, B., and Line, P., “Consideration in Wind Design of Wood Structures,” *Proceedings of International Wood Engineering Conference*, New Orleans, LA, Oct. 28-31, Vol. 4, pp. 332-338, 1996.
- Douglas, B.K., and Line, P., “System Effect in Wood Assemblies,” *Proceedings of International Wood Engineering Conference*, New Orleans, LA, Oct. 28-31, Vol. 3, pp. 371-375, 1996.
- Enjily, V., and Griffiths, R.D., “The Racking Resistance of Large Wall Panels,” *Proceedings of International Wood Engineering Conference*, New Orleans, LA, Oct. 28-31, Vol. 2, pp. 321-328, 1996.
- Easley, J.T., Foomani, M., and Dodds, R.H., “Formulas for Wood Shear Walls,” *Journal of Structural Division*, Vol. 108, No. ST11, pp. 2460-2478, 1982.
- Falk, R.H., and Itani, R.Y., “Prediction of Diaphragm Deflection,” *Proceedings of International Conference on Timber Engineering*, Seattle, WA, Sept. 19-22, Vol. 1, pp. 766-773, 1988.

- Falk, R.H. and Moody, R.C., “Wood Diaphragms: Performance Requirements and Analytical Modeling,” *Structural Design, Analysis and Testing, Proceedings of the Sessions Related to Design, Analysis and Testing at Structure Congress ‘89*, ASCE, San Francisco, CA, May 1-5, pp 101-111, 1989.
- Foschi, R.O., and Filiatrault, A., “Performance Evaluation of 3M Scotch Grip Wood Adhesives 5230 for the Static and Dynamic Design of Timber Shear Wall and Diaphragms,” *Final Report Prepared for 3M Corporation*, 43 pp, 1990.
- Foschi, R.O., “Performance Evaluation of Shear Walls and Diaphragms with Waferboard Sheathing,” *Report to the Canadian Waferboard Association by Forintek Canada Corp.*, Vancouver, British Columbia.
- Fridley, K.J., “Wood Engineering in the 21st Century: Research Needs and Goals,” *Proceedings of Workshop offered in conjunction with the SEI/ASCE Structures Congress XV*, Portland, OR, Apr. 16, pp. 371-375, 1997.
- Ge, Y-Z, V.S. Gopalaratnum, and H. Liu, “Effects of Openings on the Stiffness of Wood-Frame Walls,” *Forest Products Journals*, Vol. 41, No 1. Forest Products Research Society, Madison, WI, pp65-70, 1991.
- Gebremedhin, K.G., and Niu, K.T., “Three-Dimensional Building Stiffness Model for Post-Frame Buildings,” *Proceedings of International Wood Engineering Conference*, New Orleans, LA, Oct. 28-31, Vol. 2, pp. 45-52, 1996.
- Gobat, J. I., and Atkinson, D.C., *The FElt System: User’s Guide and Reference Manual*, *Computer Science Technical Report CS94-376*, University of California, San Diego, 2000.
- Goodman, J.R. and Klasi, M.L., “Testing of Wall Stiffness on the Crownpointe Manufactured Home”, South Dakota School of Mines and Technology, 1996.

- Goodman, J.R., Schmidt, R.J., Criswell, M., and Stewart, A.H., “Laterally Loaded Manufactured Homes,” *Proceedings of International Wood Engineering Conference*, New Orleans, LA, Oct. 28-31, Vol. 4, pp. 589-595, 1996.
- Griffiths, D.R., “Determining the Racking Resistance of Timber Framed Walls,” *Proceedings of the Pacific Timber Engineering Conference*, Auckland, New Zealand, Vol. 1, pp. 504-512, 1984.
- Gupta, A.K., and Kuo, G.P., “Behavior of Wood-Frame Shear Walls,” *Journal of Structural Engineering*, Vol. 111, No.8, pp. 1722-1733, 1985.
- Gupta, A.K., and Kuo, G.P., “Modeling of a Wood-Framed House,” *Journal of Structural Engineering*, Vol. 113, No. 2, pp. 260-278, 1987.
- Gupta, A.K., and Kuo, G.P., “Wood-Frame Shear Walls with Uplifting,” *Journal of Structural Engineering*, Vol. 113, No. 2, pp. 241-259, 1987.
- Gutkowski, R. M. and Castillo, A. L., “Single- and Double- Sheathed Wood Shear Wall Study,” *Journal of Structural Engineering*, Vol. 114, No. 6, pp. 1268-1284, 1988.
- He, M., “*A Study of Wood Based Shear Walls Sheathed with Oversize Oriented Strand Board Panels*,” Master’s Thesis, University of British Columbia, Vancouver, Canada, 1997.
- He, M., Magnusson, H., Lam, F., and Prion, H., “Cyclic Performance of Perforated Wood Shear Walls with Oversize OSB Panels,” *Journal of Structural Engineering*, Vol. 125, No. 1, pp.10-18, 1999.

- He, M., Lam, F., and Foschi, R.O., “ Modeling Three-Dimensional Timber Light-Frame Building,” *Journal of Structural Engineering*, Vol. 127, No. 8, pp. 901-913, 2001.
- Heine, C. P., “*Effect of Overturning Restraint on the Performance of Fully Sheathed and Perforated Timber Framed Shear Walls*,” Master’s Thesis, Virginia Polytechnic Institute and State University, Blacksburg, VA, 1997.
- Heine, C.P., and Dolan, J.D., “Dynamic Performance of Perforated Light-Frame Shear Walls with Various End Restraints,” *Forest Product Journal*, Vol. 51, No. 7/8, 2001.
- Itani, R. Y., and Cheung, C. K., “Nonlinear Analysis of Sheathed Wood Diaphragms,” *Journal of Structural Engineering*, Vol. 110, No. 9, pp. 2137-2147, 1984.
- Jablin, M.C., and Schmidt, R.J., “Finite Element Modeling of Manufactured Homes,” *Proceedings of International Wood Engineering Conference*, New Orleans, LA, Oct. 28-31, Vol. 3, pp. 170-177, 1996.
- Johnson, A. C., “*Monotonic and Cyclic Performance of Long Shear Walls with Openings*,” Master’s Thesis, Virginia Polytechnic Institute and State University, Blacksburg, VA, 1997.
- Johnson, A., and Dolan, J.D., “Performance of Long Shear Walls with Openings,” *Proceedings of International Wood Engineering Conference*, New Orleans, LA, Oct. 28-31, Vol. 2, pp. 337-344, 1996.

- Källsner, B., “Panels as Wind-Bracing Elements in Timber-Framed Walls,” *Wood Technology Report Nr. 56*, Swedish Institute for Wood Technology research, Stockholm, Sweden, 1984.
- Kasal, B., Leichti, R.J., and Itani, R.Y., “Nonlinear Finite Element Model of Complete Light-Frame Wood Structures,” *Journal of Structural Engineering*, Vol. 120, No. 1, pp. 100-119, 1994.
- Kasal, B., and Leichti, R.J., “Nonlinear Finite Element Model for Light-Frame Stud Walls,” *Journal of Structural Engineering*, Vol. 118, No. 11, pp. 3122-3134, 1992.
- Kamiya, F., “Configuration of Wood Sheathed Walls and Its Racking Resistance,” *Bulletin of the Forestry and Forest Products Research Institute*, Japan, No. 340, pp. 169-186, 1986.
- Kamiya, F., “Buckling Theory of Sheathed Walls: Linear Analysis,” *Journal of Structural Engineering*, Vol. 113, No. 9, pp. 2009-2022, 1987.
- Karacabeyli, E., and Ceccotti, A., “Test Results on the Lateral Resistance of Nailed Shear Walls,” *Proceedings of International Wood Engineering Conference*, New Orleans, LA, Oct. 28-31, Vol. 2, pp. 179-188, 1996.
- Koerner, B.D., Schmidt, R.J., and Goodman, J.R., “Lateral Load Testing and Analysis of Manufactured Homes,” *Proceedings of the World Conference on Timber Engineering*, British Columbia, Canada, July 31 – August 3, 2000.
- Lacy, J.M., Larson, T.K., and Richins, W.D., “Defining Hurricane Winds – Engineers Capture Georges,” *Structure*, pp. 22-26, 1999.

- Lam, F., Prion, H., and He, M., “Lateral Resistance of Wood Shear Walls with Large Sheathing Panels,” *Journal of Structural Engineering*, Vol. 123, No. 12, pp. 1666-1673, 1997.
- Lee, M., Lin, H.T., Nelson, E.L., Fowler, D.W. and Wheat, D.L., “Strength Behavior of Shear Walls Used in Mobile Homes,” *Report DHUD82-2*, Department of Civil Engineering, University of Texas, Austin, TX, June, 1982.
- Levitan, M., “Wind Loading on Wood Structures,” *Proceedings of International Wood Engineering Conference*, New Orleans, LA, Oct. 28-31, Vol. 4, pp. 328-331, 1996.
- Line, P., and Douglas, B.K., “Perforated Shear Wall Design Method,” *Proceedings of International Wood Engineering Conference*, New Orleans, LA, Oct. 28-31, Vol. 2, pp. 345-352, 1996.
- McCutcheon W.J., “Computer Programming for Structural Analysis of Wood Walls and Floors,” *Proceedings of International Conference on Timber Engineering*, Seattle, WA, Sept. 19-22, Vol. 2, pp. 909-914, 1988.
- McCutcheon, W. J., “Racking Deformations in Wood Shear Walls,” *Journal of Structural Engineering*, Vol. 111, No. 2, pp 257-269, 1985.
- McDowall, C.G., and Hilligan, A.F., “Racking Resistance of Short Lengths of Particleboard Sheathed, Timber Framed Wall Panels,” *Proceedings of the Second Pacific Engineering Conference*, Seattle, Washington, Vol. 2, pp. 95-99, 1989.
- Moody, R.C., and Schmidt, R.J., “Lateral Loading of Wood Frame Houses – Analysis and Performance,” *Proceedings of International Conference on Timber Engineering*, Seattle, WA, Sept. 19-22, Vol. 2, pp. 62-72, 1988.

- Naik, T.R., Kaliszky, S.K., and Soltis, L.A., “Mechanical Nonlinear Shear Wall Model,” *Journal of Engineering Mechanics*, Vol. 110, No. 12, 1984.
- Nelson, E.L., Fowler, D.W. and Wheat, D.L., “Structural Behavior of Wood Shear Wall Assemblies,” *Journal of Structural Engineering*, Vol. 111, No. 3, pp 654-666, 1985.
- Ohashi, Y. and Sakamoto, I, “Effect of Horizontal Diaphragm on Behavior of Wooden Dwellings Subjected to Lateral Loads – Experimental Study on a Real Size Frame Model,” *Proceedings of International Conference on Timber Engineering*, Seattle, WA, Sept. 19-22, Vol. 2, pp. 112-120, 1988.
- Oliva, M.G., and Wolfe, R.W., “Contribution of Gypsum Wallboard to Racking Performance of Walls,” *Proceedings of International Conference on Timber Engineering*, Seattle, WA, Sept. 19-22, Vol. 1, pp. 759-765, 1988.
- Paevere, P.J., Foliente, G.C., and Kasal, B., “Load-Sharing and redistribution in a One-Story Wood-Frame Building,” *Journal of Structural Engineering*, Vol. 129, No. 9, pp 1275-1283, 2003.
- Patton-Mallory, M., Gutkowski, R.M., and Soltis, L.A., “Racking Performance of Light-Frame Walls Sheathed on Two Sides,” *Research Paper FPL 448*, U.S. Department of Agriculture, Forest Service, Forest Products Laboratory, Madison, WI, 1984.
- Patton-Mallory, M., Wolfe, R.W., Soltis, L.A., and Gutkowski, R.M., “Light-Frame Shear Wall Length and Opening Effects,” *Journal of Structural Engineering*, Vol. 111, No. 10, pp. 2227-2239, 1985.

- Patton-Mallory, M., and McCutcheon, W.J., “Predicting Racking Performance of Walls Sheathed on Both Sides,” *Forest Products Journal*, Vol. 37, No.9, pp. 27-32, 1987.
- Pellicane, P.J., “Nail/Glue Joints in Wood,” *Forest Products Journal*, Vol. 41, No. 11/12, pp. 33-35, 1991.
- Philips, T.L., Itani, R.Y., and McLean, D.I., “Lateral Load Sharing by Diaphragms in Wood-Framed Buildings,” *Journal of Structural Engineering*, Vol. 119, No. 5, pp. 1556-1571, 1993.
- Polensek, A., “Finite Element Analysis of Wood-Stud Walls,” *Journal of Structural Engineering*, Vol. 102, No.7, pp.1317-1335, 1976.
- Reardon, G.F., “Effects of Non-Structural Cladding on Timber Framed House Construction,” *Proceedings of International Conference on Timber Engineering*, Seattle, WA, Sept. 19-22, Vol. 2, pp. 276-284, 1988.
- Richins, W.D., Lacy, J.M., Larson, T.K., Rahl, T.E., Schmidt, R.J., Koerner, B.D., and Pandey, A.K., “Full-Scale Testing of a Single-Wide Manufactured Home,” *Proceedings of the World Conference on Timber Engineering*, British Columbia, Canada, July 31 – August 3, 2000.
- Richins, W.D., Lacy, J.M., Larson, T.K., Snow, S.D., Schmidt, R.J., Goodman, J.R., and Beaudoin, D.K., “Manufactured Home Testing in Naturally Occurring High Winds,” *Journal of Architectural Engineering* (Unpublished).
- Richins, W.D., Rahl, T.E., Lacy, J.M., Larson, T.K., Flood, M.N., Schmidt, R.J., Koerner, B.D., Pandey, A.K., Stewart, A.H., and Walters, F., “Full-Scale Structural

Testing of a Single-Wide Manufactured Home, Oakwood Model 1320; 13 ft x 62 ft,” *INEEL Report*, INEEL/EXT-1999-301, March 1999.

- Richins, W.D., Larson, T.K., Schmidt, R.J., and Goodman, J.R., “Testing Manufactured Homes for High Winds,” *Proceedings of PATH Conference on Durability and Disaster Mitigation in Wood Frame Housing*, Madison, WI, Nov. 6-8, 2000.
- Richins, W.D., Larson, T.K., Snow, S.D., Schmidt, R.J., Goodman, J.R., and Beaudoin, D.K., “Full-Scale Testing of Manufactured Home in Naturally Occurring High Winds,” *Proceedings of Americas Conference on Wind Engineering*, Clemson, SC, June 4-6, 2001.
- Richins, W.D., Larson, T.K., Blakeley, J.E., Rahl, T.E., Twitchell, G.A., Kobbe, R.G., Crawford, A.L., and B.D., Pandey, “Lateral Load Testing of a Double-Wide Manufactured Home,” *INEEL Report*, INEEL/EXT-03-00191, April 2003.
- Riley, M.A., and Vega, R.E., “Results of Shear Resistance Tests of Manufactured Home Walls,” *NIST Report*, May 2003.
- Salenikovich, A.J., “*Racking Performance of Light-Framed Shear Walls*,” Ph.D. Dissertation, Virginia Polytechnic Institute and State University, Blacksburg, VA, 2000.
- Schmidt, R.J., “Three Dimensional Modeling of Light Frame Buildings Under Lateral Loading,” *Research Report*, Department of Civil Engineering, University of Wyoming, Laramie, WY, 1990.

- Schmidt, R.J., Goodman, J.R., Richins, and, Pandey, A.K., “Improved Design of Manufactured Homes for Hazardous Winds,” *Proceedings of the World Conference on Timber Engineering*, British Columbia, Canada, July 31 – August 3, 2000.
- Schmidt, R.J. and Moody, R.C., “Modeling of Laterally Loaded Light-Frame Buildings,” *Journal of Structural Engineering*, Vol. 115, No. 1, pp 201-217, 1989.
- Skaggs, J.D., and Rose, J.D., “Cyclic Load Testing of Wood Structural Panel Shear Walls,” *Proceedings of International Wood Engineering Conference*, New Orleans, LA, Oct. 28-31, Vol. 2, pp. 195-200, 1996.
- Stewart, A.H., Kliewer, A., Goodman, J.R., and Salsbury, E.M., “Full-Scale Tests of Manufactured Houses Under Simulated Wind Loads,” *Proceedings of International Conference on Timber Engineering*, Seattle, WA, Sept. 19-22, Vol. 2, pp 97-111, 1988.
- Stewart, A.H., Kliewer, A., Goodman, J.R., and Salsbury, E.M., “Lateral Force Distribution on Manufactured Housing From Full-Scale Testing,” *Structural Design, Analysis and Testing, Proceedings of the Sessions Related to Design, Analysis and Testing at Structure Congress '89*, ASCE, San Francisco, CA, May 1-5, pp 112-123, 1989.
- Stricklin, D.L., Schiff, S.D., and Rosowsky, D.V., “Uplift Capacity of Light-Frame Wood Stud Walls,” *Proceedings of International Wood Engineering Conference*, New Orleans, LA, Oct. 28-31, Vol. 4, pp. 471-480, 1996.
- Sugiyama, H., and Matsumoto, T., “A Simplified Method of Calculating the Shear Strength of a Plywood-Sheathed Shear Walls with Opening I. Evaluation of the

Racking Load of Shear Wall Without Openings,” *Mokuzai Gakkaishi*, Vol. 39, No. 1, pp. 75-79, 1993.

- Sugiyama, H., and Matsumoto, T., “Empirical Equations for the Estimation of Racking Strengths of a Plywood-Sheathed Shear Wall with Openings,” *Summaries of Technical Papers of the Annual Meeting*, Architectural Institute of Japan, 1994.
- Suzuki, S., Sugiyama, H., and Takemura, Y., “Behavior of Bearing Walls in the Wooden North-American-Type Full-Size Building (No. 1),” *Trans. Of A.I.J.*, No. 269, pp. 58-59, 1978.
- Thurston, S. J., “Report on Racking Resistance of Long Sheathed Timber Framed Walls with Openings,” *BRANZ Study report SR 54*, 1993.
- Thurston, S. J. and Flack, P. F., “Cyclic Load Performance of Timber Sheathed Bracing Walls,” *Central Laboratories Report 5-80/10*, Ministry of Works and Development, Wellington, New Zealand, 1980.
- Toothman, A.J., “*Monotonic and Cyclic Performance of Light-Frame Shear Walls with Various Sheathing Materials*,” Master’s Thesis, Virginia Polytechnic Institute and State University, Blacksburg, VA, 2003.
- Tuomi, R.L., and McCutcheon, W.J., “Racking Strength of Light-Frame Nailed Walls,” *Journal of Structural Engineering*, Vol 104, No. 7, pp. 1131-1140, 1978.
- Tuomi, R.L., and McCutcheon, W.J., “Testing of Full Scale House Under Simulated Snowloads and Windloads,” *Res. Pap. FPL-234*, USDA Forest Serv., *Forest Product Laboratory*, 1974.
- White, M. W., “*Parametric Study of Timber Shear Walls*,” Ph.D. Dissertation, Virginia Polytechnic Institute and State University, Blacksburg, VA, 1995.

- White, M, and Dolan, J.D., “Seismic Response of Timber Shear Walls,” *Proceedings of International Wood Engineering Conference*, New Orleans, LA, Oct. 28-31, Vol. 2, pp. 329-336, 1996.
- Wickens, H.G., and Griffiths, D.R., “Timber Frame Walls: Design For Racking Resistance,” *Proceedings of International Wood Engineering Conference*, New Orleans, LA, Oct. 28-31, Vol. 2, pp. 37-45, 1996.
- Wickens, H.G., and Griffiths, D.R., “The Derivation of Design Data from UK Timber Frame Wall Racking Test,” *Proceedings of International Wood Engineering Conference*, New Orleans, LA, Oct. 28-31, Vol. 4, pp. 3-9, 1996.
- Wolfe R. W., “Contribution of Gypsum Wallboard to the Racking Resistance of Light-Frame Walls,” *Research Paper FPL 439*, United States Department of Agriculture, Forest Products Laboratory, Madison, WI, 1983.
- Yasumura, M., “Racking Resistance of Wooden Frame Walls with Various Openings,” *International Council for Building Research Studies and Documentation, Working Commission W18 – Timber Structures, CIB – W18, IUFRO S 5.02*, Volume II, Meeting Nineteen, Florence, Italy, 1986.
- Yasumura, M., Nishiyama, I., Murota, T., and Yamaguchi, N., “Experiments of Three-Storied Wooden Frame Building Subjected to Horizontal Load,” *Proceedings of International Conference on Timber Engineering*, Seattle, WA, Sept. 19-22, Vol. 2, pp. 262-275, 1988.
- Yasumura, M., Ohta, H., and Fukuda, I., “Design of Wood-Framed Building with Shear Walls and Moment Frames,” *Proceedings of International Wood Engineering Conference*, New Orleans, LA, Oct. 28-31, Vol. 4, pp. 81-88, 1996.

Appendix A: Equivalent In-Plane Properties for Orthotropic Shell Element

A.1 Introduction

The procedures used to derive the equivalent material properties for the orthotropic shell elements are outlined in this section. The derivation is based on smearing the studs and sheathings into an equivalent orthotropic shell.

A.2 Equivalent In-Plane Properties

It is assumed that only studs provide stiffness along the vertical direction (y -direction) and only sheathings provide stiffness along horizontal direction (x -direction) as shown in *Figure A.1*. The overall thickness of an equivalent orthotropic shell element is assumed to be the sum of thicknesses of sheathings and studs.

Overall thickness of an equivalent orthotropic shell for the shear wall with OSB and Gypsum sheathing = $7/16$ in + 3.5 in + $5/16$ in = 4.25 in

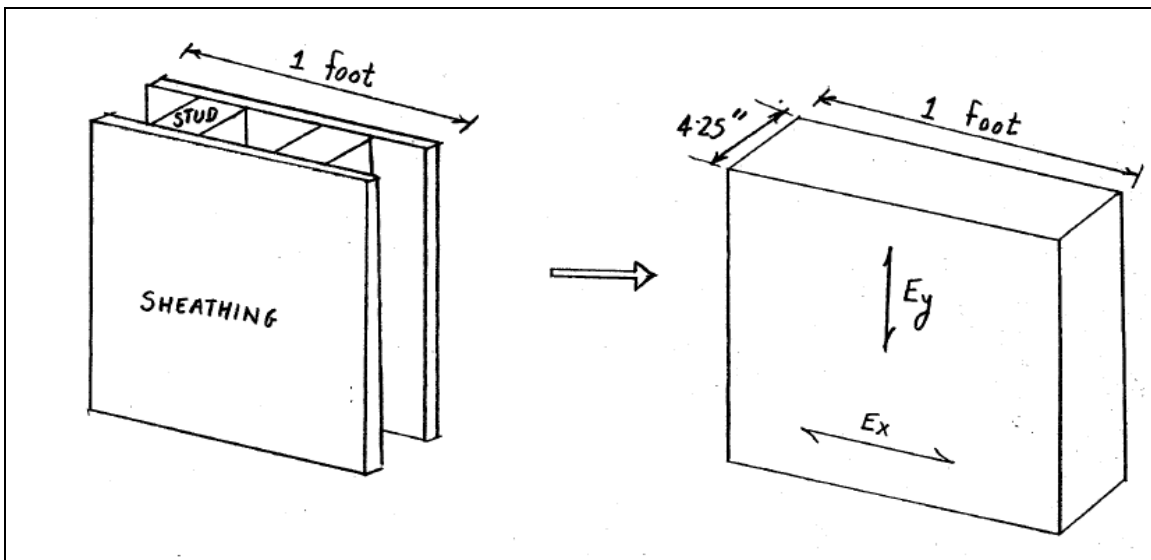


Figure A.1: Equivalent Orthotropic Shell

A.2.1 Along y-direction

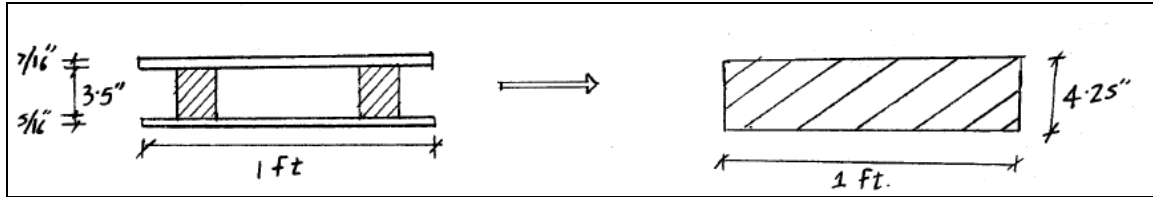


Figure A.2: Equivalent Orthotropic Shell Properties along y-Direction

Spacing of Studs = 16 in. on center

The area of stud per foot of shear wall is given by,

$$A_{STUD} = \frac{12}{16} \cdot (1.5in \times 3.5in) = 3.9375in^2 / ft$$

The modulus of Elasticity of Studs, $E_{STUD} = 1.2 \times 10^6 psi$

The area per foot of orthotropic shear wall, $A_{ORTHOSHELL} = 12 in \times 4.25 in = 51 in^2/ft$

Thus, the modulus of elasticity along the y-direction, E_y , is given by

$$E_y = \frac{E_{STUD} \cdot A_{STUD}}{A_{ORTHOSHELL}} = \frac{(1.2 \times 10^6) \cdot (3.9375)}{51} = 92647 psi$$

A.2.2 Along x-direction

The area of OSB sheathing per foot of the shear wall is given by,

$$A_{OSB} = 12 \times 7 / 16 = 5.25in^2$$

Similarly, the area of Gypsum board per foot of shear wall is given by,

$$A_{GYPSUM} = 12 \times 5 / 16 = 3.75in^2$$

The modulus of Elasticity of OSB sheathing, $E_{OSB} = 1.4922 \times 10^5 psi$, and

The modulus of Elasticity of Gypsum board, $E_{GYPSUM} = 2.545 \times 10^5 psi$

The area per foot of orthotropic shear wall, $A_{ORTHOSHELL} = 12 in \times 4.25 in = 51 in^2/ft$

Thus, for a shear wall with OSB and Gypsum sheathing, the modulus of elasticity along the x -direction, E_x , is given by

$$E_x = \frac{(E_{OSB} \cdot A_{OSB}) \cdot (E_{GYPSUM} \cdot A_{GYPSUM})}{A_{ORTHOSHELL}} = \frac{[(1.492 \times 5.25) \cdot (2.545 \times 3.75)] \times 10^5}{51} = 34074 \text{ psi}$$